

Looking for the first galaxies: Lensing or blank fields?

A. Maizy¹, J. Richard², M. A. De Leo³, R. Pelló¹, and J. P. Kneib⁴

¹ Laboratoire d'Astrophysique de Toulouse-Tarbes, CNRS, Université de Toulouse, 14 Av. Edouard-Belin, F-31400 Toulouse, France
e-mail: alexandre.maizy@ast.obs-mip.fr e-mail: roser@ast.obs-mip.fr

² Institute for Computational Cosmology, Department of Physics, Durham University, South Road, Durham, DH1 3LE, UK
e-mail: johan.richard@durham.ac.uk

³ Instituto de Astronomía, UNAM, Apartado Postal 70-264, 04510 México DF, Mexico
e-mail: madeleo@astroscu.unam.mx

⁴ OAMP, Laboratoire d'Astrophysique de Marseille, UMR 6110 traverse du Siphon, 13012 Marseille, France
e-mail: jean-paul.kneib@oamp.fr

Received ; accepted

ABSTRACT

Context. The identification and study of the first galaxies remains one of the most exciting topics in observational cosmology. The determination of the best possible observing strategies is a very important choice in order to build up a representative sample of spectroscopically confirmed sources at high- z ($z \gtrsim 7$), beyond the limits of present-day observations.

Aims. This paper is intended to precisely address the relative efficiency of lensing and blank fields in the identification and study of galaxies at $6 \lesssim z \lesssim 12$.

Methods. The detection efficiency and field-to-field variance are estimated from direct simulations of both blank and lensing fields observations. Present known luminosity functions in the UV are used to determine the expected distribution and properties of distant samples at $z \gtrsim 6$ for a variety of survey configurations. Different models for well known lensing clusters are used to simulate in details the magnification and dilution effects on the background distant population of galaxies.

Results. The presence of a strong-lensing cluster along the line of sight has a dramatic effect on the number of observed sources, with a positive magnification bias in typical ground-based “shallow” surveys ($AB \lesssim 25.5$). The positive magnification bias increases with the redshift of sources and decreases with both depth of the survey and the size of the surveyed area. The maximum efficiency is reached for lensing clusters at $z \sim 0.1 - 0.3$. Observing blank fields in shallow surveys is particularly inefficient as compared to lensing fields if the UV LF for LBGs is strongly evolving at $z \gtrsim 7$. Also in this case, the number of $z \geq 8$ sources expected at the typical depth of JWST ($AB \sim 28 - 29$) is much higher in lensing than in blank fields (e.g. a factor of ~ 10 for $AB \lesssim 28$). All these results have been obtained assuming that number counts derived in clusters are not dominated by sources below the limiting surface brightness of observations, which in turn depends on the reliability of the usual scalings applied to the size of high- z sources.

Conclusions. Blank field surveys with a large field of view are needed to prove the bright end of the LF at $z \gtrsim 6 - 7$, whereas lensing clusters are particularly useful for exploring the mid to faint end of the LF.

Key words. galaxies : formation – galaxies : high redshift – galaxies : photometry – galaxies : clusters : lensing –

1. Introduction

Constraining the abundance of $z > 7$ sources remains an important challenge of modern cosmology. Recent WMAP results place the first building blocks of galaxies at redshifts $z = 11.0 \pm 1.4$, suggesting that reionization was an extended process (Dunkley et al. 2009). Distant star-forming systems could have been responsible for a significant part of the cosmic reionization. Considerable advances have been made during the last years in the observation of the early Universe with the discovery of galaxies at $\sim 6-7$, close to the end of the reionization epoch (e.g. Hu et al. 2002; Kodaira et al. 2003; Cuby et al. 2003; Kneib et al. 2004; Stanway et al. 2004; Bouwens et al. 2004a, 2006; Iye et al. 2006; Bradley et al. 2008; Zheng et al. 2009), and the first prospects up to $z \sim 10$ (Pelló et al. 2004; Richard et al. 2006; Stark et al. 2007; Richard et al. 2008; Bouwens et al. 2008, 2009a).

High- z surveys are mainly based on two different and complementary techniques: the dropout (Lyman- α Break) identification, which is an extrapolation of the drop-out technique used

for Lyman-Break Galaxies (LBGs, Steidel et al. 1999) to higher redshifts (e.g. Bouwens et al. 2006; Richard et al. 2006, 2008), and the narrow-band (NB) imaging aimed at detecting Lyman α emitters (LAEs, e.g. Taniguchi et al. 2005; Iye et al. 2006; Kashikawa et al. 2006; Willis et al. 2006; Cuby et al. 2007). Using the former technique, Bouwens et al. (2008) found a strong evolution in the abundance of galaxies between $z \sim 7-8$ and $z \sim 3-4$, the SFR density being much smaller at very high- z up to the limits of their survey, in particular towards the bright end of the Luminosity Function (LF). A strong evolution is also observed in the number density of sources detected with NB techniques, which seems to be much smaller at $z \geq 7$ than in the $z \sim 5 - 7$ interval (Iye et al. 2006; Cuby et al. 2007; Willis et al. 2008).

Both dropout and NB approaches require a subsequent spectroscopic confirmation of the selected candidates. For now approximately ten galaxies beyond $z \sim 6.5$ are known with secure spectroscopic redshifts (Hu et al. 2002; Kodaira et al. 2003; Cuby et al. 2003; Taniguchi et al. 2005; Iye et al. 2006). All samples beyond this redshift are mainly supported by photometric considerations (Kneib et al. 2004; Bouwens et al. 2004b,

2006; Richard et al. 2006, 2008; Bradley et al. 2008). This situation is expected to dramatically improve in the near future with the arrival of a new generation of multi-object spectrographs in the near-IR, such as MOIRCS/Subaru, Flamingos2/Gemini-S (~ 2009), or EMIR/GTC¹ (~ 2012), with well suited field of view, spectral resolution and sensitivity. These forthcoming facilities should provide spectroscopic confirmation for a large number of $z > 7$ candidates identified from deep photometric surveys, and the first characterization of the physical properties of these sources (e.g. IMF, stellar populations, fraction of AGN, ...).

The aim of this paper is to determine the best possible observing strategies in order to build up a representative sample of spectroscopically confirmed $z \geq 7$ galaxies. The photometric pre-selection of high- z candidates could be achieved either in blank fields or in lensing clusters. This later technique, also first referred to as the “gravitational telescope” by Zwicky, has proven highly successful in identifying a large fraction of the most distant galaxies known today thanks to magnifications by typically 1-3 magnitudes in the cluster core (e.g. Ellis et al. 2001; Hu et al. 2002; Kneib et al. 2004; Bradley et al. 2008; Zheng et al. 2009; Bradač et al. 2009). The presence of a strong lensing cluster in the surveyed field introduces two opposite effects on number counts as compared to blank fields. In one hand, gravitational magnification increases the number of faint sources by improving the detection towards the faint end of the LF. On the other hand, the reduction of the effective surface by the same magnification factor leads to a dilution in observed counts. The global positive/negative magnification bias obviously depends on the slope of the number counts, as pointed out by Broadhurst et al. (1995).

This paper addresses the relative efficiency of surveys conducted on blank and lensing fields as a function of the relevant parameters, namely the redshift of the sources, the redshift and properties of the lensing clusters and the survey characteristics (i.e. area, photometric depth...). This calculation requires a detailed simulation of observations using lensing models, and realistic assumptions for the properties of background sources according to present-day observational results, in particular for the luminosity function and typical sizes of $z > 7$ galaxies.

The paper is organized as follows. In Section 2 we describe the simulations performed in order to determine the relative detection efficiency for high- z sources, both in lensing and blank fields. Section 3 presents the results, in particular the detection efficiency achieved as a function of redshift for both sources and lensing clusters, together with a discussion on the influence of lensing cluster properties and field-to-field variance. A discussion is presented in Section 4 on the relative efficiency as a function of survey parameters, and a comparison between simulations and present surveys. Conclusions are given in Section 5.

Throughout this paper, we adopt a concordance cosmological model, with $\Omega_\Lambda = 0.7$, $\Omega_m = 0.3$, and $H_0 = 70 \text{ km s}^{-1} \text{ Mpc}^{-1}$. All magnitudes are given in the AB system. Conversion values between Vega and AB systems for the filters used in this paper are typically $C_{AB} = 0.95, 1.41$ and 1.87 in J, H and K respectively, with $m_{AB} = m_{Vega} + C_{AB}$.

2. Simulations of lensing and blank field observations

2.1. Simulation parameters

This section describes the ingredients used in the simulations to implement different assumptions that would affect our efficiency in detecting high redshift galaxies. There are three important aspects to be considered in the comparison between lensing and blank fields. The first one is the LF and typical sizes of sources. The second one concerns the properties of the lensing clusters, in particular their mass distribution and redshift. The third one is related to the survey parameters, namely the photometric depth and the size of the field. All these aspects are discussed in this section. Table 1 provides the list of parameters used in these simulations, together with the range of values explored.

2.1.1. Source Properties

These simulations are focused on the detection of sources in the redshift range $6 < z < 12$, a relevant domain for spectroscopic follow-up with near-infrared instruments. The lower limit of this redshift domain overlaps with current photometric surveys measuring the LF at $z \sim 6 - 7$ (e.g. Bouwens et al. 2007). However, the LF is still largely unconstrained beyond $z \geq 7$ because of the lack of spectroscopic confirmation of photometric samples and the relatively small size of the surveyed volumes.

The abundance of background sources at these redshifts is given by the luminosity function $\phi(L)$, with L the rest-frame UV luminosity at 1500 \AA . $\phi(L)$ is the most basic description of the galaxy population from an observer point of view. We adopt a parametrization based on the analytical Schechter function (Schechter 1976):

$$\phi(L) dL = \phi^* \left(\frac{L}{L^*}\right)^{-\alpha} \exp\left(-\frac{L}{L^*}\right) d\left(\frac{L}{L^*}\right) \quad (1)$$

The slope at faint luminosities α , the characteristic luminosity L^* and the normalization factor Φ^* have been constrained by several photometric surveys targeting Lyman Break Galaxies (LBG) at high redshift ($z \geq 4$) (Ouchi et al. 2004, Beckwith et al. 2006, Bouwens et al. 2007, Bouwens et al. 2008, McLure et al. 2009, Henry et al. 2009). Three different representative cases are being discussed in our simulations, basically exploring our present knowledge (or lack of knowledge) of the overall shape of the LF at $z \geq 6$ (Table 1):

- An “optimistic” scenario where LBGs show no-evolution from $z \sim 6$, with the LF parameters as determined by Beckwith et al. (2006). Indeed, the LF at $z \sim 6$ found by these authors display the same shape as for $z \sim 3$ (Steidel et al. 1999), but a 3 times smaller normalization factor (but see, e.g., McLure et al. 2009).
- A constant LF based on robust measurements by Bouwens et al. (2007) at $z \sim 6$ in the Hubble UDF, but using the more recent fit parameters from Bouwens et al. (2008). As compared to model (a), this LF exhibits a turnover towards the bright end.
- The evolutionary LF recently proposed by Bouwens et al. (2008), which includes an important dimming of L^* with increasing redshift. This LF represents the “pessimistic” case with respect to the case (a), with very few high-luminosity galaxies.

The size of the sources is a relevant parameter in this study, given the finite resolution of instruments, and the fact that grav-

¹ <http://www.ucm.es/info/emir/>

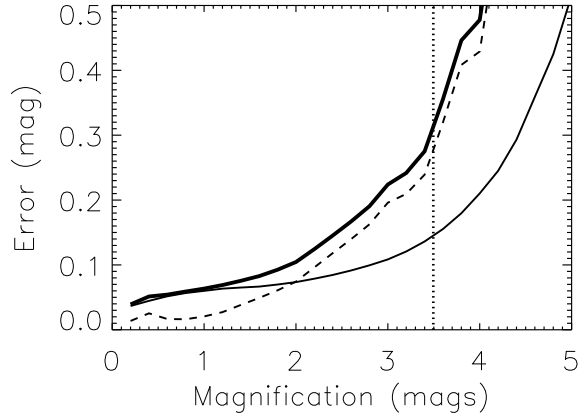


Fig. 2. Typical error in the magnification factor μ , as a function of the magnification for Abell 1835. The solid curve gives the statistical error derived from the MCMC model, while the dashed curve gives the systematic error between two choices of parametrization (see text for details). The thick solid curve is the quadratic sum of both errors, used later in the calculation. The vertical line represents the conservative upper limit of $\mu=25$.

itional magnification preserves surface brightness. High redshift galaxies are expected to be very small at $z > 7$, typically $\lesssim 0.1''$ on the sky (*e.g.* Barkana & Loeb 2000). Recent observations of photometric candidates support this idea (Bouwens et al. 2008, Oesch et al. 2009). This means that a large fraction of lensed sources should remain spatially unresolved in ground-based surveys, even with a strong gravitational magnification (hereafter μ) of ~ 10 . The high resolution capability of JWST is clearly needed for resolving such faint galaxies. In the present simulations and for detection purposes, we consider all sources at $z > 6$ as spatially unresolved. However, galaxy morphology and image sampling are important when discussing the efficiency of surveys based on space facilities, as discussed in Sect. 4.2.

2.1.2. Lensing effects

The present simulations address the effect of lensing by a foreground galaxy cluster. Several well-studied examples of lensing clusters are used in order to evaluate the influence of different mass distributions on the final results. Reference lensing clusters usually display several multiply-imaged systems with redshift measurements, allowing us to model their lensing properties accurately. Lensing clusters considered in these simulations have been previously used as gravitational telescopes to search for high redshift dropouts and LAEs. We take advantage of this situation to perform a direct comparison between our estimates and available observations. Finally, we selected clusters with different redshifts, total mass distributions and morphologies, because all of these factors are susceptible to affect the way they magnify background galaxies.

We selected three clusters satisfying the previous criteria: Abell 1689, Abell 1835 and AC114. Abell 1689 is one of the most spectacular gravitational telescopes, having the largest Einstein radius observed to date ($45''$). Both optical dropouts (Bradley et al. 2008) and Lyman- α emitters (Stark et al. 2007) candidates have been reported in the background of this cluster. Abell 1835 and AC114 are both massive, X-ray luminous

clusters, previously used in our deep near-infrared survey for high redshift dropouts with VLT/ISAAC (Richard et al. 2006). Finally, these three clusters constitute the sample used by the ZEN2 survey for LAEs in narrow-band images (Willis et al. 2008).

We used the most recent mass models available for the reference clusters to derive the magnification maps (see Table 1) although simulation results are found to be weakly sensitive to modeling details. Each lensing cluster has been modeled in a similar way using the public lensing software Lenstool², including the new MCMC optimization method (Jullo et al. 2007) providing bayesian estimates on each parameter derived from the model.

The structure of mass models is given by a sum of individual dark matter subcomponents of two different types: large scale components, reproducing the cluster-scale behavior of dark matter, and small scale potentials centered on each cluster galaxy, reproducing the effect of substructure. Each lensing potential is parametrized by a Pseudo-Isothermal Elliptical Mass Distribution model (PIEMD, Kassiola & Kovner 1993), with a projected mass density Σ given by:

$$\Sigma(x, y) = \frac{\sigma_0^2}{2G} \frac{r_{cut}}{r_{cut} - r_{core}} \left[\frac{1}{(r_{core}^2 + \rho^2)^{1/2}} - \frac{1}{(r_{cut}^2 + \rho^2)^{1/2}} \right], \quad (2)$$

where $\rho^2 = [(x - x_c)/(1 + \epsilon)]^2 + [(y - y_c)/(1 - \epsilon)]^2$, (x_c, y_c) stands for the central position with respect to the BCG (cD or central Bright Cluster Galaxy), $\epsilon = (a - b)/(a + b)$ is the ellipticity, σ_0 is the central velocity dispersion and (r_{core}, r_{cut}) are two characteristic radii. For each lensing potential, the position of x and y axis is given by the position angle θ . The total mass of this profile is proportional to $r_{cut} \sigma_0^2$. The PIEMD parametrization, easily linked to the observed geometry of elliptical lensing galaxies, has been widely used to model the strong lensing properties of massive clusters (Smith et al. 2005; Richard et al. 2007; Limousin et al. 2007).

A good approximation of the angular distance of the critical line, corresponding to maximum magnification in a flat universe, is given by the Einstein radius θ_E :

$$\theta_E = \frac{4\pi \sigma_0^2}{c^2} \frac{D_A(z_s) - D_A(z_c)}{D_A(z_s)} \quad (3)$$

where $D_A(z)$ stands for the angular distance at redshift z . Source and cluster redshifts are, respectively, z_s and z_c .

The value of θ_E provides a fair estimate of the extension of the strongly magnified area ($\mu > 10$) in the image plane. This value quantifies the power of a gravitational telescope to magnify background sources. Equation 3 shows that, for a given source redshift z_s , θ_E depends on σ_0^2 and on the cluster redshift z_c .

For the three clusters mentioned before, there is a significant variation in redshift ($z_{c0} \sim 0.17 - 0.3$) and in σ_0 (taken from the mass models and reported in Table 1), Abell 1689 being $\sim 30\%$ more massive and less distant than AC114, for instance. We explored a wider range of cluster redshifts in our simulations, producing fiducial lensing clusters by adjusting z_c between 0.1 and 0.8 in the three cases, assuming no evolution in the cluster properties. This is clearly an over-simplistic and conservative assumption, as massive clusters of galaxies undergo a dynamical evolution during cluster assembly at high redshift.

² <http://www.oamp.fr/cosmology/lenstool>

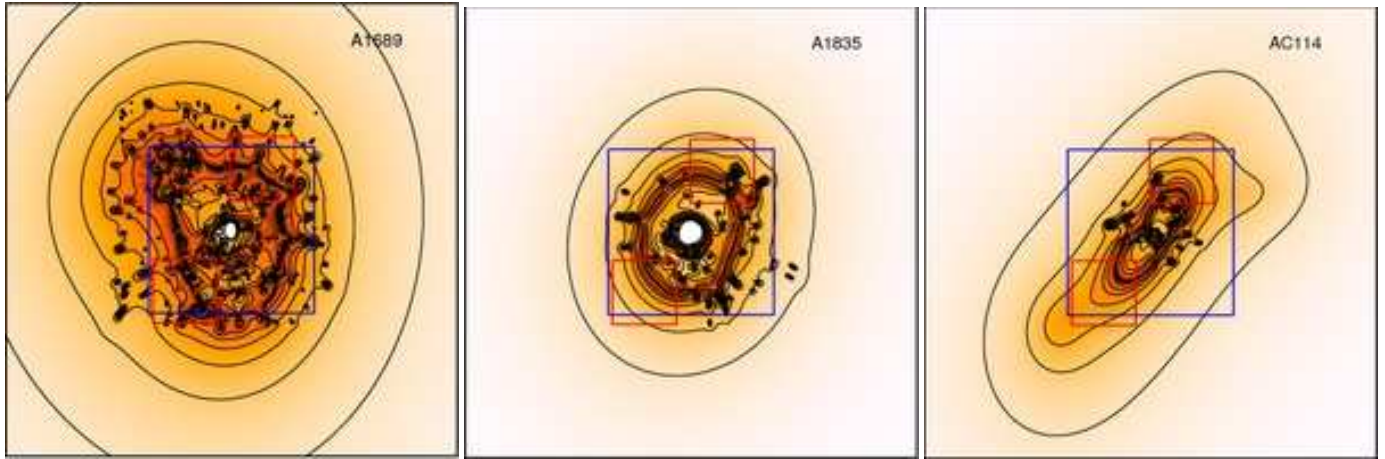


Fig. 1. Magnification maps for the three clusters at $z_s = 8$ used in this study (from left to right A1689, A1835 and AC114 respectively). The global size of the image corresponds to the $6' \times 6'$ FOV whereas the blue and red squares correspond respectively to $2.2' \times 2.2'$ and $0.85' \times 0.85'$ FOV (see Sect. 2.1.3). Black contours represent different magnification regimes with increasing magnification values from 0.5 to 3 mags towards the cluster center.

The relevance of the MCMC approach of the cluster mass modeling is to derive relevant statistical errors in the magnification factors. Fig. 2 illustrates the typical errors in the magnification at a given position of the lensing field, in the case of the lensing cluster Abell 1835. Similar errors in the magnification are found in the case of the two other clusters, as all of them have ≥ 5 multiple systems constraining independent regions of the cluster cores, the majority of them having spectroscopic redshifts. For reasonable magnification factors (≤ 3 magnitudes), this error is always smaller than 0.1 magnitudes (or $\sim 10\%$ relative error in flux). For larger magnifications factors, corresponding to the vicinity ($\leq 2''$) of the critical lines, the error can reach much higher values. The *systematic errors* in the magnification factors, due to the choice of the parametrization when building the lensing model, can be estimated for Abell 1835, which have been modelled by Richard et al. (2009, submitted) using both PIEMD profiles and Navarro-Frenk-White (NFW, Navarro et al. 1997) profiles for the cluster-scale mass distributions. The comparison of magnifications from both models, at a given position, gives an estimate of the systematic error in the magnification, which dominate at large μ (Figure 2), reaching typical values of 0.3 magnitudes. We adopted a conservative upper limit of $\mu = 25$ to avoid singularities in the magnification determination. This is justified by the finite resolution of instruments, and the limited knowledge on the precise location of the critical lines at such high z (typically $\sim 1''$). The affected area is not significant once averaged over the entire field of view. Nevertheless, the quadratic sum of the statistical and systematic errors in the magnification is later used to derive errors in the number density calculations when looking at lensing fields.

2.1.3. Survey Simulations

In addition to cluster and source properties, the main ingredients to consider in the simulations are the following:

- The typical field of view (FOV) of near-IR instruments for 8-10 meters class telescopes and space facilities. The former typically range between a few and $10'$ on a side (e.g. $\sim 6' \times 6'$ for EMIR/GTC, $\sim 7' \times 7'$ for Hawk-I/VLT). The later are usually smaller (e.g. $\sim 1' \times 1'$ for NICMOS/HST, $\sim 2.2' \times 2.2'$ for JWST or WFC3-IR/HST). Fig. 1 presents the compari-

son between these typical FOV values and the magnification regimes found in lensing clusters. The references for the different instruments used in the simulations are presented in Table 1.

- The limiting magnitudes of present near-IR surveys based on ground-based and space observations tailored to select LBGs at $z \geq 6$. The former are typically limited to $AB \sim 25.5$ (see Sect. 2.1.1), whereas the later could reach as deep as $AB \sim 29$ with JWST (see Sect. 3.5 and 4).

The shallow magnitude limit of $AB \sim 25.5$ achieved on ground-based observations should allow us to detect galaxies with a UV continuum corresponding to a $SFR \sim 40/\mu M_\odot/yr$ at $z \sim 10$, whereas the typical depth for JWST should be $\sim 1/\mu M_\odot/yr$.

We can relate the UV luminosities of high redshift galaxies with the expected Lyman- α emission line by converting L into a star formation rate SFR using the calibrations from Kennicutt (1998):

$$SFR(M_\odot \text{ yr}^{-1}) = 1.4 \cdot 10^{-28} L (\text{ergs Hz}^{-1} \text{ s}^{-1}) \quad (4)$$

The expected Lyman- α luminosity produced at the equilibrium can be written as:

$$L_{Ly_\alpha} (\text{ergs s}^{-1}) = (1 - f_{esc}) f_\alpha SFR(M_\odot \text{ yr}^{-1}) \quad (5)$$

where f_{esc} is the escape fraction of Lyman- α photons and f_α the Lyman- α production rate per unit of star formation. Assuming no reddening, the typical values for f_α range between $2.44 \cdot 10^{42}$ and $6.80 \cdot 10^{42} \text{ ergs.s}^{-1}$ (Schaerer 2002). We use these scaling relations when discussing the detectability of Lyman- α in lensing fields.

2.2. Implementation

We explicitly compute the expected number counts $N(z, m_0)$ of sources at the redshift z brighter than a limiting magnitude m_0 by a pixel-to-pixel integration of the (magnified) source plane as a function of redshift, using the sources and lensing cluster models described in the previous subsections. Number counts are integrated hereafter within a redshift slice $\Delta z = 1$ around z , unless otherwise indicated. With respect to a blank field, the

Parameter	Explored range				Reference
LF (a)	(< z >= 6.0)	$\alpha = 1.6,$	$\phi^* = 0.4 \cdot 10^{-3} \text{ Mpc}^{-3},$	$M^* = -21.07$	Beckwith et al. (2006)
LF (b)	(< z >= 5.9)	$\alpha = 1.74,$	$\phi^* = 1.1 \cdot 10^{-3} \text{ Mpc}^{-3},$	$M^* = -20.24$	Bouwens et al. (2008)
LF (c)	(3.8 < z < 7.4)	$\alpha = 1.74,$	$\phi^* = 1.1 \cdot 10^{-3} \text{ Mpc}^{-3},$	$M^* = -21.02 + 0.36 (z - 3.8)$	Bouwens et al. (2008)
Source redshift	$z_s = 6 - 12$				
Lensing cluster	Abell 1689	$z_{c0} = 0.178,$	$\sigma_0 = 1320 \text{ km/s},$	$N_{\text{sub}} = 266$	Limousin et al. (2007)
	Abell 1835	$z_{c0} = 0.25,$	$\sigma_0 = 1210 \text{ km/s},$	$N_{\text{sub}} = 90$	Smith(2005) Richard(2009)
	AC114	$z_{c0} = 0.31,$	$\sigma_0 = 1080 \text{ km/s},$	$N_{\text{sub}} = 28$	Natarajan et al. (1998)
Cluster redshift z_c	0.1 – 0.8				
Survey strategy	GTC/EMIR	FOV=6' × 6',	pix: 0.2''/pixel,	depth: $\Delta z = 1$	Garzón et al. (2007)
	JWST/NIRCam	FOV=2.2' × 2.2',	pix: 0.06''/pixel,	depth: $\Delta z = 1$	Rieke et al. (2005)
	HST/NICMOS	FOV=0.85' × 0.85',	pix: 0.2''/pixel,	depth: $\Delta z = 1$	Thompson (1998)

Table 1. Summary of the parameters included in our simulations. For each entry, we give the range of values explored and reference to the relevant publication. LF(a) is the same as in Steidel et al. (1999), but Φ^* is a factor of 3 smaller (see Sect. 2.1.1).

magnification pushes the limit of integration to fainter magnitudes, whereas the dilution effect reduces the effective volume by the same factor.

An important effect to take into account in cluster fields is light contamination coming from the large number of bright cluster galaxies, which reduces the surface area reaching the maximum depth, and consequently prevents the detection of faint objects, especially in the vicinity of the cluster center. This contamination effect can be as high as 20% of the total surface (Richard et al. 2006), whereas it is almost negligible in blank field surveys.

We created bright-objects masks by measuring the central position (x_c, y_c) and shape parameters (a, b, θ) of galaxies in the three cluster fields, each object being approximated by an ellipse during this process. We used SExtractor (Bertin & Arnouts 1996) in combination with reasonably deep and wide ground-based images available from the ESO archive (larger than 6' × 6' used in these simulations). The characteristics of these images are summarized in Table 2. They were reduced using standard IRAF routines. The image mask $M(x, y)$ produced is the superposition of ellipses for all objects in the photometric catalog where pixels belonging to object domains were flagged. Ellipses correspond to $1 - \sigma$ isophotes over the background sky. In other words, only images lying on empty regions have been included in the lensed samples, thus providing a lower limit for detections in lensing fields. This fractional area covered by foreground galaxies ranges between 6% and 12% depending on the cluster as well as the size and central position of the field of view (Table 2). The largest hidden area corresponds to the smaller field of view centered on the cluster (JWST-like). NICMOS pointings are even smaller, but they are centered on the critical lines in our study and avoid the crowded central regions of the cluster. In blank fields, this value doesn't exceed 3-4%. In the next sections, we have taken into account this correction in the calculations of number counts, both in blank fields and lensing fields.

Including the object mask $M(x, y)$, number counts $N(z, m_0)$ are given by the following expression:

$$N(z, m_0) = \phi^* \int_{x,y} M(x, y) \int_{L(\mu, z, m_0)}^{\infty} \frac{C_V(x, y, z)}{\mu(x, y, z)} \left(\frac{L(\mu, z, m_0)}{L^*} \right)^\alpha \cdot \exp\left(-\frac{L(\mu, z, m_0)}{L^*}\right) d\left(\frac{L}{L^*}\right) dx dy \quad (6)$$

where $\mu(x, y, z)$ is the magnification induced by the lensing field, $C_V(x, y, z)$ is the covolume associated with a single spatial

resolution element pixel with $\Delta z = 1$ and (L^*, ϕ^*, α) are the parameters of the LF.

A conservative upper limit of $\mu = 25$ was adopted in the vicinity of the critical lines in order to avoid singularities in the magnification/dilution determination. This is justified by the finite resolution of instruments, and the limited knowledge on the precise location of the critical lines at such high- z (typically $\sim 1''$).

When exploring the impact of cluster redshift, we assumed no evolution in the physical parameters r_{core} , r_{cut} and σ of individual potentials, thus keeping the total mass of the cluster constant in this process. Variations in z_c from the original redshift z_{c0} of the cluster produce a geometrical effect on the central positions (x_{ci}, y_{ci}) of each PIEMD potential i , measured from a reference position (x_0, y_0) which coincides with the center of the BCG:

$$\begin{aligned} x_{ci}(z_c) - x_0 &= \frac{D_A(z_c)}{D_A(z_{c0})} (x_{ci}(z_{c0}) - x_0) \\ y_{ci}(z_c) - y_0 &= \frac{D_A(z_c)}{D_A(z_{c0})} (y_{ci}(z_{c0}) - y_0) \end{aligned} \quad (7)$$

Similarly, we produced fiducial masks at different cluster redshifts z_c based on the reference mask at z_{c0} and adjusting the parameters of the galaxy ellipses, applying the same scaling relations on (x_c, y_c) . The sizes a and b were scaled by $D_A(z_{c0})/D_A(z_c)$.

3. Results

As discussed above, lensing introduces two opposite trends on the observed sample as compared to blank fields : gravitational magnification by a factor μ , increasing the expected number of sources and thus the total number of objects, and reduction of the effective surface by the same factor thus leading to a dilution in expected counts. This effect was first studied by Broadhurst et al. (1995).

If we consider, for a given redshift z , the cumulative abundance of sources (per unit of solid angle) with a luminosity greater than L and by redshift bin, the magnification bias will change depending on μ according to

$$n'_{\text{lensing}}(> L, z) = N(> L/\mu, z)/\mu(z) \quad (8)$$

$$\simeq \mu^{\beta(z)-1} n(> L, z) \quad (9)$$

where β is the logarithmic slope of $n(L, z)$ assuming that this function is well represented by a power law in this interval of

Cluster	Instrument and Reference	Filter	Exposure Time	Depth (5σ , AB)	Mask area $6' \times 6'$,	$2.2' \times 2.2'$,	$0.85' \times 0.85'$
Abell 1689	ISAAC/VLT Moorwood (1997)	SZ	14.4 ksec	26.0	7%	12%	10%
Abell 1835	FORS/VLT Appenzeller et al. (1998)	V	19.6 ksec	27.0	6%	10%	8%
AC114	SOFI/NTT Moorwood et al. (1998)	K	10.8 ksec	22.0	6%	9%	7%

Table 2. Characteristics of the images used to produce the foreground object’s mask for each cluster field, the three last columns representing the fractional surface area covered by the foreground galaxies in each cluster, for the three reference field of view, EMIR-like, JWST-like and NICMOS-like respectively

luminosities : $\beta = -d(\ln n)/d(\ln L)$. The effect on number counts is as follows:

- if $\beta(z) > 1$ the number counts will increase with respect to a blank field, and
- if $\beta(z) < 1$ there will be an opposite trend: i.e. a depletion in number counts

With increasing depth, the β parameter will decrease in a greater or lesser amount depending on the LF, the FOV (because it determines the mean μ) and the redshift of sources, leading to a depletion in number counts in lensing fields as compared to a blank fields. With these simple considerations, we expect lensing clusters to be more efficient than blank fields in relatively shallow surveys.

The efficiency of using lensing clusters as gravitational telescopes to find high- z galaxies can be quantified with simple assumptions taking advantage of the properties of the sources explained in Sect. 2. In this section, we discuss the results obtained by exploring the relevant intervals in the parameter space. We present a comparison between the number counts expected in lensing and blank fields, as a function of source redshift and for different LFs. The influence of lensing cluster properties and redshift is also studied, as well as the expected field to field variance.

3.1. The influence of the field of view

Here we discuss on the influence of the FOV in the simulations for typical surveys. The influence of the limiting magnitude will be discussed in Sect. 4. Three different FOV are considered here:

- $6' \times 6'$ (“EMIR-like” aperture)
- $2.2' \times 2.2'$ (“JWST-like” or “WFC3/HST” aperture)
- $0.85' \times 0.85'$ (NICMOS/HST aperture)

In the last case, the FOV is centered along the critical lines in order to achieve the highest mean magnification (Fig. 1).

The limiting magnitude is $AB \lesssim 25.5$, a value ranging between $L_*(z=6)$ and $3L_* - 5L_*$ at redshift $z_s \sim 7$ to 10. The cluster model corresponds to AC114, but the results are qualitatively the same with other models. Fig. 3 displays the relative gain in number counts between lensing and blank fields as a function of sources redshift, for the three values of the FOV mentioned above, and for the three LF adopted in the present simulations.

The largest gain is obtained for the smallest FOV, as expected from geometrical considerations, because the mean magnification decreases with increasing FOV, and in this case $\beta \gtrsim 1$ given the shallow depth ($AB \lesssim 25.5$). For a given FOV, the difference between lensing and blank field results strongly depends on the shape of the LF. Hence, the comparison between lensing and blank field number counts is likely to yield strong constraints on the LF, provided that field-to-field variance is small enough. This issue is addressed in Sect. 3.5. In the following subsections, we adopt a $6' \times 6'$ FOV unless otherwise indicated.

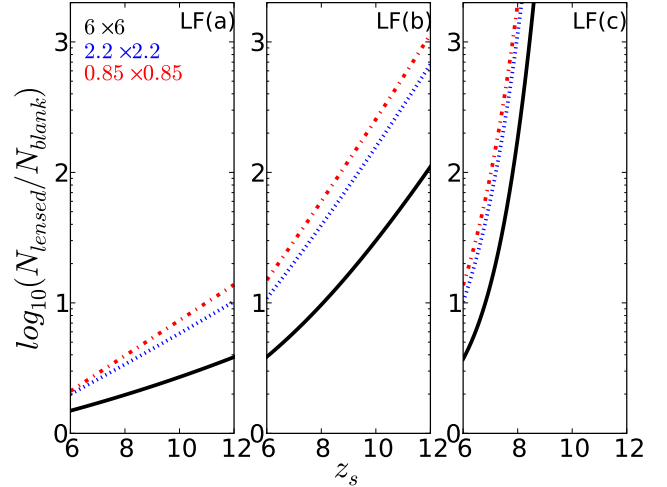


Fig. 3. Relative gain in number counts between lensing and blank fields as a function of the source redshift, with $\Delta z = 1$, for different fields of view: $6' \times 6'$ in black, $2.2' \times 2.2'$ in blue dotted line and $0.85' \times 0.85'$ in red dot-dashed line (from bottom to top). The three panels from left to right represent the 3 values of the LF, (a), (b) and (c) respectively.

3.2. Lensing versus Blank field efficiency

In this section, we study the effects of lensing clusters on source counts, using lensing models for the three reference clusters. We compute the expected number of sources brighter than m_0 , the typical apparent magnitude reached in ground-based near-IR surveys. The comparison between expected number counts of galaxies in a typical $6' \times 6'$ FOV, up to $m_0 \leq 25.5$, per redshift bin $\Delta z = 1$, in a blank field and in the field of a strong lensing cluster are presented in Fig. 4 in logarithmic scale.

We also estimate the error on number counts due to the uncertainties on magnification factors (Sect. 2.1.2). The choice of the LF has no influence on the following results. Field to field variance dominate the error budget whatever the regime. Statistical errors and systematic errors on lensing models are smaller but not negligible as their contribution is less sensitive than field to field variance to the number of objects. In particular, when the number of detected sources is relatively high (i.e. when field to field variance is relatively small), they reach $\sim 15\%$ of the error budget in the worst cases (e.g. for LF(a) at $z \sim 6$ in a $6' \times 6'$ FOV), and typically $\leq 2\%$ when the number of sources is relatively small (e.g. for LF(c) at $z \sim 8$, for any FOV).

As shown in Fig. 4, the presence of a strong lensing cluster has a dramatic effect on the observed number of sources, with a positive magnification effect. Strong lensing fields are a factor between 2 and 10 more efficient than blank fields for the most optimistic LF (a), the gain increasing for the LFs (b) and (c), reaching a factor between 10 and 100 in the $z \sim 6 - 12$ domain.

A positive magnification bias is observed, increasing with the redshift of the sources, and also increasing from optimistic to pessimistic values of the LF. This trend is indeed expected given the steep shape of the LF around the typical luminosity limits achieved in ground-based “shallow” surveys.

Quantitatively (cf Table 3 and Fig. 4), if the LF for LBGs was nearly constant between $z \sim 4$ and 12, we could always detect at least one object over the redshift range of interest. At $z \sim 6$, we expect up to between 7-10 sources, and at $z \sim 12$ between 0.7 and 1 galaxies should be detected in a lensing field. Even in a blank field, until $z \sim 8-9$ at least one LBG could be found in such a large field of view. With more realistic (pessimistic) values of the LF (e.g. Bouwens et al. 2006, 2008), blank fields are particularly inefficient as compared to lensing fields. The size of the surveyed area would need to increase by at least a factor of ~ 10 in order to reach a number of detections similar to the one achieved in a lensing field around $z \sim 6-8$, and this factor increases with redshift. Note however that given a limiting (apparent) magnitude, blank and lensing fields do not explore the same intrinsic luminosities (see also Sect.4).

As seen in Fig. 4 and Table 3, there are also some differences between the results found in the three lensing clusters, although they are smaller than the differences between lensing and blank fields for a given LF. The number of expected sources behind A1689 is a factor of two (at $z \sim 6$) and a factor of three ($z \sim 8$) larger than in the other clusters for the realistic LFs (b) and (c), whereas the difference is only $\sim 10-30\%$ for LF (a). The influence of lensing properties is studied in Sect. 3.4.

From the results above, it seems that lensing fields allow us to detect a larger number of $z \geq 6$ sources based on their UV continuum, with some cluster to cluster differences. This result is essentially due to the shape of the LF. For magnitude limited samples selected within a given field of view, the positive magnification bias increases with the redshift of the sources and decreases with both the depth of the survey and the size of the surveyed area. The last trend is purely geometric, as discussed in the previous section. The differential behaviour between blank and lensing regimes strongly depends on the shape of the LF. The comparison between blank and lensing field observations could be of potential interest in constraining the LF, provided that field-to-field variance is sufficiently small. This issue is addressed in the following sections.

3.3. Redshift of the lensing cluster

The redshift of the lensing cluster is a potentially important parameter when defining an “ideal” sample of gravitational telescopes. Based on geometrical considerations, we expect the magnification bias to decrease with cluster redshift (z_c) after reaching a maximum efficiency at some point, depending on cluster properties and the size of the surveyed field. The field of view considered here is typically a few square arcminutes, essentially including the region around the critical lines where magnification factors are the highest. Further down, we study the impact of z_c on the magnification bias.

Using the non-evolution assumption presented in Sect. 2.2, we compute the expected number counts for the three reference models (A1689, A1835 and AC114) with cluster redshifts ranging between $z=0.1$ and 0.8, with a $\Delta z = 0.1$ step. A step $\Delta z = 0.05$ is used in the $z=0.1-0.3$ interval, in order to refine the sampling around the maximum value. We use the same depth and field size as in previous section. The effect of cluster redshift is clearly seen in Fig. 6 representing the number of objects

as a function of cluster redshift (for the three reference models), at a fixed redshift of $z=8$ for sources.

The global effect of z_c on number counts as a function of the source redshift is displayed in Fig. 5. This figure directly compares to Fig. 4 in the previous section. Table 4 presents the z_c value which corresponds to a maximum in the expected number counts at $z=8$. This value depends slightly on the source redshift and LF. In addition to the $\Delta z_c = + - 0.05$ when changing the LF, there is also an increase of z_c with higher values of z_s , up to $+0.05$ towards $z_s = 12$. The search efficiency of distant galaxies in lensing fields is maximised when using clusters at low redshift ($z_c \sim 0.1-0.3$). Although the field of view considered here is relatively large for near-IR surveys and close to present-day cameras, it is the limiting factor at $z_c \leq 0.1$, where an increasing fraction of the strong-magnification area is lost with decreasing z_c . Also, in this z_c regime, the field of view concentrates on the central region of the cluster where bright cluster galaxies mask an important fraction of the strong-magnification area. The high magnification region represents an increasingly small percentage of the field with increasing z_c . Number counts in this regime asymptotically tend towards a limiting value with increasing z_c (Fig. 5), which still is a substantial gain with respect to a blank field of the same size. The non-evolution assumption in cluster properties has a weak effect on this conclusion. Indeed, clusters far from relaxation will be even more ineffective as a gravitational lenses in the strongest magnification regime. The results obtained are hence an optimistic upper limit on number counts for realistic clusters beyond the optimal regime $z_c \sim 0.1-0.3$.

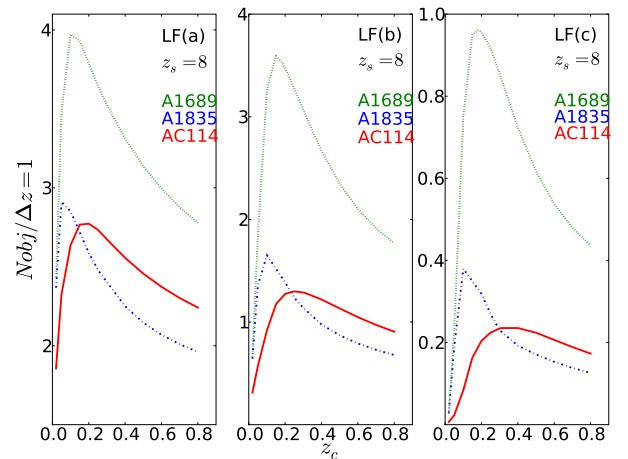


Fig. 6. Expected number of objects as a function of the cluster redshift for a fixed redshift of sources ($z_s = 8$) and with the same depth and field size as in previous section. Three cluster models are displayed: A1689 (green dotted line), A1835 (blue dot-dashed line) and AC114 (red solid line). Panels from left to right display respectively LF (a), (b) and (c).

3.4. Influence of lensing cluster properties

In this section we focus on the differences between lensing cluster properties and their influence on expected source counts. As seen in previous sections, A1689-like clusters are expected to be more efficient irrespective of the cluster redshift. To understand this effect, we study the magnification regimes for a reference

Table 3. Total number of objects expected within a $6' \times 6'$ FOV (up to $H_{AB} \leq 25.5$, $\Delta z = 1$) from the three LF adopted in these simulations. Uncertainties correspond to $1 - \sigma$ level in magnification and lensing modeling.

	Blank field			Lensed field								
	6	7	8	A1689 $z_c = 0.184$			A1835 $z_c = 0.253$			AC114 $z_c = 0.310$		
z	6	7	8	6	7	8	6	7	8	6	7	8
LF (a)	4.61	2.43	1.31	$8.63^{+0.86}_{-0.76}$	$5.66^{+0.62}_{-0.59}$	$3.83^{+0.47}_{-0.44}$	$6.69^{+0.61}_{-0.58}$	$4.00^{+0.42}_{-0.39}$	$2.48^{+0.29}_{-0.27}$	$7.07^{+0.65}_{-0.61}$	$4.27^{+0.44}_{-0.41}$	$2.66^{+0.31}_{-0.29}$
LF (b)	1.30	0.39	0.13	$10.07^{+1.808}_{-1.608}$	$5.66^{+1.24}_{-1.08}$	$3.53^{+0.89}_{-0.75}$	$4.69^{+0.78}_{-0.69}$	$2.21^{+0.47}_{-0.41}$	$1.23^{+0.30}_{-0.25}$	$4.96^{+0.80}_{-0.71}$	$2.35^{+0.47}_{-0.41}$	$1.28^{+0.30}_{-0.25}$
LF (c)	1.30	0.07	< 0.01	$10.07^{+1.808}_{-1.608}$	$3.08^{+0.84}_{-0.71}$	$0.96^{+0.38}_{-0.29}$	$4.69^{+0.78}_{-0.69}$	$1.04^{+0.27}_{-0.23}$	$0.28^{+0.10}_{-0.08}$	$4.96^{+0.80}_{-0.71}$	$1.03^{+0.26}_{-0.22}$	$0.24^{+0.09}_{-0.07}$

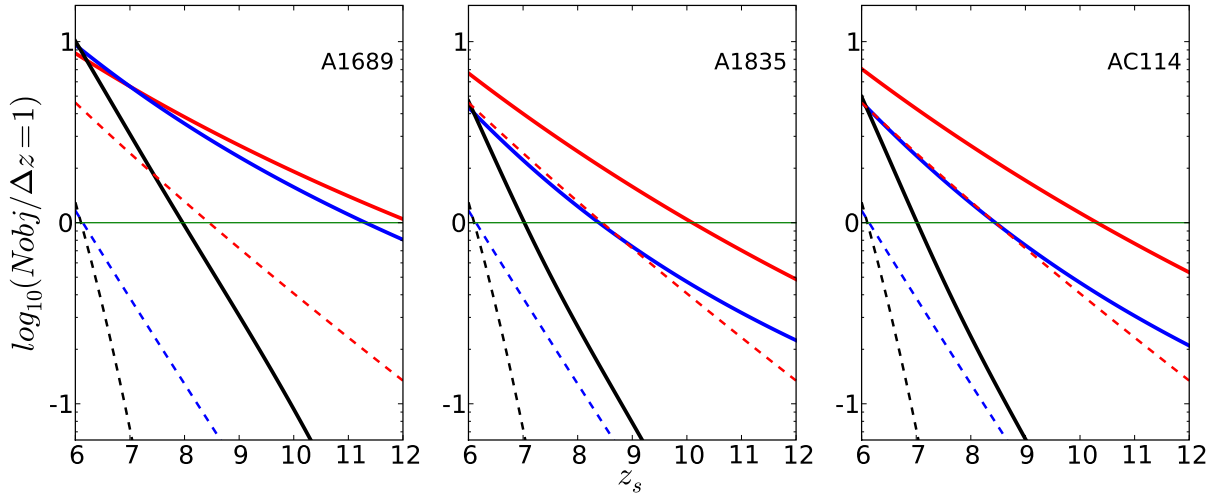


Fig. 4. Comparison between the expected number counts of galaxies in a typical $6' \times 6'$ FOV, up to $H_{AB} \leq 25.5$, per redshift bin $\Delta z = 1$, in a blank field (dashed lines) and in the field of lensing cluster (solid lines) (left to right respectively A1689, A1835 and AC114). Expected counts are obtained by the integration of 3 different luminosity functions (a), (b) and (c) from top to bottom. The limit of one source detected in the field of view is indicated by an horizontal line to guide the eye.

Table 4. Redshift of the cluster which maximizes the number of objects detected at $z=8$ for the three LF respectively from top to bottom (a), (b) and (c)

LF	A1689	A1835	AC114
actual z_c	0.184	0.253	0.310
(a)	0.10	0.05	0.25
(b)	0.15	0.10	0.25
(c)	0.20	0.10	0.30

source plane fixed at $z_s = 8$. The distribution of the magnification regimes in the image plane varies from cluster to cluster. Histograms in Fig. 7 represent the percentage of the image plane (for the $6' \times 6'$ FOV) as a function of the associated magnification. To perform this calculation, cluster redshifts were standardized to identical values for a better understanding of the phenomenon. As seen in the figure, A1689 shows a different regime at $z_c \lesssim 0.8$ as compared to the other clusters. While the percentage of the surface affected by strong magnification ($\mu > 10$) does not exceed 5% in A1835 and AC114, it is as high as 8 – 10% in A1689, depending on z_c . Nevertheless, this difference between clusters tends to fade with increasing cluster redshift due to projection effects, the fraction of highly magnified pixels becoming smaller with respect to the whole FOV. We also note that AC114 and A1835 models have a similar behaviour with minor differ-

ences (A1835-like clusters being more effective at very low z_c while the AC114 model is more efficient for intermediate z_c).

Another way of understanding this phenomenon is presented in the Fig. 8, where the effective covolume for the $6' \times 6'$ FOV is traced as a function of the effective magnitude, for a magnitude-limited survey with $AB \leq 25.5$. Magnification in lensing fields provides an enhanced depth for a magnitude-limited survey, where the effective (lensing corrected) covolume surveyed decreases with increasing effective depth. The behavior of A1689 in Fig. 8 illustrates the situation for this particularly efficient cluster, allowing us to study a $\sim 100 Mpc^3$ volume to $AB \sim 29.0$ with a relatively modest observational investment. Except for some particularly efficient lensing clusters (such as A1689), most lensing fields should behave the same way as A1835 or AC114.

3.5. Field to field variance

In this section, we address the expected field-to-field variance affecting our previous results in order to estimate its impact in blank and lensed fields. We used two different approaches: the two-point correlation function estimation proposed by Trenti & Stiavelli (2008) and a pencil beam tracer through the Millenium simulation.

The first estimate is based on the method implemented by Trenti & Stiavelli (2008). This method for the calculation of the

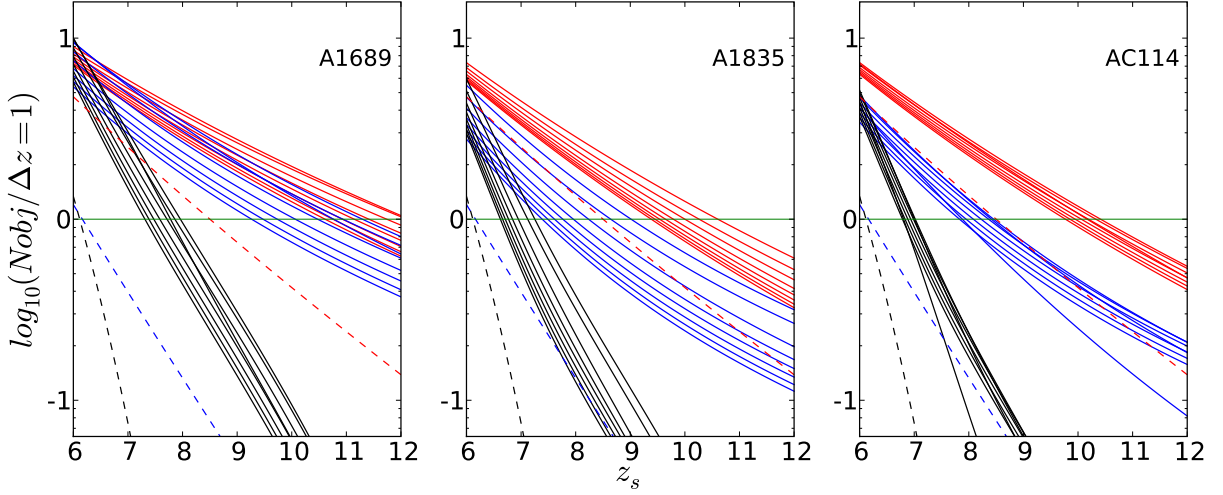


Fig. 5. The same as Fig. 4 but using different assumptions for the redshift of the clusters, with $z_c \in [0.1, 0.8]$ and a 0.1 step (for more details see Sect. 3.3)

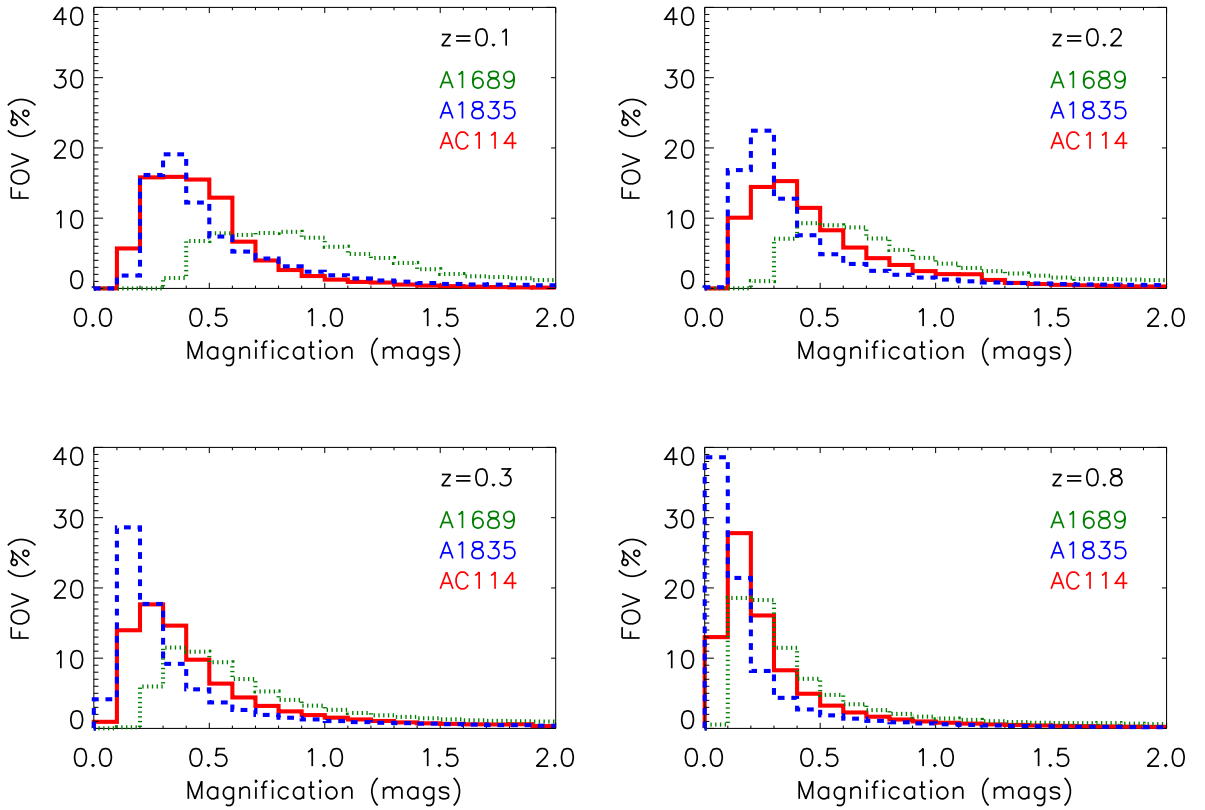


Fig. 7. Histogram representing the percentage of the surface ($6' \times 6'$ FOV) as a function of the magnification for different redshifts of cluster ($z_c=0.1, 0.2, 0.3, 0.8$), using the same color codes for the three clusters as in Fig. 6 (A1689: green dotted line, A1835: blue dot-dashed line and AC114: red solid line)

cosmic variance is based on the two points correlation function $\xi(r)$ of the sample (Peebles 1993). Field o field variance is given by

$$\sigma_v^2 = \frac{\int_V \int_V d^3x_1 d^3x_2 \xi(|x_1 - x_2|)}{\int_V \int_V d^3x_1 d^3x_2} \quad (10)$$

where V represents the volume of the survey.

We focus on the redshift interval $z \sim 6 - 8$ using the present “shallow” survey parameters (see Sect. 4.1), both in blank and lensing fields. Here we use the same parameters as in Sect. 3.2, i.e. typical FOV $6' \times 6'$, $m_{AB} = 25.5$ and $\Delta_z = 1$.

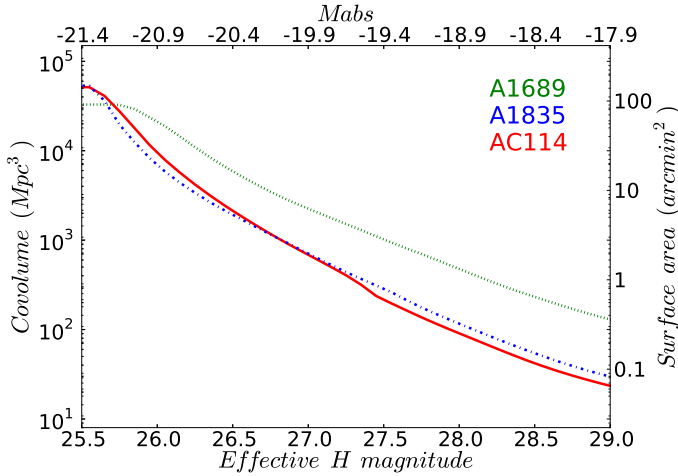


Fig. 8. The effective (lensing corrected) covolume sampled at $z=6.5-7.5$ by each cluster is given as a function of effective H_{AB} magnitude limit, for a magnitude-limited survey of $6' \times 6'$ FOV with $H_{AB} \leq 25.5$. The three clusters are displayed with the same colors and line codes as in Fig. 6.

We define the total fractional error of the counts N following Trenti & Stiavelli (2008) (this is the so-called field-to-field standard deviation or the, again, improperly called “cosmic variance”) as :

$$v_r = \frac{\sqrt{\langle N^2 \rangle - \langle N \rangle^2}}{\langle N \rangle} \quad (11)$$

Results are presented in the Table 5 for the three LF considered, and for the three typical clusters used in the simulations. We note an important field to field variance with such a limiting magnitude ($AB \sim 25.5$) either in blank or lensing fields due to the small number counts previously derived from calculations (see Table 3). Nevertheless, the variance is smaller behind gravitational telescopes with the same differential trends mentioned before between the three clusters, i.e. A1689 exhibits a stronger magnification bias (see Sect. 3.4) than the other clusters which have a similar behavior. Besides, with increasing redshift of sources, the expected number counts decrease leading to a larger field to field variance.

The second estimate was based on the Millennium simulation, carried out by the Virgo Consortium and described in detail in Springel et al. (2005) and Lemson & Virgo Consortium (2006). The simulation follows $N = 2160^3$ particles of mass $8.6 \cdot 10^8 h^{-1} M_\odot$ within a co-moving box of size $500 h^{-1} Mpc$ on a side. The cosmological model is a Λ CDM model with small differences in the cosmological parameters adopted in Sect. 1, but without impact on the final results. These cosmological parameters are consistent with recent determinations from the combined analysis of the 2dFGRS and 3rd year WMAP data (Sanchez & Baugh 2006). Given its high resolution and large volume, the Millennium simulation allows us to follow in enough details the formation history of a representative sample of high redshift galaxy environments. With these prescriptions and a realistic beam tracer we can study the field-to-field variations in the number counts of star forming galaxies at the epoch of interest.

Our pencil beam tracer is similar to the one developed by Kitzbichler & White (2006). We trace through the simulation box a parallelepiped where the base is a parallelogram, whose size is given by the reference field of view in comoving units, and the depth is the comoving depth arbitrarily taken to $\Delta z = 1$.

Table 6. Number counts for $m_{AB} \leq 25.5$ and field to field uncertainties (v_r) calculated from the Millenium simulation in a $6' \times 6'$ blank field, for different source redshifts

	$z_s = 6$	$z_s = 7$	$z_s = 8$
$\langle N \rangle$	2.74	1.10	0.39
v_r	68%	100%	168%

The variation of angular distance versus redshift in the redshift interval of the selection window considered was properly taken into account. This $500h^{-1}Mpc$ edge box is more than 2000 times larger than the effective volume probed by the $6' \times 6'$ FOV : $\sim 10.7 \times 10.7 \times 323.0(Mpc/h)^3$ for instance at $z=6$. We carried out 10000 Monte Carlo realizations of the beam-tracing procedure by randomly varying the initial position of the beam in order to calculate the typical number counts of galaxies and the associated standard deviation in the field of view with the same hypothesis.

Although this procedure is well suited to determine the field to field variance, several studies on this topic suggest an over-prediction on the abundance of massive galaxies at high redshift (e.g. Kitzbichler & White 2007). For this reason, we consider this second approach as a cross check yielding a lower limit for the field to field variance. Results obtained from the Millenium simulation are displayed in Table 6. They are in fair agreement with those obtained with the first method.

Field to field variance on number counts obviously depends on the depth of the survey. In order to compare our results with existing photometric surveys, we calculated the number counts of sources in blank and lensing fields (here AC114) with the evolving LF(c) for different deeper magnitude limits ($m_{lim} = 27.0, 28.0$ and 29.0), in our reference field of view using the same parameters as in Sect. 3.2 (see Table 7). The correlation function was used to derive the cosmic variance. The total fractional error (v_r) strongly decreases with increasing photometric depth, as expected given the increasing number of sources detected in such a large FOV (e.g. at $m_{lim} = 29.0$, the total number of sources is 1000 times larger than in the “shallow” survey), both in blank and lensing fields. The fractional error appears slightly larger in lensing than in blank fields at $z=6$, but this effect reverses with increasing source redshift. These estimates for the blank field can be compared to present-day surveys. For instance, the field to field variations obtained by Bouwens et al. (2006) for a single ACS pointing at $z \sim 6$ for a limiting magnitude $z_{850} \sim 29$ is 35%. Using the same observational constraints (FOV, depth, ...), our simulations yield a $v_r \sim 30\%$, a value which is smaller but fairly compatible with the results quoted by Bouwens et al. (2006).

4. Discussion

4.1. Survey parameters and efficiency

As discussed in Sect. 2.1.3, the FOV and the limiting magnitude are two important survey parameters used in these simulations. The influence of the FOV for a fixed limiting magnitude strongly depends on the shape of the LF. The highest ratio in number counts between lensing and blank fields can be achieved with the smallest FOV due to simple geometrical considerations. This section specifically addresses the evolution on the survey efficiency in lensing and blank fields as a function of the limiting magnitude.

For these purposes, we use the same approach as in Sect. 3.2 to derive number counts within a $6' \times 6'$ FOV in blank fields

Table 5. Number counts, field to field variance calculated with the correlation function both in blank and lensing fields, for $z = 6, 7$ and 8 within a $6' \times 6'$ FOV, for a shallow survey with $AB \leq 25.5$. Field to field variance in lensing fields includes $1 - \sigma$ magnification errors.

	Blank field			Lensed field								
	6	7	8	A1689			A1835			AC114		
z_s	6	7	8	6	7	8	6	7	8	6	7	8
LF (a)	4.61	2.43	1.31	$8.63^{+0.86}_{-0.76}$	$5.66^{+0.62}_{-0.59}$	$3.83^{+0.47}_{-0.44}$	$6.69^{+0.61}_{-0.58}$	$4.00^{+0.42}_{-0.39}$	$2.48^{+0.29}_{-0.27}$	$7.07^{+0.65}_{-0.61}$	$4.27^{+0.44}_{-0.41}$	$2.66^{+0.31}_{-0.29}$
v_r	58%	75%	97%	$47^{+1}_{-1}\%$	$56^{+2}_{-2}\%$	$66^{+3}_{-3}\%$	$51^{+1}_{-1}\%$	$63^{+2}_{-2}\%$	$77^{+3}_{-3}\%$	$50^{+1}_{-1}\%$	$62^{+2}_{-2}\%$	$75^{+3}_{-3}\%$
LF (b)	1.30	0.39	0.13	$10.07^{+1.808}_{-1.608}$	$5.66^{+1.24}_{-1.08}$	$3.53^{+0.89}_{-0.75}$	$4.69^{+0.78}_{-0.69}$	$2.21^{+0.47}_{-0.41}$	$1.23^{+0.30}_{-0.25}$	$4.96^{+0.80}_{-0.71}$	$2.35^{+0.47}_{-0.41}$	$1.28^{+0.30}_{-0.25}$
v_r	96%	165%	283%	$45^{+2}_{-2}\%$	$56^{+4}_{-4}\%$	$68^{+5}_{-6}\%$	$60^{+3}_{-3}\%$	$79^{+6}_{-7}\%$	$101^{+9}_{-10}\%$	$57^{+4}_{-4}\%$	$77^{+6}_{-6}\%$	$100^{+8}_{-9}\%$
LF (c)	1.30	0.07	< 0.01	$10.07^{+1.808}_{-1.608}$	$3.08^{+0.84}_{-0.71}$	$0.96^{+0.38}_{-0.29}$	$4.69^{+0.78}_{-0.69}$	$1.04^{+0.27}_{-0.23}$	$0.28^{+0.10}_{-0.08}$	$4.96^{+0.80}_{-0.71}$	$1.03^{+0.26}_{-0.22}$	$0.24^{+0.09}_{-0.07}$
v_r	96%	383%	-	$45^{+2}_{-2}\%$	$70^{+6}_{-7}\%$	$113^{+17}_{-16}\%$	$60^{+3}_{-3}\%$	$108^{+12}_{-10}\%$	$197^{+39}_{-25}\%$	$57^{+4}_{-4}\%$	$108^{+12}_{-10}\%$	$211^{+38}_{-29}\%$

Table 7. Field to field variance for 3 different magnitude limits : $m_{lim} = 27.0, 28.0$ and 29.0 , in a $6' \times 6'$ blank field and lensing field (behind AC114) for the LF(c). Field to field variance in lensing fields includes $1 - \sigma$ magnification errors.

	$m_{lim} = 27.0$		$m_{lim} = 28.0$		$m_{lim} = 29.0$	
	$\langle N \rangle$	v_r	$\langle N \rangle$	v_r	$\langle N \rangle$	v_r
Blank field						
$z = 6$	65.58	27%	256.71	21%	681.92	18%
$z = 7$	19.01	38%	107.27	26%	352.52	21%
$z = 8$	4.17	62%	39.78	34%	170.04	26%
$z = 10$	0.05	471%	2.92	72%	29.73	39%
$z = 12$	< 0.00	-	0.04	494%	2.56	77%
Lensing field						
$z = 6$	$83.88^{+6.60}_{-6.28}$	$26^{+0}_{-0}\%$	$253.92^{+13.20}_{-12.86}$	$23^{+0}_{-0}\%$	$537.27^{+17.23}_{-17.22}$	$22^{+0}_{-0}\%$
$z = 7$	$31.05^{+3.21}_{-3.00}$	$33^{+1}_{-1}\%$	$122.49^{+8.16}_{-7.85}$	$26^{+1}_{-1}\%$	$318.64^{+13.88}_{-13.66}$	$24^{+0}_{-0}\%$
$z = 8$	$10.03^{+1.39}_{-1.27}$	$45^{+1}_{-2}\%$	$54.01^{+4.57}_{-4.33}$	$31^{+1}_{-1}\%$	$174.64^{+9.75}_{-9.46}$	$26^{+0}_{-0}\%$
$z = 10$	$0.72^{+0.20}_{-0.16}$	$129^{+14}_{-14}\%$	$7.44^{+1.06}_{-0.96}$	$55^{+2}_{-2}\%$	$41.28^{+3.58}_{-3.39}$	$37^{+1}_{-2}\%$
$z = 12$	$0.06^{+0.03}_{-0.02}$	$411^{+107}_{-78}\%$	$0.64^{+0.17}_{-0.14}$	$137^{+15}_{-14}\%$	$6.46^{+0.92}_{-0.83}$	$59^{+2}_{-2}\%$

and behind lensing clusters. AC114 is used here as a representative lensing cluster. Fig. 9 displays the expected number counts as a function of the redshift of sources, for different depths ($AB \leq 26.0, 27.0, 28.0$ and 29.0). An opposite trend between blank and lensing fields appears, depending once again on the LF and on the redshift of sources. With increasing limiting magnitude, the efficiency of the survey towards a foreground cluster diminishes and becomes less effective than in blank fields leading to a negative magnification bias for the faintest limiting magnitudes (e.g. for LF(a) between $AB \sim 27.0 - 28.0$, for LF(b) between $AB \sim 28.0 - 29.0$ and for LF(c) beyond $AB \sim 29.0$). This trend, however, is highly sensitive to the FOV. In particular, the negative magnification bias appears towards the typical magnitudes achieved by space facilities (JWST). Fig. 10 displays the same results as in Fig. 9 but for a $2.2' \times 2.2'$ FOV (JWST-like). The main characteristics remain broadly unchanged, the general trends are just exacerbated, the inversion happening to lesser depth.

Lensing and blank field surveys do not explore the same intrinsic luminosities, as shown in Fig. 11 and 12. These figures compare the expected number density of sources as a function of their intrinsic UV luminosity (or equivalent SFR) for different limiting magnitudes ranging from $AB \leq 25.5$ to 29.0 . In the case of lensing fields, two different results are given, depending on the FOV around the cluster center. In this particular case, the source redshift is arbitrarily fixed to $z_s = 8$, assuming a strongly evolving LF(c), and the lensing cluster is AC114.

In summary, the number of $z > 8$ sources expected at the typical depth of JWST ($AB \sim 28 - 29$) is much higher in lensing than in blank fields if the UV LF is rapidly evolving with redshift (LF(c)), as suggested by Bouwens et al. (2008). The trend should be the opposite if the LF remains unchanged between $z \sim 6$ and 8. Lensing clusters are the only way to study the faintest building blocks of galaxies, with typical $SFR \leq 0.1$ to $1 M_\odot/\text{yr}$. On the contrary, wide field surveys covering 10^3 to 10^4 arcmin^{-2} are needed to set reliable constraints on the brightest part of the LF at $z \geq 6$, i.e. for galaxies with $SFR \geq 10 M_\odot/\text{yr}$.

4.2. Influence of galaxy morphology and image sampling

Gravitational magnification (e.g. in the tangential direction) induces an elongation of images along the shear direction while preserving the resolution in the perpendicular direction and the surface brightness of high redshift galaxies. All the comparisons between lensing and blank fields in our simulations assumed that observations were conducted with the same instrument setup in terms of FOV and spatial sampling, and with the same observational conditions, in particular the same limiting surface brightness and PSF. However, when comparing magnitude-limited samples in lensing and blank fields, it is worth discussing the influence of galaxy morphology and image sampling on the present results. In particular, the evolution in the surface brightness of high redshift sources is susceptible to hinder the search efficiency in clusters if, for instance, number counts in clusters were dominated by sources below the limiting surface brightness.

As explained in Sect. 2.1.1, all the previous results have been obtained assuming that galaxies at $z > 7$ are compact as compared to spatial sampling. Indeed, high redshift sources are expected to be very small, typically $\lesssim 0.10$ on the sky, based on cosmological simulations (e.g. Barkana & Loeb 2000), in such a way that the high resolution capability of JWST is needed for resolving such faint galaxies. Recent observations of LBGs candidates in the HUDF fully support this idea (Bouwens et al. 2008, 2009b; Oesch et al. 2009). In a recent paper, Oesch et al. (2009) measured the average intrinsic size of $z \sim 7 - 8$ LBGs to be 0.7 ± 0.3 kpc. These galaxies are found to be extremely compact, with very little evolution in their half-light radii between $z \sim 6$ and 7 , roughly consistent with galaxies having constant comoving sizes, at least within the observed luminosity domain $\sim 0.1 - 1L^*(z = 3)$. Smaller physical sizes are expected for higher redshift and/or intrinsically fainter galaxies, based on the scaling of the dark matter halo mass or the disk circular velocity (Mo et al. 1998). This differential trend is actually observed between the bright ($\sim 0.3 - 1L^*$) and the faint ($\sim 0.12 - 0.3L^*$) samples of Oesch et al. (2009).

If all high- z galaxies exhibit the same compact and uniform morphology, the effective mean surface brightness of a lensed galaxy will be brighter or fainter with respect to a blank field galaxy with the same apparent magnitude depending on the spatial resolution (in practice, the instrumental PSF). The majority of lensed sources should remain spatially unresolved on their width on seeing-limited ground-based surveys, and even on their tangential direction up to a gravitational magnification $\mu \sim 5 - 10$. Hence, the apparent surface brightness of a lensed source is actually brighter than that of a blank field galaxy of similar apparent magnitude (by roughly $-2.5 \log(\mu)$ mags for a spatially unresolved galaxy). This situation is typically found in the “shallow and wide” near-IR surveys discussed above (e.g. for the $6' \times 6'$ FOV), where lensing clusters are particularly efficient.

On the contrary, for a fixed apparent magnitude, the effective mean surface brightness of a lensed galaxy is expected to become fainter with respect to a blank field galaxy when the image resolution is similar or better than its (lensed maximum) half-light radius, reaching $\sim 2.5 \log(\mu)$ mags in the worst case. This situation is typically expected in the “deep and narrow” near-IR surveys with space facilities. In practice, the best spatial resolution presently achieved with HST/WFC3 in the near-IR is ~ 0.10 , reaching 0.065 with JWST/NIRCam, i.e. the typical size of the brightest $z \sim 7 - 8$ LBGs candidates presently identified. Therefore, the majority of lensed sources should remain spatially unresolved on their width. A lensed source entering the

apparent-magnitude limited sample because of its magnification μ has also a smaller physical size, by a factor of μ (assuming a constant M/L scaling with the halo mass) or $\mu^{1/2}$ (assuming a constant M/L scaling with the halo circular velocity), leading to an apparent increase on its surface brightness with respect to blank-field observations of the same galaxy. Given the spatial resolution achieved with HST and JWST, this intrinsic-size effect tends to compensate the image dilution described above, in such a way that the actual surface brightness of the lensed galaxy should get close to the surface brightness of a blank field galaxy of similar apparent magnitude.

For the reasons explained above, and to the best of present knowledge, we do not expect the apparent-magnitude limited number counts derived in clusters to be strongly biased by sources below the limiting surface brightness, provided that the usual scalings apply to the size of high- z sources.

4.3. Comparison with current survey results

We have compared our simulation results to recent observations looking for high- z LBGs. For instance, the discovery of a bright $z = 7.6 \pm 0.4$ lensed galaxy by Bradley et al. (2008), with $AB=24.7$ (intrinsic $AB \sim -22.6$), in a $2.5' \times 2.5'$ FOV survey around A1689 is in fair agreement with our expectations. Indeed, given the survey characteristics and including $\sim 100\%$ variance for $z_s = 7.6 \pm 0.4$, we expect between 0.2 and 0.8 such bright objects in this lensing field, if the LF remains constant between $z \sim 4$ and 8 (LF(a)). In case of a strongly evolving LF(c), the expected number of sources in this survey is 0.12 (i.e. ranging between 0 and 0.5 with $\sim 200\%$ variance) making the discovery of this bright source particularly fortunate. Our results for lensing fields are also consistent with the number of $z \sim 7.5$ LBGs found by Richard et al. (2008), to the depth of their survey, using LF(b) or (c). Quantitatively, Richard et al. (2008) detected 5 sources with 12 pointings over 6 clusters. With our simulations, $2.6^{+0.7}_{-0.6}$ objects with a variance of $\sim 75\%$ are expected with the LF(c) model. We also compared with the surface density of $z \sim 7$ candidates in the deep near-IR data behind clusters obtained by Bouwens et al. (2009a). Bouwens et al. (2009a) found a surface density of $0.05^{+0.11}_{-0.04} \text{ arcmin}^{-2}$ with $AB \leq 25.5$ with a typical NICMOS3 FOV. With the strongly evolving LF(c) and the same survey characteristics used in our simulations, we expect a surface density of 0.01 arcmin^{-2} behind a typical cluster such as AC114, with a variance of $\sim 110\%$. This result shows a relatively good agreement by taking into account field to field variance.

4.4. Lyman Break versus NB searches

In this section, we discuss on the relative efficiency of blank and lensing fields on the detection of LAEs based on either NB surveys or the spectroscopic follow up of LBGs at $z > 6$. Although the observational effort required to select $z \geq 7$ candidates using the dropout technique seems relatively cheap as compared to the NB approach, the two approaches are complementary, as emphasized by the fact that many objects found by Lyman α emission remain weak or undetected in the continuum (e.g. Rhoads & Malhotra 2001, Kodaira et al. 2003, Cuby et al. 2003, Taniguchi et al. 2005). A quantitative comparison between the properties of LAEs and LBGs at $z \geq 7$ within the same volume should provide important information on the Lyman α transmission, SFR and other properties of these high- z galaxies.

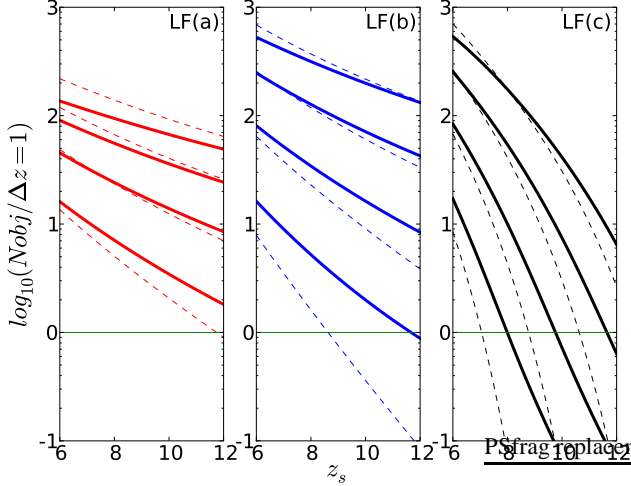


Fig. 9. Expected number counts of objects as a function of the redshift of sources in a $6' \times 6'$ FOV, for different limiting magnitudes 26.0, 27.0, 28.0 and 29.0 from bottom to top respectively. This calculation is provided both in blank (dotted line) and lensing fields (solid line) (here AC114) and for the three LFs (from right to left, (a) in red, (b) in blue and (c) in black)

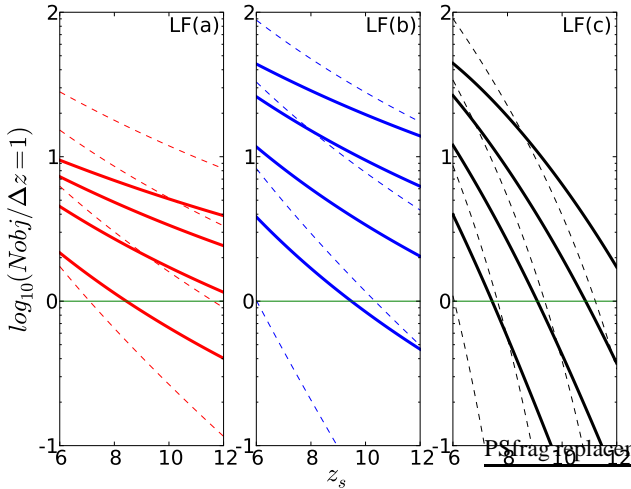


Fig. 10. The same as Fig. 9 but for a $2.2' \times 2.2'$ FOV. Some differences appear in comparison with the Fig. 9. For example, the total numbers of high- z galaxies expected behind lensing clusters (solid lines) and the field (dashed lines) are much larger at low limiting magnitude ($m_{AB} = 26.0$) but this phenomenon is reversed for deeper surveys ($m_{AB} = 28.0 - 29.0$) (see text for details).

Since the pioneering Large Area Lyman Alpha Survey (LALA, Rhoads & Malhotra (2001), Rhoads et al. (2003)), different NB surveys in blank fields have provided interesting galaxy samples in the $z \sim 5 - 7$ interval, e.g. the large sample of Ly α emitters at $z \sim 5.7$ by Hu et al. (2004), the $z \sim 6.17$ and 6.53 galaxies found respectively by Cuby et al. (2003) and Rhoads et al. (2004), the two $z \sim 6.6$ galaxies detected by Kodaira et al. (2003), and the galaxy at a redshift $z=6.96$ found by Iye et al. (2006). In the latter case, which should be representative of $z \sim 7$ samples, the authors used a combination of NB

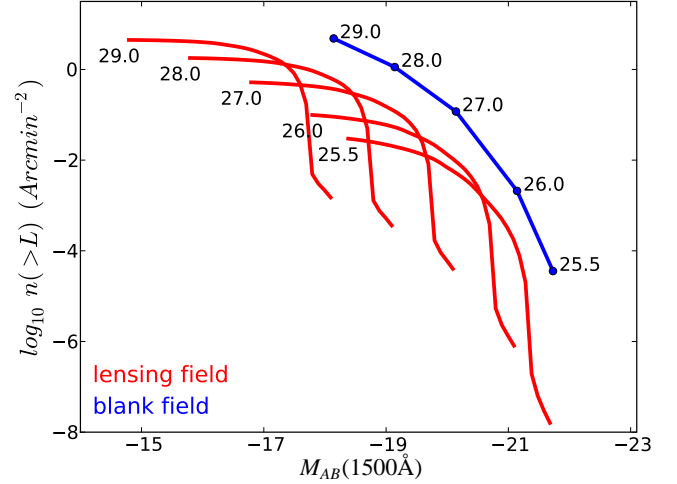


Fig. 11. Cumulative surface density of sources as a function of their intrinsic UV luminosity, in blank fields (blue solid line) and in the lensing fields with FOV ~ 5 arcmin 2 (JWST-like, red solid line), for different photometric depths ranging from shallow ($AB \sim 25.5$) to deep ($AB \sim 29.0$) surveys and a strongly evolving LF(c). The source redshift is arbitrarily fixed at $z=8$, with $\Delta z = 1$

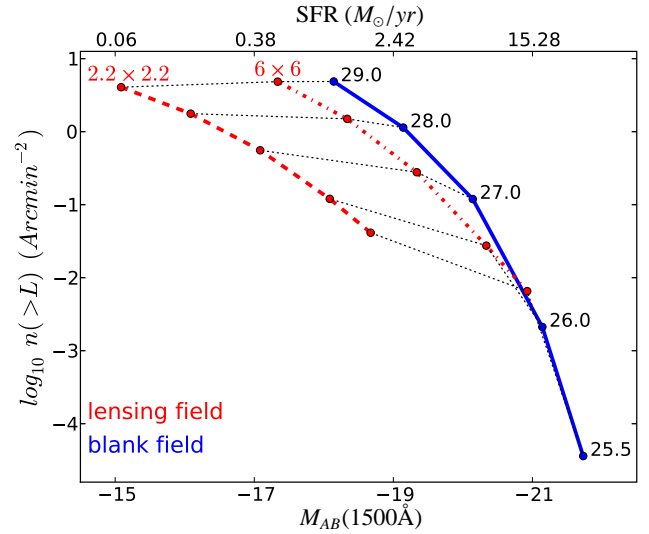


Fig. 12. Cumulative surface density of sources as a function of their intrinsic UV luminosity and SFR, in blank fields (blue solid line) and in the lensing fields with FOV $6' \times 6'$ (red dotted line) and $2.2' \times 2.2'$ (JWST-like, red dashed line), for different photometric depths ranging from shallow ($AB \sim 25.5$) to deep ($AB \sim 29.0$) surveys and a strongly evolving LF(c). The mean magnification over the whole the field is used to derive the lensing points, the true distribution is displayed in Fig. 11. The source redshift is arbitrarily fixed at $z=8$, with $\Delta z = 1$. The conversion from absolute magnitude to SFR is provided in Sect. 2.1.3 using the calibrations from Kennicutt (1998).

imaging at 8150\AA (SuprimeCam) and broad-band photometry in the optical bands to select candidates for a subsequent spectroscopic follow up with DEIMOS/Keck. Their confirmation rate is relatively high (18 sources out of 26 candidates), leading to 0.03 sources/arcmin 2 and redshift bin $\delta z = 0.1$. Similar results

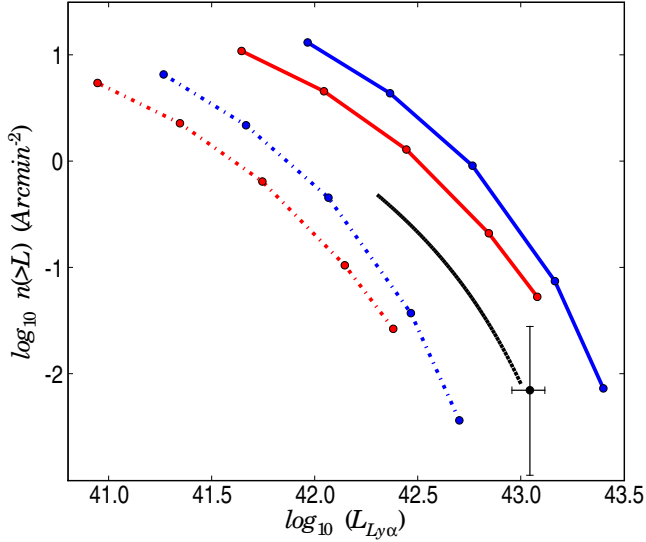


Fig. 13. Cumulative surface density of observed sources as a function of their Lyman alpha luminosity ($6' \times 6'$ FOV, $\Delta_z = 1$, redshift of sources fixed at 6.6 for the LF(c)). The density is calculated in blank (blue solid line) and in lensing fields (red solid line) for different limiting magnitudes (from right to left: 25.5, 26.0, 27.0, 28.0 and 29.0). Dashed lines display number counts corrected by transmission value $\epsilon \sim 10\%$ (dashed red line in lensing fields and dashed blue line in blank field). For comparison, raw number counts extracted from the spectroscopic sample of LAEs by Kashikawa et al. (2006) are also given (black solid line). The number density derived from Iye et al. (2006) at $z = 6.96$ is also indicated, together with corresponding error bars (see text for details). As in Fig. 12, the magnification used to derive the lensing points is averaged over the entire field.

are reported by Kashikawa et al. (2006). All these sources have important Lyman α fluxes (a few $\times 10^{-17}$ erg cm^{-2} s^{-1}), and display broad Lyman α lines ($\sigma_{\nu} \sim 200$ km/s). A strong evolution is found in the number density of LAEs at $z \geq 7$ with respect to the $z \sim 5 - 7$ interval (Iye et al. 2006, Willis et al. 2006, Cuby et al. 2007).

The number of LAEs expected within a sample of LBGs at $z \geq 6$ can be estimated using the distribution of Lyman- α equivalent widths derived for the spectroscopic sample of LBGs at $z \sim 3$ by Shapley et al. (2003), assuming no evolution in the population of LAEs with respect to LBGs. This simplistic scaling should be enough for the simulation needs. We introduce a factor ϵ , defined below, which can be linked to the Lyman α transmission as follows:

$$\epsilon = \frac{L_{1500}}{L_{\text{Ly}\alpha}(1+z)} = \frac{1}{W_{\text{Ly}\alpha}} \quad (12)$$

where L_{1500} is the UV monochromatic luminosity at 1500 Å, $L_{\text{Ly}\alpha}$ is the Lyman- α luminosity and $W_{\text{Ly}\alpha}$ is the Lyman- α equivalent width. With this simple assumption, the average value for the Lyman- α equivalent width is ~ 10 Å, corresponding to $\epsilon \sim 10\%$. This value can be used to derive a rough estimate of expected number density of LAEs, from a population of LBGs. In addition, the number density is also corrected to take into account of the fraction of the LBGs sample displaying Ly α in emission.

Fig. 13 displays the cumulative number counts of sources at $z \sim 6.6$ integrated from the LF(c) as a function of the Lyman- α luminosity, scaled according to the UV luminosities (cf Sect. 2.1.1) in the typical $6' \times 6'$ FOV, together with a comparison of observations in a similar redshift domain ($z_s \sim 6.6$ for Kashikawa spectroscopic sample of LAEs and Iye et al. 2006 at $z=6.96$).

The number density of LBGs at $z=7$ (with $\delta z = 0.1$, close to the band-width of NB surveys) ranges between 0.001 (LF(c)) and 0.02 (LF(a)) sources/ arcmin^2 for a survey limited to $H(AB) \leq 25.5$, depending on the LF. Lensing clusters improve these numbers by a factor ranging between 6 (for LF(c)) and 2 (for LF(a)). In case of a deep survey limited to $H(AB) \leq 29.0$, the number densities reach 1 (LF(c)) to 2 (LF(a)) sources/ arcmin^2 . In this case, there is a negative magnification bias of the order of 20%. These numbers, obtained with a simplistic model, are between a factor of ~ 10 (for bright sources) and a few (for faint sources) smaller than the number densities obtained by Kashikawa et al. (2006) for their spectroscopic sample. With increasing z_s (see Fig. 9) for instance at $z=9$ with the strongly evolving LF(c), no sources can be detected for a shallow survey limited to $H(AB) \leq 25.5$ and for a deeper limited survey ($H(AB) \leq 29.0$), a minimum of 3 arcmin^2 surveyed area is needed to obtain 1 source in a blank field. In a lensing field with the (LF(c)), these number densities reach 0.002 for $H(AB) \leq 25.5$ and 0.32 sources/ arcmin^2 for $H(AB) \leq 29.0$. The relatively low-efficiency of lensing clusters with NB techniques in the $z \geq 9$ domain has been recently confirmed by the results of Willis et al. (2008).

The preselection of $z \geq 6 - 7$ candidates in lensing fields has two main advantages with respect to blank fields. In the shallow ($AB \leq 25.5$) regime, there is an increase by a factor $\sim 8 - 10$ on the number of sources detected and a moderate gain in depth for a given exposure time (i.e. ~ 0.5 magnitudes at $AB \sim 25.5$). In the deep-survey regime ($AB \leq 28 - 29$), there is a gain in intrinsic depth, for a number of candidates which remains essentially constant (i.e. ~ 0.8 mags gain at $AB \leq 28$). The relative efficiency of lensing with respect to blank field counts in Fig. 12 depends on the FOV. The two predictions get close to each other with increasing values of the FOV in lensing surveys, and the trend goes in the opposite direction for smaller FOV. This trend is the same for both LBGs and LAEs. To explore the bright end of the LF, blank field surveys are needed with a large FOV, whereas lensing clusters are particularly useful to explore the faint end of the LF. This trend is further discussed in the next Section.

4.5. Towards the ideal survey: constraining the Luminosity Function of high- z sources

All present photometric surveys aimed at constraining the UV LF at $z > 7$, either space or ground-based, are still dramatically small in terms of effective surface. Wide and deep optical+near-IR surveys in lensing and blank fields are needed to set strong constraints on the LF and on the star-formation density at $z > 7$. An important issue is the combination between photometric depth and surveyed area which is needed to identify a representative number of photometric candidates, or to reach a significant non-detection limit in order to constrain the LF of $z > 7$ sources.

There are three different aspects to consider when designing an “ideal” survey aiming at constraining the LF: the depth and the area of the survey, and the corresponding field to field variance. In order to address these issues, we have computed the expected field to field variance corresponding to lensing and

blank field surveys, for different survey configurations (area and depth). A summary of these results is given in Table 8 for different number of lensing clusters, and for two representative depths in the H-band (i.e. a “shallow” survey with $AB \leq 25.5$, and a “deep” survey with $AB \leq 28.0$) assuming a strongly evolving LF(c) in all cases. This table complements the results given in Tables 5 and 7 for blank and lensing fields as a function of depth. In all cases, we use AC114 as a reference for lensing clusters.

Regarding field-to-field variance in number counts, results are expected to be similar in blank and lensing fields for a relatively wide FOV ($\sim 40 - 50 \text{ arcmin}^2$; see Sect. 3.5 and Table 7). As shown in Table 8, a deep lensing survey using ~ 10 clusters should be able to reach a variance $\leq 20\%$ on sources at $6 \leq z \leq 8$, irrespective of the actual LF. This value is better than present-day photometric surveys in blank fields, typically reaching 30-35% for $AB \leq 29.0$ (e.g. Bouwens et al. 2008), which in turn is rather close to what could be achieved in a single lensing cluster for $AB \leq 28.0$.

A different survey strategy consists of increasing the number of lensing clusters with a shallow limiting magnitude. In this case, a few tens of lensing clusters (typically between 10 and 50, depending on the LF) are needed to reach a variance of $\sim 30\%$ at $z \leq 8$. Note that the difference in exposure time between the shallow and deep surveys reported in Table 8 is a factor ~ 100 , and that ~ 10 pointings are needed on blank fields in order to reach the same number of $z \sim 6 - 8$ sources as in a single “shallow” lensing field.

In the case of a strongly evolving LF(c), photometric surveys should reach a minimum depth of $AB \sim 28$ to achieve fair statistics on $z \sim 9 - 10$ sources using a lensing cluster (Table 7). In this case we expect between 20 ($z=9$, $\sim 40\%$ variance) and 8 ($z=10$, $\sim 40\%$ variance) sources per lensing cluster in a $\sim 40 \text{ arcmin}^2$ FOV. The efficiency is a factor of 10 smaller at $z \sim 10$ in blank fields. Fair statistics at $z \sim 12$ should require a minimum depth close to $AB \sim 29$ both in lensing and blank fields.

Constraining the LF of star forming galaxies at $z \geq 7$ should require the combination of blank and lensing field observations. This is illustrated for instance in Fig. 11 and 12 for an example at $z_s = 8$. A survey towards a lensing cluster has several advantages. It increases the total number of sources available for spectroscopic follow up, and it helps extending the sample towards the faint edge of the LF and towards the highest possible limits in redshift. On the other hand, blank fields are needed to achieve fair statistics on the bright edge of the LF. Thus an “ideal” survey should combine both blank and lensing fields. Given the numbers presented in previous sections, a blank field used for these purposes should be a factor ranging between ~ 10 and 100 times larger than a lensing field (depending on the redshift domain, photometric depth, and actual LF) in order to efficiently complete the survey towards $L > L^*$. This should be possible with the new upcoming surveys, such as the WIRCAM ultra deep survey (WUDS) at CFHT ($\sim 400 \text{ arcmin}^2$, with $YJHK \leq 25.5$), UKIDSS-UDS ($\sim 2700 \text{ arcmin}^2$, with $YJHK \leq 25$) or Ultra-Vista ($\sim 2600 \text{ arcmin}^2$, with $YJH \leq 26$, $K \leq 25.6$). The optimum number of lensing fields ranges between $\sim 10 - 20$ (for $z \sim 6 - 8$ studies with “shallow” photometry) to a few (for “deep” surveys targeting $z \sim 8 - 12$ sources).

5. Summary and conclusions

We have evaluated the relative efficiency of lensing clusters with respect to blank fields in the identification and study of $z \geq 6$ galaxies. The main conclusions of this study are given below.

For magnitude-limited samples of LBGs at $z \geq 6$, the magnification bias increases with the redshift of sources and decreases with both the depth of the survey and the size of the surveyed area. Given the typical near-IR FOV in lensing fields, the maximum efficiency is reached for clusters at $z \sim 0.1 - 0.3$, with maximum cluster-to-cluster differences ranging between 30 and 50% in number counts, depending on the redshift of sources and the LF.

The relative efficiency of lensing with respect to blank fields strongly depends on the shape of the LF, for a given photometric depth and FOV. The comparison between lensing and blank field number counts is likely to yield strong constraints on the LF.

The presence of a strong-lensing cluster along the line of sight has a dramatic effect on the observed number of sources, with a positive magnification effect in typical ground-based “shallow” surveys ($AB \leq 25.5$). The positive magnification bias increases with the redshift of sources, and also from optimistic to pessimistic values of the LF. In case of a strongly evolving LF at $z \geq 7$, as proposed by Bouwens et al. (2008), blank fields are particularly inefficient as compared to lensing fields. For instance, the size of the surveyed area in ground-based observations would need to increase by a factor of ~ 10 in blank fields with respect to a typical $\sim 30 - 40 \text{ arcmin}^2$ survey in a lensing field, in order to reach the same number of detections at $z \sim 6 - 8$, and this merit factor increases with redshift. All these results have been obtained assuming that number counts derived in clusters are not dominated by sources below the limiting surface brightness of observations, which in turn depends on the reliability of the usual scalings applied to the size of high- z sources.

Ground-based “shallow” surveys are dominated by field-to-field variance reaching ~ 30 to 50% in number counts between $z \sim 6$ and 8 in a unique $\sim 30 - 40 \text{ arcmin}^2$ lensing field survey (or in a 400 arcmin^2 blank field), assuming a strongly evolving LF.

The number of $z > 8$ sources expected at the typical depth of JWST ($AB \sim 28 - 29$) is much higher in lensing than in blank fields if the UV LF is rapidly evolving with redshift (i.e. a factor of ~ 10 at $z \sim 10$ with $AB \leq 28$).

Blank field surveys with a large FOV are needed to probe the bright edge of the LF at $z \geq 6 - 7$, whereas lensing clusters are particularly useful to explore the mid to faint end of the LF.

Acknowledgements. We are grateful to D. Schaerer, A. Hempel, J.F. Le Borgne and E. Egami for useful comments. We acknowledge financial support from the European Commissions ALFA-II programme through its funding of the Latin-America European Network for Astrophysics and Cosmology (LENAC). This work was also supported by the French *Centre National de la Recherche Scientifique*, the French *Programme National de Cosmologie* (PNC) and *Programme National de Galaxies* (PNG). JR acknowledges support from a EU Marie-Curie fellowship.

References

- Appenzeller, I., Fricke, K., Fürtig, W., et al. 1998, *The Messenger*, 94, 1
- Barkana, R. & Loeb, A. 2000, *ApJ*, 531, 613
- Beckwith, S. V. W., Stiavelli, M., Koekemoer, A. M., et al. 2006, *AJ*, 132, 1729
- Bertin, E. & Arnouts, S. 1996, *A&AS*, 117, 393
- Bouwens, R. J., Illingworth, G. D., Blakeslee, J. P., & Franx, M. 2006, *ApJ*, 653, 53
- Bouwens, R. J., Illingworth, G. D., Bradley, L. D., et al. 2009a, *ApJ*, 690, 1764
- Bouwens, R. J., Illingworth, G. D., Franx, M., & Ford, H. 2007, *ApJ*, 670, 928
- Bouwens, R. J., Illingworth, G. D., Franx, M., & Ford, H. 2008, *ApJ*, 686, 230
- Bouwens, R. J., Illingworth, G. D., Oesch, P. A., et al. 2009b, *ArXiv e-prints*
- Bouwens, R. J., Illingworth, G. D., Thompson, R. I., et al. 2004a, *ApJ*, 606, L25
- Bouwens, R. J., Thompson, R. I., Illingworth, G. D., et al. 2004b, *ApJ*, 616, L79
- Bradač, M., Treu, T., Applegate, D., et al. 2009, *ArXiv e-prints*
- Bradley, L. D., Bouwens, R. J., Ford, H. C., et al. 2008, *ArXiv e-prints*, 802
- Broadhurst, T. J., Taylor, A. N., & Peacock, J. A. 1995, *ApJ*, 438, 49
- Cuby, J.-G., Hiben, P., Lidman, C., et al. 2007, *A&A*, 461, 911

Table 8. Field to field variance, including $1 - \sigma$ errors on the magnification factor, expected in a lensing survey, as a function of the number of clusters, for the three LFs (a), (b) and (c) (from top to bottom respectively). Simulations were performed using the same approaches in Sect. 3.5 (i.e. $6' \times 6'$ FOV, ...) for two different depths: $AB \leq 25.5$ (shallow survey) and $AB \leq 28.0$ (deep survey)

v_r LF(a)/ $N_{clusters}$	1	6	10	20	50	100
$z = 6$						
Shallow	50 $^{+3}_{-3}$ %	28 $^{+1}_{-1}$ %	24 $^{+1}_{-1}$ %	19 $^{+0}_{-0}$ %	14 $^{+0}_{-0}$ %	10 $^{+0}_{-0}$ %
Deep	25 $^{+1}_{-1}$ %	17 $^{+0}_{-0}$ %	15 $^{+0}_{-0}$ %	12 $^{+0}_{-0}$ %	9 $^{+0}_{-0}$ %	7 $^{+0}_{-0}$ %
$z = 7$						
Shallow	62 $^{+2}_{-2}$ %	33 $^{+1}_{-1}$ %	28 $^{+1}_{-1}$ %	22 $^{+0}_{-0}$ %	16 $^{+0}_{-0}$ %	12 $^{+0}_{-0}$ %
Deep	29 $^{+1}_{-1}$ %	19 $^{+0}_{-0}$ %	17 $^{+0}_{-0}$ %	13 $^{+0}_{-0}$ %	10 $^{+0}_{-0}$ %	7 $^{+0}_{-0}$ %
$z = 8$						
Shallow	75 $^{+3}_{-3}$ %	39 $^{+1}_{-2}$ %	32 $^{+1}_{-1}$ %	25 $^{+0}_{-1}$ %	18 $^{+0}_{-0}$ %	13 $^{+0}_{-0}$ %
Deep	32 $^{+1}_{-1}$ %	21 $^{+0}_{-0}$ %	18 $^{+0}_{-0}$ %	15 $^{+0}_{-0}$ %	11 $^{+0}_{-0}$ %	8 $^{+0}_{-0}$ %
v_r LF(b)/ $N_{clusters}$	1	6	10	20	50	100
$z = 6$						
Shallow	57 $^{+4}_{-4}$ %	40 $^{+2}_{-2}$ %	33 $^{+2}_{-2}$ %	26 $^{+1}_{-1}$ %	18 $^{+0}_{-0}$ %	14 $^{+0}_{-0}$ %
Deep	23 $^{+1}_{-1}$ %	14 $^{+0}_{-0}$ %	13 $^{+0}_{-0}$ %	10 $^{+0}_{-0}$ %	8 $^{+0}_{-0}$ %	6 $^{+0}_{-0}$ %
$z = 7$						
Shallow	77 $^{+6}_{-6}$ %	40 $^{+2}_{-2}$ %	33 $^{+1}_{-1}$ %	25 $^{+0}_{-1}$ %	18 $^{+0}_{-0}$ %	13 $^{+0}_{-0}$ %
Deep	24 $^{+1}_{-1}$ %	17 $^{+0}_{-0}$ %	15 $^{+0}_{-0}$ %	12 $^{+0}_{-0}$ %	9 $^{+0}_{-0}$ %	7 $^{+0}_{-0}$ %
$z = 8$						
Shallow	100 $^{+8}_{-9}$ %	48 $^{+2}_{-3}$ %	40 $^{+2}_{-2}$ %	30 $^{+1}_{-1}$ %	21 $^{+0}_{-0}$ %	15 $^{+0}_{-0}$ %
Deep	28 $^{+1}_{-1}$ %	19 $^{+0}_{-0}$ %	16 $^{+0}_{-0}$ %	13 $^{+0}_{-0}$ %	10 $^{+0}_{-0}$ %	7 $^{+0}_{-0}$ %
v_r LF(c)/ $N_{clusters}$	1	6	10	20	50	100
$z = 6$						
Shallow	57 $^{+4}_{-4}$ %	40 $^{+2}_{-2}$ %	33 $^{+1}_{-1}$ %	26 $^{+1}_{-1}$ %	18 $^{+0}_{-0}$ %	14 $^{+0}_{-0}$ %
Deep	23 $^{+0}_{-0}$ %	14 $^{+0}_{-0}$ %	13 $^{+0}_{-0}$ %	10 $^{+0}_{-0}$ %	8 $^{+0}_{-0}$ %	6 $^{+0}_{-0}$ %
$z = 7$						
Shallow	108 $^{+12}_{-10}$ %	51 $^{+3}_{-4}$ %	42 $^{+2}_{-2}$ %	32 $^{+1}_{-1}$ %	22 $^{+1}_{-1}$ %	16 $^{+0}_{-0}$ %
Deep	26 $^{+1}_{-1}$ %	18 $^{+0}_{-0}$ %	15 $^{+0}_{-0}$ %	12 $^{+0}_{-0}$ %	9 $^{+0}_{-0}$ %	7 $^{+0}_{-0}$ %
$z = 8$						
Shallow	211 $^{+38}_{-29}$ %	92 $^{+8}_{-8}$ %	73 $^{+6}_{-6}$ %	53 $^{+4}_{-4}$ %	35 $^{+1}_{-1}$ %	25 $^{+1}_{-1}$ %
Deep	31 $^{+1}_{-1}$ %	21 $^{+0}_{-0}$ %	18 $^{+0}_{-0}$ %	15 $^{+0}_{-0}$ %	11 $^{+0}_{-0}$ %	8 $^{+0}_{-0}$ %

Cuby, J.-G., Le Fèvre, O., McCracken, H., et al. 2003, A&A, 405, L19
Dunkley, J., Komatsu, E., Nolta, M. R., et al. 2009, ApJS, 180, 306
Ellis, R., Santos, M. R., Kneib, J.-P., & Kuijken, K. 2001, ApJ, 560, L119
Garzón, F., Abreu, D., Barrera, S., et al. 2007, in Revista Mexicana de Astronomía y Astrofísica, vol. 27, Vol. 29, Revista Mexicana de Astronomía y Astrofísica Conference Series, 12–17
Henry, A. L., Siana, B., Malkan, M. A., et al. 2009, ApJ, 697, 1128

Hu, E. M., Cowie, L. L., Capak, P., et al. 2004, AJ, 127, 563
Hu, E. M., Cowie, L. L., McMahon, R. G., et al. 2002, ApJ, 568, L75
Iye, M., Ota, K., Kashikawa, N., et al. 2006, Nature, 443, 186
Jullo, E., Kneib, J.-P., Limousin, M., et al. 2007, New Journal of Physics, 9, 447
Kashikawa, N., Shimasaku, K., Malkan, M. A., et al. 2006, ApJ, 648, 7
Kassiola, A. & Kovner, I. 1993, in Liege International Astrophysical Colloquia, Vol. 31, Liege International Astrophysical Colloquia, ed. J. Surdej,

- D. Fraipont-Caro, E. Gosset, S. Refsdal, & M. Remy, 571–+
 Kennicutt, R. C. 1998, *ApJ*, 498, 541
 Kitzbichler, M. G. & White, S. D. M. 2006, *MNRAS*, 366, 858
 Kitzbichler, M. G. & White, S. D. M. 2007, *MNRAS*, 376, 2
 Kneib, J.-P., Ellis, R. S., Santos, M. R., & Richard, J. 2004, *ApJ*, 607, 697
 Kodaira, K., Taniguchi, Y., Kashikawa, N., et al. 2003, *PASJ*, 55, L17
 Lemson, G. & Virgo Consortium, t. 2006, *ArXiv Astrophysics e-prints*
 Limousin, M., Richard, J., Jullo, E., et al. 2007, *ApJ*, 668, 643
 McLure, R. J., Cirasuolo, M., Dunlop, J. S., Foucaud, S., & Almaini, O. 2009, *MNRAS*, 395, 2196
 Mo, H. J., Mao, S., & White, S. D. M. 1998, *MNRAS*, 295, 319
 Moorwood, A., Cuby, J.-G., & Lidman, C. 1998, *The Messenger*, 91, 9
 Moorwood, A. F. 1997, in *Society of Photo-Optical Instrumentation Engineers (SPIE) Conference Series*, Vol. 2871, *Society of Photo-Optical Instrumentation Engineers (SPIE) Conference Series*, ed. A. L. Ardeberg, 1146–1151
 Natarajan, P., Kneib, J.-P., Smail, I., & Ellis, R. S. 1998, *ApJ*, 499, 600
 Navarro, J. F., Frenk, C. S., & White, S. D. M. 1997, *ApJ*, 490, 493
 Oesch, P. A., Bouwens, R. J., Carollo, C. M., et al. 2009, *ArXiv e-prints*
 Ouchi, M., Shimasaku, K., Okamura, S., et al. 2004, *ApJ*, 611, 660
 Peebles. 1993, *Physics Today*, 46, 87
 Pelló, R., Schaerer, D., Richard, J., Le Borgne, J.-F., & Kneib, J.-P. 2004, *A&A*, 416, L35
 Rhoads, J. E., Dey, A., Malhotra, S., et al. 2003, *AJ*, 125, 1006
 Rhoads, J. E. & Malhotra, S. 2001, *ApJ*, 563, L5
 Rhoads, J. E., Xu, C., Dawson, S., et al. 2004, *ApJ*, 611, 59
 Richard, J., Kneib, J.-P., Jullo, E., et al. 2007, *ApJ*, 662, 781
 Richard, J., Pelló, R., Schaerer, D., Le Borgne, J.-F., & Kneib, J.-P. 2006, *A&A*, 456, 861
 Richard, J., Stark, D. P., Ellis, R. S., et al. 2008, *ApJ*, 685, 705
 Rieke, M. J., Kelly, D., & Horner, S. 2005, in *Society of Photo-Optical Instrumentation Engineers (SPIE) Conference Series*, Vol. 5904, *Society of Photo-Optical Instrumentation Engineers (SPIE) Conference Series*, ed. J. B. Heaney & L. G. Burriesci, 1–8
 Sanchez, A. G. & Baugh, C. M. 2006, *ArXiv Astrophysics e-prints*
 Schaerer, D. 2002, *A&A*, 382, 28
 Schechter, P. 1976, *ApJ*, 203, 297
 Shapley, A. E., Steidel, C. C., Pettini, M., & Adelberger, K. L. 2003, *ApJ*, 588, 65
 Smith, G. P., Kneib, J.-P., Smail, I., et al. 2005, *MNRAS*, 359, 417
 Springel, V., White, S. D. M., Jenkins, A., et al. 2005, *Nature*, 435, 629
 Stanway, E. R., Bunker, A. J., McMahon, R. G., et al. 2004, *ApJ*, 607, 704
 Stark, D. P., Ellis, R. S., Richard, J., et al. 2007, *ApJ*, 663, 10
 Steidel, C. C., Adelberger, K. L., Giavalisco, M., Dickinson, M., & Pettini, M. 1999, *ApJ*, 519, 1
 Taniguchi, Y., Ajiki, M., Nagao, T., et al. 2005, *PASJ*, 57, 165
 Thompson, R. I. 1998, in *Bulletin of the American Astronomical Society*, Vol. 30, *Bulletin of the American Astronomical Society*, 1326–+
 Trenti, M. & Stiavelli, M. 2008, *ApJ*, 676, 767
 Willis, J., Courbin, F., Kneib, J.-P., & Minniti, D. 2006, *New Astronomy Review*, 50, 70
 Willis, J. P., Courbin, F., Kneib, J.-P., & Minniti, D. 2008, *MNRAS*, 384, 1039
 Zheng, W., Bradley, L. D., Bouwens, R. J., et al. 2009, *ApJ*, 697, 1907

Looking for the first galaxies: Lensing or blank fields?

A. Maizy¹, J. Richard², M. A. De Leo³, R. Pelló¹, and J. P. Kneib⁴

¹ Laboratoire d'Astrophysique de Toulouse-Tarbes, CNRS, Université de Toulouse, 14 Av. Edouard-Belin, F-31400 Toulouse, France
e-mail: alexandre.maizy@ast.obs-mip.fr e-mail: roser@ast.obs-mip.fr

² Institute for Computational Cosmology, Department of Physics, Durham University, South Road, Durham, DH1 3LE, UK
e-mail: johan.richard@durham.ac.uk

³ Instituto de Astronomía, UNAM, Apartado Postal 70-264, 04510 México DF, Mexico
e-mail: madeleo@astroscu.unam.mx

⁴ OAMP, Laboratoire d'Astrophysique de Marseille, UMR 6110 traverse du Siphon, 13012 Marseille, France
e-mail: jean-paul.kneib@oamp.fr

Received ; accepted

ABSTRACT

Context. The identification and study of the first galaxies remains one of the most exciting topics in observational cosmology. The determination of the best possible observing strategies is a very important choice in order to build up a representative sample of spectroscopically confirmed sources at high- z ($z \geq 7$), beyond the limits of present-day observations.

Aims. This paper is intended to precisely address the relative efficiency of lensing and blank fields in the identification and study of galaxies at $6 \leq z \leq 12$.

Methods. The detection efficiency and field-to-field variance are estimated from direct simulations of both blank and lensing fields observations. Present known luminosity functions in the UV are used to determine the expected distribution and properties of distant samples at $z \geq 6$ for a variety of survey configurations. Different models for well known lensing clusters are used to simulate in details the magnification and dilution effects on the background distant population of galaxies.

Results. The presence of a strong-lensing cluster along the line of sight has a dramatic effect on the number of observed sources, with a positive magnification bias in typical ground-based “shallow” surveys ($AB \leq 25.5$). The positive magnification bias increases with the redshift of sources and decreases with both depth of the survey and the size of the surveyed area. The maximum efficiency is reached for lensing clusters at $z \sim 0.1 - 0.3$. Observing blank fields in shallow surveys is particularly inefficient as compared to lensing fields if the UV LF for LBGs is strongly evolving at $z \geq 7$. Also in this case, the number of $z \geq 8$ sources expected at the typical depth of JWST ($AB \sim 28 - 29$) is much higher in lensing than in blank fields (e.g. a factor of ~ 10 for $AB \leq 28$). **All these results have been obtained assuming that number counts derived in clusters are not dominated by sources below the limiting surface brightness of observations, which in turn depends on the reliability of the usual scalings applied to the size of high- z sources.**

Conclusions. Blank field surveys with a large field of view are needed to prove the bright end of the LF at $z \geq 6 - 7$, whereas lensing clusters are particularly useful for exploring the mid to faint end of the LF.

Key words. galaxies : formation – galaxies : high redshift – galaxies : photometry – galaxies : clusters : lensing –

1. Introduction

Constraining the abundance of $z > 7$ sources remains an important challenge of modern cosmology. Recent WMAP results place the first building blocks of galaxies at redshifts $z = 11.0 \pm 1.4$, suggesting that reionization was an extended process (?). Distant star-forming systems could have been responsible for a significant part of the cosmic reionization. Considerable advances have been made during the last years in the observation of the early Universe with the discovery of galaxies at $\sim 6-7$, close to the end of the reionization epoch (e.g. ?????????), and the first prospects up to $z \sim 10$ (??????).

High- z surveys are mainly based on two different and complementary techniques: the dropout (Lyman- α Break) identification, which is an extrapolation of the drop-out technique used for Lyman-Break Galaxies (LBGs, ?) to higher redshifts (e.g. ???), and the narrow-band (NB) imaging aimed at detecting Lyman α emitters (LAEs, e.g. ?????). Using the former technique, ? found a strong evolution in the abundance of galaxies between $z \sim 7-8$ and $z \sim 3-4$, the SFR density being much smaller at very

high- z up to the limits of their survey, in particular towards the bright end of the Luminosity Function (LF). A strong evolution is also observed in the number density of sources detected with NB techniques, which seems to be much smaller at $z \geq 7$ than in the $z \sim 5 - 7$ interval (???)

Both dropout and NB approaches require a subsequent spectroscopic confirmation of the selected candidates. For now approximately ten galaxies beyond $z \sim 6.5$ are known with secure spectroscopic redshifts (?????). All samples beyond this redshift are mainly supported by photometric considerations (?????). This situation is expected to dramatically improve in the near future with the arrival of a new generation of multi-object spectrographs in the near-IR, such as MOIRCS/Subaru, Flamingos2/Gemini-S (~ 2009), or EMIR/GTC¹ (~ 2012), with well suited field of view, spectral resolution and sensitivity. These forthcoming facilities should provide spectroscopic confirmation for a large number of $z > 7$ candidates identified from deep photometric surveys, and the first characterization of the

physical properties of these sources (e.g. IMF, stellar populations, fraction of AGN, ...).

The aim of this paper is to determine the best possible observing strategies in order to build up a representative sample of spectroscopically confirmed $z \geq 7$ galaxies. The photometric pre-selection of high- z candidates could be achieved either in blank fields or in lensing clusters. This later technique, also first referred to as the “gravitational telescope” by Zwicky, has proven highly successful in identifying a large fraction of the most distant galaxies known today thanks to magnifications by typically 1-3 magnitudes in the cluster core (e.g. ?????). The presence of a strong lensing cluster in the surveyed field introduces two opposite effects on number counts as compared to blank fields. In one hand, gravitational magnification increases the number of faint sources by improving the detection towards the faint end of the LF. On the other hand, the reduction of the effective surface by the same magnification factor leads to a dilution in observed counts. The global positive/negative magnification bias obviously depends on the slope of the number counts, as pointed out by ?.

This paper addresses the relative efficiency of surveys conducted on blank and lensing fields as a function of the relevant parameters, namely the redshift of the sources, the redshift and properties of the lensing clusters and the survey characteristics (i.e. area, photometric depth...). This calculation requires a detailed simulation of observations using lensing models, and realistic assumptions for the properties of background sources according to present-day observational results, in particular for the luminosity function and typical sizes of $z > 7$ galaxies.

The paper is organized as follows. In Section 2 we describe the simulations performed in order to determine the relative detection efficiency for high- z sources, both in lensing and blank fields. Section 3 presents the results, in particular the detection efficiency achieved as a function of redshift for both sources and lensing clusters, together with a discussion on the influence of lensing cluster properties and field-to-field variance. A discussion is presented in Section 4 on the relative efficiency as a function of survey parameters, and a comparison between simulations and present surveys. Conclusions are given in Section 5.

Throughout this paper, we adopt a concordance cosmological model, with $\Omega_\Lambda = 0.7$, $\Omega_m = 0.3$, and $H_0 = 70 \text{ km s}^{-1} \text{ Mpc}^{-1}$. All magnitudes are given in the AB system. Conversion values between Vega and AB systems for the filters used in this paper are typically $C_{AB} = 0.95, 1.41$ and 1.87 in J, H and K respectively, with $m_{AB} = m_{Vega} + C_{AB}$.

2. Simulations of lensing and blank field observations

2.1. Simulation parameters

This section describes the ingredients used in the simulations to implement different assumptions that would affect our efficiency in detecting high redshift galaxies. There are three important aspects to be considered in the comparison between lensing and blank fields. The first one is the LF and typical sizes of sources. The second one concerns the properties of the lensing clusters, in particular their mass distribution and redshift. The third one is related to the survey parameters, namely the photometric depth and the size of the field. All these aspects are discussed in this section. Table 1 provides the list of parameters used in these simulations, together with the range of values explored.

2.1.1. Source Properties

These simulations are focused on the detection of sources in the redshift range $6 < z < 12$, a relevant domain for spectroscopic follow-up with near-infrared instruments. The lower limit of this redshift domain overlaps with current photometric surveys measuring the LF at $z \sim 6 - 7$ (e.g. ?). However, the LF is still largely unconstrained beyond $z \geq 7$ because of the lack of spectroscopic confirmation of photometric samples and the relatively small size of the surveyed volumes.

The abundance of background sources at these redshifts is given by the luminosity function $\phi(L)$, with L the rest-frame UV luminosity at 1500 \AA . $\phi(L)$ is the most basic description of the galaxy population from an observer point of view. We adopt a parametrization based on the analytical Schechter function (?):

$$\phi(L) dL = \phi^* \left(\frac{L}{L^*}\right)^{-\alpha} \exp\left(-\frac{L}{L^*}\right) d\left(\frac{L}{L^*}\right) \quad (1)$$

The slope at faint luminosities α , the characteristic luminosity L^* and the normalization factor Φ^* have been constrained by several photometric surveys targeting Lyman Break Galaxies (LBG) at high redshift ($z \geq 4$) (? , ? , ? , ? , ?). Three different representative cases are being discussed in our simulations, basically exploring our present knowledge (or lack of knowledge) of the overall shape of the LF at $z \geq 6$ (Table 1):

- An “optimistic” scenario where LBGs show no-evolution from $z \sim 6$, with the LF parameters as determined by ?. Indeed, the LF at $z \sim 6$ found by these authors display the same shape as for $z \sim 3$ (?), but a 3 times smaller normalization factor (but see, e.g., ?).
- A constant LF based on robust measurements by ? at $z \sim 6$ in the Hubble UDF, but using the more recent fit parameters from ?. As compared to model (a), this LF exhibits a turnover towards the bright end.
- The evolutionary LF recently proposed by ?, which includes an important dimming of L^* with increasing redshift. This LF represents the “pessimistic” case with respect to the case (a), with very few high-luminosity galaxies.

The size of the sources is a relevant parameter in this study, given the finite resolution of instruments, and the fact that gravitational magnification preserves surface brightness. High redshift galaxies are expected to be very small at $z > 7$, typically $\lesssim 0.1''$ on the sky (e.g. ?). Recent observations of photometric candidates support this idea (? , ?). This means that a large fraction of lensed sources should remain spatially unresolved in ground-based surveys, even with a strong gravitational magnification (hereafter μ) of ~ 10 . The high resolution capability of JWST is clearly needed for resolving such faint galaxies. In the present simulations and for detection purposes, we consider all sources at $z > 6$ as spatially unresolved. **However, galaxy morphology and image sampling are important when discussing the efficiency of surveys based on space facilities, as discussed in Sect. 4.2.**

2.1.2. Lensing effects

The present simulations address the effect of lensing by a foreground galaxy cluster. Several well-studied examples of lensing clusters are used in order to evaluate the influence of different mass distributions on the final results. Reference lensing clusters usually display several multiply-imaged systems with redshift measurements, allowing us to model their lensing properties accurately. Lensing clusters considered in these simulations have

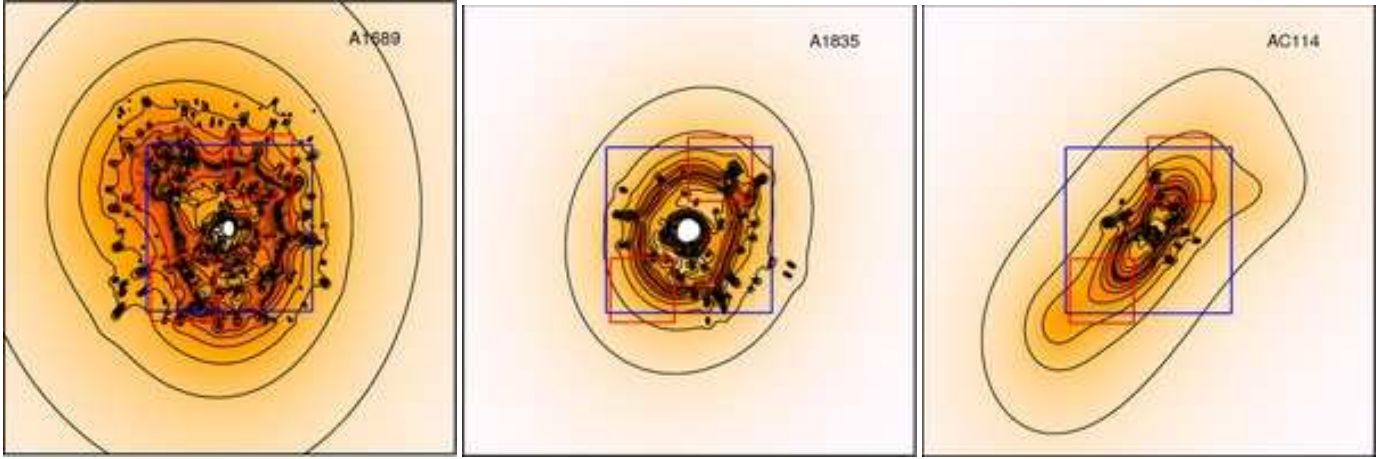


Fig. 1. Magnification maps for the three clusters at $z_s = 8$ used in this study (from left to right A1689, A1835 and AC114 respectively). The global size of the image corresponds to the $6' \times 6'$ FOV whereas the blue and red squares correspond **respectively** to $2.2' \times 2.2'$ and $0.85' \times 0.85'$ FOV (see Sect. 2.1.3). Black contours represent different magnification regimes with increasing magnification values from 0.5 to 3 mags towards the cluster center.

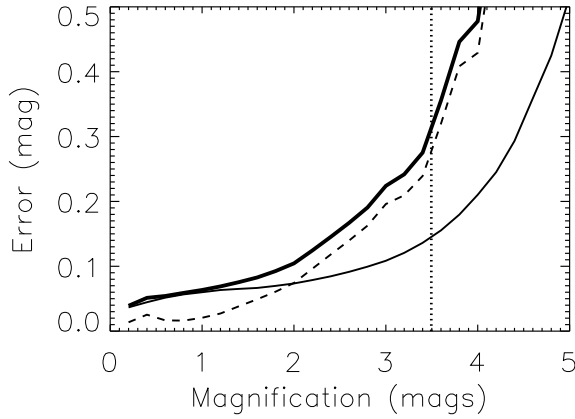


Fig. 2. Typical error in the magnification factor μ , as a function of the magnification for Abell 1835. The solid curve gives the statistical error derived from the MCMC model, while the dashed curve gives the systematic error between two choices of parametrization (see text for details). The thick solid curve is the quadratic sum of both errors, used later in the calculation. The vertical line represents the conservative upper limit of $\mu=25$.

been previously used as gravitational telescopes to search for high redshift dropouts and LAEs. We take advantage of this situation to perform a direct comparison between our estimates and available observations. Finally, we selected clusters with different redshifts, total mass distributions and morphologies, because all of these factors are susceptible to affect the way they magnify background galaxies.

We selected three clusters satisfying the previous criteria: Abell 1689, Abell 1835 and AC114. Abell 1689 is one of the most spectacular gravitational telescopes, having the largest Einstein radius observed to date ($45''$). Both optical dropouts (?) and Lyman- α emitters (?) candidates have been reported in the background of this cluster. Abell 1835 and AC114 are both massive, X-ray luminous clusters, previously used in our deep near-infrared survey for high redshift dropouts with VLT/ISAAC (?).

Finally, these three clusters constitute the sample used by the ZEN2 survey for LAEs in narrow-band images (?).

We used the most recent mass models available for the reference clusters to derive the magnification maps (see Table 1) although simulation results are found to be weakly sensitive to modeling details. Each lensing cluster has been modeled in a similar way using the public lensing software Lenstool², including the new MCMC optimization method (?) providing bayesian estimates on each parameter derived from the model.

The structure of mass models is given by a sum of individual dark matter subcomponents of two different types: large scale components, reproducing the cluster-scale behavior of dark matter, and small scale potentials centered on each cluster galaxy, reproducing the effect of substructure. Each lensing potential is parametrized by a Pseudo-Isothermal Elliptical Mass Distribution model (PIEMD, ?), with a projected mass density Σ given by:

$$\Sigma(x, y) = \frac{\sigma_0^2}{2G} \frac{r_{cut}}{r_{cut} - r_{core}} \left[\frac{1}{(r_{core}^2 + \rho^2)^{1/2}} - \frac{1}{(r_{cut}^2 + \rho^2)^{1/2}} \right], \quad (2)$$

where $\rho^2 = [(x - x_c)/(1 + \epsilon)]^2 + [(y - y_c)/(1 - \epsilon)]^2$, (x_c, y_c) stands for the central position with respect to the BCG (cD or central Bright Cluster Galaxy), $\epsilon = (a - b)/(a + b)$ is the ellipticity, σ_0 is the central velocity dispersion and (r_{core}, r_{cut}) are two characteristic radii. For each lensing potential, the position of x and y axis is given by the position angle θ . The total mass of this profile is proportional to $r_{cut} \sigma_0^2$. The PIEMD parametrization, easily linked to the observed geometry of elliptical lensing galaxies, has been widely used to model the strong lensing properties of massive clusters (???)

A good approximation of the angular distance of the critical line, corresponding to maximum magnification in a flat universe, is given by the Einstein radius θ_E :

$$\theta_E = \frac{4\pi \sigma_0^2}{c^2} \frac{D_A(z_s) - D_A(z_c)}{D_A(z_s)} \quad (3)$$

where $D_A(z)$ stands for the angular distance at redshift z . Source and cluster redshifts are, respectively, z_s and z_c .

² <http://www.oamp.fr/cosmology/lenstool>

The value of θ_E provides a fair estimate of the extension of the strongly magnified area ($\mu > 10$) in the image plane. This value quantifies the power of a gravitational telescope to magnify background sources. Equation 3 shows that, for a given source redshift z_s , θ_E depends on σ_0^2 and on the cluster redshift z_c .

For the three clusters mentioned before, there is a significant variation in redshift ($z_{c0} \sim 0.17 - 0.3$) and in σ_0 (taken from the mass models and reported in Table 1), Abell 1689 being $\sim 30\%$ more massive and less distant than AC114, for instance. We explored a wider range of cluster redshifts in our simulations, producing fiducial lensing clusters by adjusting z_c between 0.1 and 0.8 in the three cases, assuming no evolution in the cluster properties. This is clearly an over-simplistic and conservative assumption, as massive clusters of galaxies undergo a dynamical evolution during cluster assembly at high redshift.

The relevance of the MCMC approach of the cluster mass modeling is to derive relevant statistical errors in the magnification factors. Fig. 2 illustrates the typical errors in the magnification at a given position of the lensing field, in the case of the lensing cluster Abell 1835. Similar errors in the magnification are found in the case of the two other clusters, as all of them have ≥ 5 multiple systems constraining independent regions of the cluster cores, the majority of them having spectroscopic redshifts. For reasonable magnification factors (≤ 3 magnitudes), this error is always smaller than 0.1 magnitudes (or $\sim 10\%$ relative error in flux). For larger magnifications factors, corresponding to the vicinity ($\leq 2''$) of the critical lines, the error can reach much higher values. The *systematic errors* in the magnification factors, due to the choice of the parametrization when building the lensing model, can be estimated for Abell 1835, which have been modelled by Richard et al.(2009, submitted) using both PIEMD profiles and Navarro-Frenk-White (NFW, ?) profiles for the cluster-scale mass distributions. The comparison of magnifications from both models, at a given position, gives an estimate of the systematic error in the magnification, which dominate at large μ (Figure 2), reaching typical values of 0.3 magnitudes. We adopted a conservative upper limit of $\mu = 25$ to avoid singularities in the magnification determination. This is justified by the finite resolution of instruments, and the limited knowledge on the precise location of the critical lines at such high z (typically $\sim 1''$). The affected area is not significant once averaged over the entire field of view. Nevertheless, the quadratic sum of the statistical and systematic errors in the magnification is later used to derive errors in the number density calculations when looking at lensing fields.

2.1.3. Survey Simulations

In addition to cluster and source properties, the main ingredients to consider in the simulations are the following:

- The typical field of view (FOV) of near-IR instruments for 8-10 meters class telescopes and space facilities. The former typically range between a few and $10'$ on a side (e.g. $\sim 6' \times 6'$ for EMIR/GTC, $\sim 7' \times 7'$ for Hawk-I/VLT). The later are usually smaller (e.g. $\sim 1' \times 1'$ for NICMOS/HST, $\sim 2.2' \times 2.2'$ for JWST or WFC3-IR/HST). Fig. 1 presents the comparison between these typical FOV values and the magnification regimes found in lensing clusters. The references for the different instruments used in the simulations are presented in Table 1.
- The limiting magnitudes of present near-IR surveys based on ground-based and space observations tailored to select LBGs

at $z \geq 6$. The former are typically limited to $AB \sim 25.5$ (see Sect. 2.1.1), whereas the later could reach as deep as $AB \sim 29$ with JWST (see Sect. 3.5 and 4).

The shallow magnitude limit of $AB \sim 25.5$ achieved on ground-based observations should allow us to detect galaxies with a UV continuum corresponding to a SFR $\sim 40/\mu M_\odot/\text{yr}$ at $z \sim 10$, whereas the typical depth for JWST should be $\sim 1/\mu M_\odot/\text{yr}$.

We can relate the UV luminosities of high redshift galaxies with the expected Lyman- α emission line by converting L into a star formation rate SFR using the calibrations from ?:

$$\text{SFR}(M_\odot \text{ yr}^{-1}) = 1.4 \cdot 10^{-28} L \text{ (ergs Hz}^{-1} \text{ s}^{-1}) \quad (4)$$

The expected Lyman- α luminosity produced at the equilibrium can be written as:

$$L_{Ly_\alpha} \text{ (ergs s}^{-1}) = (1 - f_{esc}) f_\alpha \text{ SFR}(M_\odot \text{ yr}^{-1}) \quad (5)$$

where f_{esc} is the escape fraction of Lyman- α photons and f_α the Lyman- α production rate per unit of star formation. Assuming no reddening, the typical values for f_α range between $2.44 \cdot 10^{42}$ and $6.80 \cdot 10^{42} \text{ ergs.s}^{-1}$ (?). We use these scaling relations when discussing the detectability of Lyman- α in lensing fields.

2.2. Implementation

We explicitly compute the expected number counts $N(z, m_0)$ of sources at the redshift z brighter than a limiting magnitude m_0 by a pixel-to-pixel integration of the (magnified) source plane as a function of redshift, using the sources and lensing cluster models described in the previous subsections. **Number counts are integrated hereafter within a redshift slice $\Delta z = 1$ around z , unless otherwise indicated.** With respect to a blank field, the magnification pushes the limit of integration to fainter magnitudes, whereas the dilution effect reduces the effective volume by the same factor.

An important effect to take into account in cluster fields is light contamination coming from the large number of bright cluster galaxies, which reduces the surface area reaching the maximum depth, and consequently prevents the detection of faint objects, especially in the vicinity of the cluster center. This contamination effect can be as high as 20% of the total surface (?), whereas it is almost negligible in blank field surveys.

We created bright-objects masks by measuring the central position (x_c, y_c) and shape parameters (a, b, θ) of galaxies in the three cluster fields, each object being approximated by an ellipse during this process. We used SExtractor (?) in combination with reasonably deep and wide ground-based images available from the ESO archive (larger than $6' \times 6'$ used in these simulations). The characteristics of these images are summarized in Table 2. They were reduced using standard IRAF routines. The image mask $M(x, y)$ produced is the superposition of ellipses for all objects in the photometric catalog where pixels belonging to object domains were flagged. Ellipses correspond to $1 - \sigma$ isophotes over the background sky. In other words, only images lying on empty regions have been included in the lensed samples, thus providing a lower limit for detections in lensing fields. This fractional area covered by foreground galaxies ranges between 6% and 12% depending on the cluster as well as the size and central position of the field of view (Table 2). The largest hidden area corresponds to the smaller field of view centered on the cluster (JWST-like). NICMOS pointings are even smaller, but

Parameter	Explored range				Reference
LF (a)	(< z >= 6.0)	$\alpha = 1.6,$	$\phi^* = 0.4 \cdot 10^{-3} \text{ Mpc}^{-3},$	$M^* = -21.07$?
LF (b)	(< z >= 5.9)	$\alpha = 1.74,$	$\phi^* = 1.1 \cdot 10^{-3} \text{ Mpc}^{-3},$	$M^* = -20.24$?
LF (c)	(3.8 < z < 7.4)	$\alpha = 1.74,$	$\phi^* = 1.1 \cdot 10^{-3} \text{ Mpc}^{-3},$	$M^* = -21.02 + 0.36 (z - 3.8)$?
Source redshift	$z_s = 6 - 12$				
Lensing cluster	Abell 1689	$z_{c0} = 0.178,$	$\sigma_0 = 1320 \text{ km/s},$	$N_{\text{sub}} = 266$?
	Abell 1835	$z_{c0} = 0.25,$	$\sigma_0 = 1210 \text{ km/s},$	$N_{\text{sub}} = 90$	Smith(2005) Richard(2009)
	AC114	$z_{c0} = 0.31,$	$\sigma_0 = 1080 \text{ km/s},$	$N_{\text{sub}} = 28$?
Cluster redshift z_c	0.1 – 0.8				
Survey strategy	GTC/EMIR	FOV=6' × 6',	pix: 0.2''/pixel,	depth: $\Delta z = 1$?
	JWST/NIRCam	FOV=2.2' × 2.2',	pix: 0.06''/pixel,	depth: $\Delta z = 1$?
	HST/NICMOS	FOV=0.85' × 0.85',	pix: 0.2''/pixel,	depth: $\Delta z = 1$?

Table 1. Summary of the parameters included in our simulations. For each entry, we give the range of values explored and reference to the relevant publication. **LF(a) is the same as in ?, but Φ^* is a factor of 3 smaller (see Sect. 2.1.1).**

Cluster	Instrument and Reference	Filter	Exposure Time	Depth (5σ , AB)	Mask area 6' × 6',	2.2' × 2.2',	0.85' × 0.85'
Abell 1689	ISAAC/VLT ?	SZ	14.4 ksec	26.0	7%	12%	10%
Abell 1835	FORS/VLT ?	V	19.6 ksec	27.0	6%	10%	8%
AC114	SOFI/NTT ?	K	10.8 ksec	22.0	6%	9%	7%

Table 2. Characteristics of the images used to produce the foreground object's mask for each cluster field, the three last columns representing the fractional surface area covered by the foreground galaxies in each cluster, for the three reference field of view, EMIR-like, JWST-like and NICMOS-like respectively

they are centered on the critical lines in our study and avoid the crowded central regions of the cluster. In blank fields, this value doesn't exceed 3-4%. In the next sections, we have taken into account this correction in the calculations of number counts, both in blank fields and lensing fields.

Including the object mask $M(x, y)$, number counts $N(z, m_0)$ are given by the following expression:

$$N(z, m_0) = \phi^* \int_{x,y} M(x, y) \int_{L(\mu, z, m_0)}^{\infty} \frac{Cv(x, y, z)}{\mu(x, y, z)} \left(\frac{L(\mu, z, m_0)}{L^*} \right)^\alpha \cdot \exp\left(-\frac{L(\mu, z, m_0)}{L^*}\right) d\left(\frac{L}{L^*}\right) dx dy \quad (6)$$

where $\mu(x, y, z)$ is the magnification induced by the lensing field, $Cv(x, y, z)$ is the covolume associated with a single spatial resolution element pixel with $\Delta z = 1$ and (L^*, ϕ^*, α) are the parameters of the LF.

A conservative upper limit of $\mu = 25$ was adopted in the vicinity of the critical lines in order to avoid singularities in the magnification/dilution determination. This is justified by the finite resolution of instruments, and the limited knowledge on the precise location of the critical lines at such high- z (typically $\sim 1''$).

When exploring the impact of cluster redshift, we assumed no evolution in the physical parameters r_{core} , r_{cut} and σ of individual potentials, thus keeping the total mass of the cluster constant in this process. Variations in z_c from the original redshift z_{c0} of the cluster produce a geometrical effect on the central positions (x_{ci}, y_{ci}) of each PIEMD potential i , measured from a reference position (x_0, y_0) which coincides with the center of the BCG:

$$\begin{aligned} x_{ci}(z_c) - x_0 &= \frac{D_A(z_c)}{D_A(z_{c0})} (x_{ci}(z_{c0}) - x_0) \\ y_{ci}(z_c) - y_0 &= \frac{D_A(z_c)}{D_A(z_{c0})} (y_{ci}(z_{c0}) - y_0) \end{aligned} \quad (7)$$

Similarly, we produced fiducial masks at different cluster redshifts z_c based on the reference mask at z_{c0} and adjusting the parameters of the galaxy ellipses, applying the same scaling relations on (x_c, y_c) . The sizes a and b were scaled by $D_A(z_{c0})/D_A(z_c)$.

3. Results

As discussed above, lensing introduces two opposite trends on the observed sample as compared to blank fields : gravitational magnification by a factor μ , increasing the expected number of sources and thus the total number of objects, and reduction of the effective surface by the same factor thus leading to a dilution in expected counts. This effect was first studied by ?.

If we consider, for a given redshift z , the cumulative abundance of sources (per unit of solid angle) with a luminosity greater than L and by redshift bin, the magnification bias will change depending on μ according to

$$n'_{\text{lensing}}(> L, z) = N(> L/\mu, z)/\mu(z) \quad (8)$$

$$\simeq \mu^{\beta(z)-1} n(> L, z) \quad (9)$$

where β is the logarithmic slope of $n(L, z)$ assuming that this function is well represented by a power law in this interval of luminosities : $\beta = -d(\ln n)/d(\ln L)$. The effect on number counts is as follows:

- if $\beta(z) > 1$ the number counts will increase with respect to a blank field, and
- if $\beta(z) < 1$ there will be an opposite trend: i.e. a depletion in number counts

With increasing depth, the β parameter will decrease in a greater or lesser amount depending on the LF, the FOV (because it determines the mean μ) and the redshift of sources, leading to a depletion in number counts in lensing fields as compared to a blank fields. With these simple considerations, we expect lensing clusters to be more efficient than blank fields in relatively shallow surveys.

The efficiency of using lensing clusters as gravitational telescopes to find high- z galaxies can be quantified with simple assumptions taking advantage of the properties of the sources explained in Sect. 2. In this section, we discuss the results obtained by exploring the relevant intervals in the parameter space. We present a comparison between the number counts expected in lensing and blank fields, as a function of source redshift and for different LFs. The influence of lensing cluster properties and redshift is also studied, as well as the expected field to field variance.

3.1. The influence of the field of view

Here we discuss on the influence of the FOV in the simulations for typical surveys. The influence of the limiting magnitude will be discussed in Sect. 4. Three different FOV are considered here:

- $6' \times 6'$ (“EMIR-like” aperture)
- $2.2' \times 2.2'$ (“JWST-like” or “WFC3/HST” aperture)
- $0.85' \times 0.85'$ (NICMOS/HST aperture)

In the last case, the FOV is centered along the critical lines in order to achieve the highest mean magnification (Fig. 1).

The limiting magnitude is $AB \lesssim 25.5$, a value ranging between $L_*(z=6)$ and $3L_* - 5L_*$ at redshift $z_s \sim 7$ to 10. The cluster model corresponds to AC114, but the results are qualitatively the same with other models. Fig. 3 displays the relative gain in number counts between lensing and blank fields as a function of sources redshift, for the three values of the FOV mentioned above, and for the three LF adopted in the present simulations.

The largest gain is obtained for the smallest FOV, as expected from geometrical considerations, because the mean magnification decreases with increasing FOV, and in this case $\beta \gtrsim 1$ given the shallow depth ($AB \lesssim 25.5$). For a given FOV, the difference between lensing and blank field results strongly depends on the shape of the LF. Hence, the comparison between lensing and blank field number counts is likely to yield strong constraints on the LF, provided that field-to-field variance is small enough. This issue is addressed in Sect. 3.5. In the following subsections, we adopt a $6' \times 6'$ FOV unless otherwise indicated.

3.2. Lensing versus Blank field efficiency

In this section, we study the effects of lensing clusters on source counts, using lensing models for the three reference clusters. We compute the expected number of sources brighter than m_0 , the typical apparent magnitude reached in ground-based near-IR surveys. The comparison between expected number counts of galaxies in a typical $6' \times 6'$ FOV, up to $m_0 \leq 25.5$, per redshift bin $\Delta z = 1$, in a blank field and in the field of a strong lensing cluster are presented in Fig. 4 in logarithmic scale.

We also estimate the error on number counts due to the uncertainties on magnification factors (Sect. 2.1.2). The choice of the LF has no influence on the following results. Field to field variance dominate the error budget whatever the regime. Statistical errors and systematic errors on lensing models are smaller but not negligible as their contribution is less sensitive than field to field variance to the number of objects. In particular, when the number of detected sources is relatively high (i.e. when field to field variance is relatively small), they reach $\sim 15\%$ of the error budget in the worst cases (e.g. for LF(a) at $z \sim 6$ in a $6' \times 6'$ FOV), and typically $\leq 2\%$ when the number of sources is relatively small (e.g. for LF(c) at $z \sim 8$, for any FOV).

As shown in Fig. 4, the presence of a strong lensing cluster has a dramatic effect on the observed number of sources, with

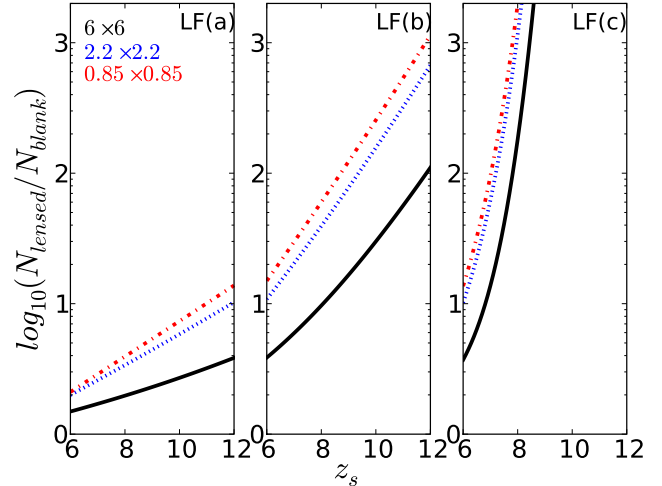


Fig. 3. Relative gain in number counts between lensing and blank fields as a function of the source redshift, with $\Delta z = 1$, for different fields of view: $6' \times 6'$ in black, $2.2' \times 2.2'$ in blue dotted line and $0.85' \times 0.85'$ in red dot-dashed line (from bottom to top). The three panels from left to right represent the 3 values of the LF, (a), (b) and (c) respectively.

a positive magnification effect. Strong lensing fields are a factor between 2 and 10 more efficient than blank fields for the most optimistic LF (a), the gain increasing for the LFs (b) and (c), reaching a factor between 10 and 100 in the $z \sim 6 - 12$ domain. A positive magnification bias is observed, increasing with the redshift of the sources, and also increasing from optimistic to pessimistic values of the LF. This trend is indeed expected given the steep shape of the LF around the typical luminosity limits achieved in ground-based “shallow” surveys.

Quantitatively (cf Table 3 and Fig. 4), if the LF for LBGs was nearly constant between $z \sim 4$ and 12, we could always detect at least one object over the redshift range of interest. At $z \sim 6$, we expect up to between 7-10 sources, and at $z \sim 12$ between 0.7 and 1 galaxies should be detected in a lensing field. Even in a blank field, until $z \sim 8 - 9$ at least one LBG could be found in such a large field of view. With more realistic (pessimistic) values of the LF (e.g. ??), blank fields are particularly inefficient as compared to lensing fields. The size of the surveyed area would need to increase by at least a factor of ~ 10 in order to reach a number of detections similar to the one achieved in a lensing field around $z \sim 6 - 8$, and this factor increases with redshift. Note however that given a limiting (apparent) magnitude, blank and lensing fields do not explore the same intrinsic luminosities (see also Sect.4).

As seen in Fig. 4 and Table 3, there are also some differences between the results found in the three lensing clusters, although they are smaller than the differences between lensing and blank fields for a given LF. The number of expected sources behind A1689 is a factor of two (at $z \sim 6$) and a factor of three ($z \sim 8$) larger than in the other clusters for the realistic LFs (b) and (c), whereas the difference is only $\sim 10 - 30\%$ for LF (a). The influence of lensing properties is studied in Sect. 3.4.

From the results above, it seems that lensing fields allow us to detect a larger number of $z \gtrsim 6$ sources based on their UV continuum, with some cluster to cluster differences. This result is essentially due to the shape of the LF. For magnitude limited samples selected within a given field of view, the positive mag-

nification bias increases with the redshift of the sources and decreases with both the depth of the survey and the size of the surveyed area. The last trend is purely geometric, as discussed in the previous section. The differential behaviour between blank and lensing regimes strongly depends on the shape of the LF. The comparison between blank and lensing field observations could be of potential interest in constraining the LF, provided that field-to-field variance is sufficiently small. This issue is addressed in the following sections.

3.3. Redshift of the lensing cluster

The redshift of the lensing cluster is a potentially important parameter when defining an “ideal” sample of gravitational telescopes. Based on geometrical considerations, we expect the magnification bias to decrease with cluster redshift (z_c) after reaching a maximum efficiency at some point, depending on cluster properties and the size of the surveyed field. The field of view considered here is typically a few square arcminutes, essentially including the region around the critical lines where magnification factors are the highest. Further down, we study the impact of z_c on the magnification bias.

Using the non-evolution assumption presented in Sect. 2.2, we compute the expected number counts for the three reference models (A1689, A1835 and AC114) with cluster redshifts ranging between $z=0.1$ and 0.8 , with a $\Delta z = 0.1$ step. A step $\Delta z = 0.05$ is used in the $z=0.1-0.3$ interval, in order to refine the sampling around the maximum value. We use the same depth and field size as in previous section. The effect of cluster redshift is clearly seen in Fig. 6 representing the number of objects as a function of cluster redshift (for the three reference models), at a fixed redshift of $z=8$ for sources.

The global effect of z_c on number counts as a function of the source redshift is displayed in Fig. 5. This figure directly compares to Fig. 4 in the previous section. Table 4 presents the z_c value which corresponds to a maximum in the expected number counts at $z=8$. This value depends slightly on the source redshift and LF. In addition to the $\Delta z_c = \pm 0.05$ when changing the LF, there is also an increase of z_c with higher values of z_s , up to $+0.05$ towards $z_s = 12$. The search efficiency of distant galaxies in lensing fields is maximised when using clusters at low redshift ($z_c \sim 0.1-0.3$). Although the field of view considered here is relatively large for near-IR surveys and close to present-day cameras, it is the limiting factor at $z_c \leq 0.1$, where an increasing fraction of the strong-magnification area is lost with decreasing z_c . Also, in this z_c regime, the field of view concentrates on the central region of the cluster where bright cluster galaxies mask an important fraction of the strong-magnification area. The high magnification region represents an increasingly small percentage of the field with increasing z_c . Number counts in this regime asymptotically tend towards a limiting value with increasing z_c (Fig. 5), which still is a substantial gain with respect to a blank field of the same size. The non-evolution assumption in cluster properties has a weak effect on this conclusion. Indeed, clusters far from relaxation will be even more ineffective as a gravitational lenses in the strongest magnification regime. The results obtained are hence an optimistic upper limit on number counts for realistic clusters beyond the optimal regime $z_c \sim 0.1-0.3$.

3.4. Influence of lensing cluster properties

In this section we focus on the differences between lensing cluster properties and their influence on expected source counts. As

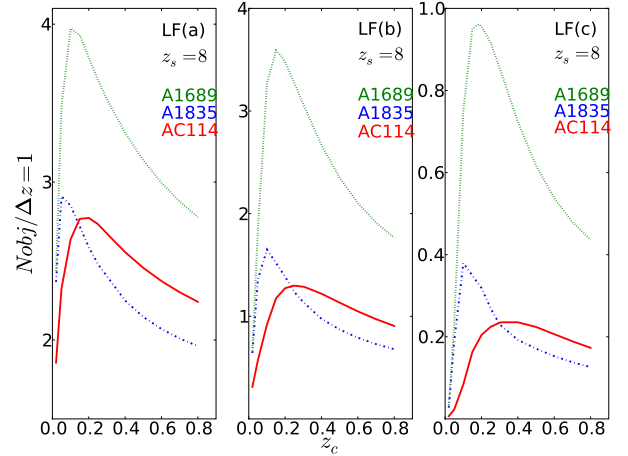


Fig. 6. Expected number of objects as a function of the cluster redshift for a fixed redshift of sources ($z_s = 8$) and with the same depth and field size as in previous section. Three cluster models are displayed: A1689 (green dotted line), A1835 (blue dot-dashed line) and AC114 (red solid line). Panels from left to right display respectively LF (a), (b) and (c).

Table 4. Redshift of the cluster which maximizes the number of objects detected at $z=8$ for the three LF respectively from top to bottom (a), (b) and (c)

LF	A1689	A1835	AC114
actual z_c	0.184	0.253	0.310
(a)	0.10	0.05	0.25
(b)	0.15	0.10	0.25
(c)	0.20	0.10	0.30

seen in previous sections, A1689-like clusters are expected to be more efficient irrespective of the cluster redshift. To understand this effect, we study the magnification regimes for a reference source plane fixed at $z_s = 8$. The distribution of the magnification regimes in the image plane varies from cluster to cluster. Histograms in Fig. 7 represent the percentage of the image plane (for the $6' \times 6'$ FOV) as a function of the associated magnification. To perform this calculation, cluster redshifts were standardized to identical values for a better understanding of the phenomenon. As seen in the figure, A1689 shows a different regime at $z_c \leq 0.8$ as compared to the other clusters. While the percentage of the surface affected by strong magnification ($\mu > 10$) does not exceed 5% in A1835 and AC114, it is as high as 8 – 10% in A1689, depending on z_c . Nevertheless, this difference between clusters tends to fade with increasing cluster redshift due to projection effects, the fraction of highly magnified pixels becoming smaller with respect to the whole FOV. We also note that AC114 and A1835 models have a similar behaviour with minor differences (A1835-like clusters being more effective at very low z_c while the AC114 model is more efficient for intermediate z_c).

Another way of understanding this phenomenon is presented in the Fig. 8, where the effective covolume for the $6' \times 6'$ FOV is traced as a function of the effective magnitude, for a magnitude-limited survey with $AB \leq 25.5$. Magnification in lensing fields provides an enhanced depth for a magnitude-limited survey, where the effective (lensing corrected) covolume surveyed decreases with increasing effective depth. The behavior of A1689 in Fig. 8 illustrates the situation for this particu-

Table 3. Total number of objects expected within a $6' \times 6'$ FOV (up to $H_{AB} \leq 25.5$, $\Delta z = 1$) from the three LF adopted in these simulations. **Uncertainties correspond to $1 - \sigma$ level in magnification and lensing modeling**

z	Blank field			Lensed field								
	6	7	8	A1689 $z_c = 0.184$			A1835 $z_c = 0.253$			AC114 $z_c = 0.310$		
				6	7	8	6	7	8	6	7	8
LF (a)	4.61	2.43	1.31	$8.63^{+0.86}_{-0.76}$	$5.66^{+0.62}_{-0.59}$	$3.83^{+0.47}_{-0.44}$	$6.69^{+0.61}_{-0.58}$	$4.00^{+0.42}_{-0.39}$	$2.48^{+0.29}_{-0.27}$	$7.07^{+0.65}_{-0.61}$	$4.27^{+0.44}_{-0.41}$	$2.66^{+0.31}_{-0.29}$
LF (b)	1.30	0.39	0.13	$10.07^{+1.808}_{-1.608}$	$5.66^{+1.24}_{-1.08}$	$3.53^{+0.89}_{-0.75}$	$4.69^{+0.78}_{-0.69}$	$2.21^{+0.47}_{-0.41}$	$1.23^{+0.30}_{-0.25}$	$4.96^{+0.80}_{-0.71}$	$2.35^{+0.47}_{-0.41}$	$1.28^{+0.30}_{-0.25}$
LF (c)	1.30	0.07	< 0.01	$10.07^{+1.808}_{-1.608}$	$3.08^{+0.84}_{-0.71}$	$0.96^{+0.38}_{-0.29}$	$4.69^{+0.78}_{-0.69}$	$1.04^{+0.27}_{-0.23}$	$0.28^{+0.10}_{-0.08}$	$4.96^{+0.80}_{-0.71}$	$1.03^{+0.26}_{-0.22}$	$0.24^{+0.09}_{-0.07}$

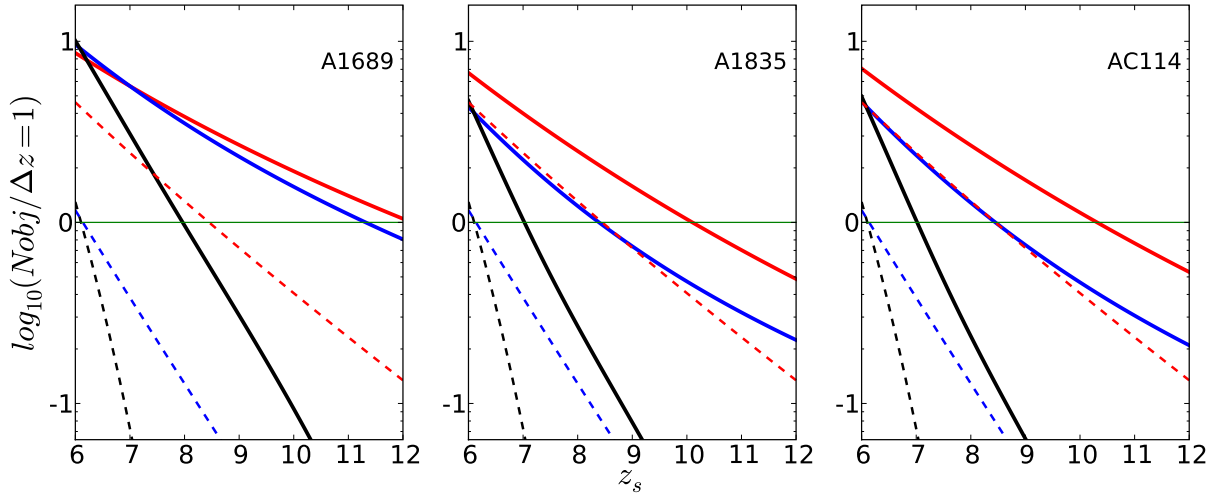


Fig. 4. Comparison between the expected number counts of galaxies in a typical $6' \times 6'$ FOV, up to $H_{AB} \leq 25.5$, per redshift bin $\Delta z = 1$, in a blank field (dashed lines) and in the field of lensing cluster (solid lines) (left to right respectively A1689, A1835 and AC114). Expected counts are obtained by the integration of 3 different luminosity functions (a), (b) and (c) from top to bottom. The limit of one source detected in the field of view is indicated by an horizontal line to guide the eye.

larly efficient cluster, allowing us to study a $\sim 100 Mpc^3$ volume to $AB \sim 29.0$ with a relatively modest observational investment. Except for some particularly efficient lensing clusters (such as A1689), most lensing fields should behave the same way as A1835 or AC114.

3.5. Field to field variance

In this section, we address the expected field-to-field variance affecting our previous results in order to estimate its impact in blank and lensed fields. We used two different approaches: the two-point correlation function estimation proposed by ? and a pencil beam tracer through the Millenium simulation.

The first estimate is based on the method implemented by ?. This method for the calculation of the cosmic variance is based on the two points correlation function $\xi(r)$ of the sample (?). Field o field variance is given by

$$\sigma_v^2 = \frac{\int_V \int_V d^3x_1 d^3x_2 \xi(|\mathbf{x}_1 - \mathbf{x}_2|)}{\int_V \int_V d^3x_1 d^3x_2} \quad (10)$$

where V represents the volume of the survey.

We focus on the redshift interval $z \sim 6 - 8$ using the present “shallow” survey parameters (see Sect. 4.1), both in blank and lensing fields. Here we use the same parameters as in Sect. 3.2, i.e. typical FOV $6' \times 6'$, $m_{AB} = 25.5$ and $\Delta z = 1$.

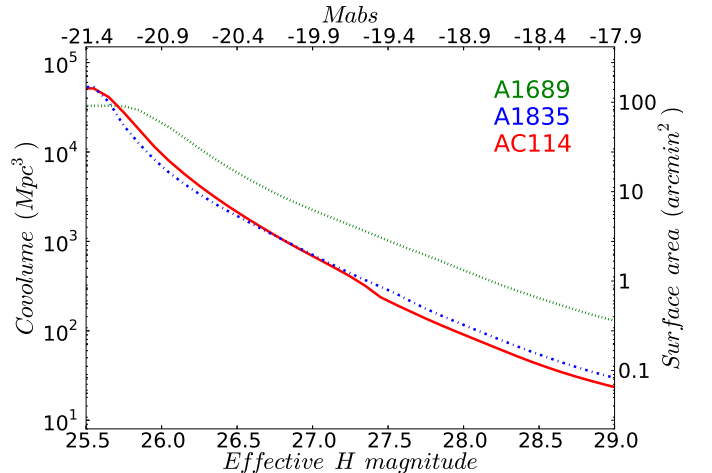


Fig. 8. The effective (lensing corrected) covolume sampled at $z=6.5-7.5$ by each cluster is given as a function of effective H_{AB} magnitude limit, for a magnitude-limited survey of $6' \times 6'$ FOV with $H_{AB} \leq 25.5$. The three clusters are displayed with the same colors and line codes as in Fig. 6.

We define the total fractional error of the counts N following ? (this is the so-called field-to-field standard deviation or the,

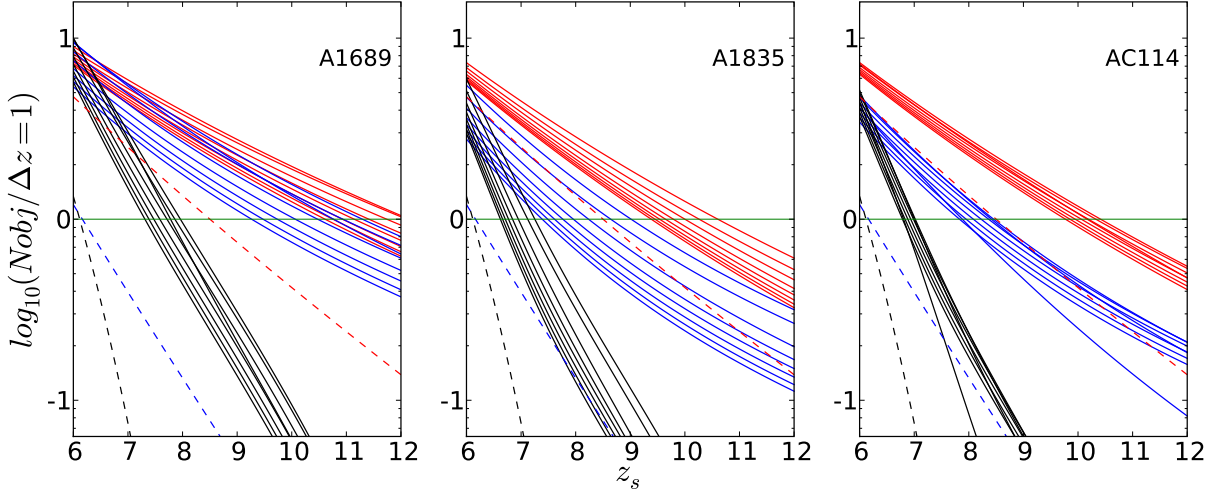


Fig. 5. The same as Fig. 4 but using different assumptions for the redshift of the clusters, with $z_c \in [0.1, 0.8]$ and a 0.1 step (for more details see Sect. 3.3)

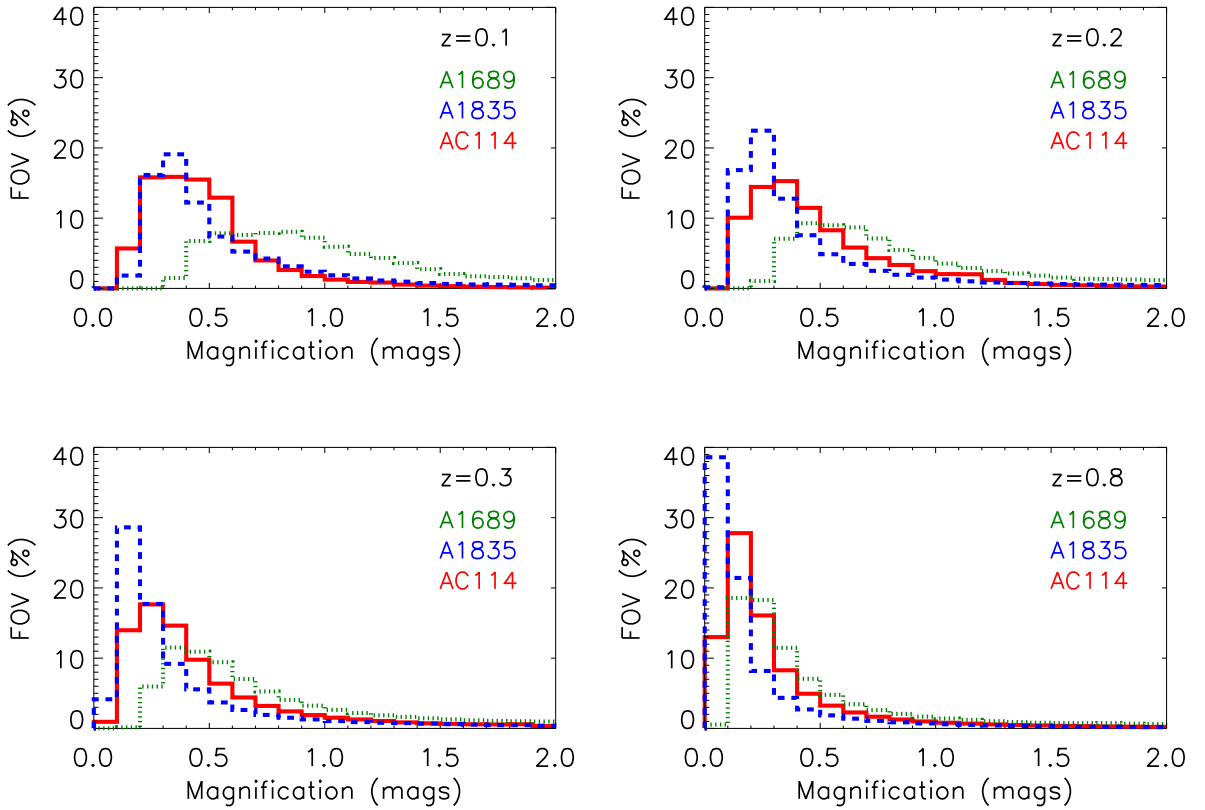


Fig. 7. Histogram representing the percentage of the surface ($6' \times 6'$ FOV) as a function of the magnification for different redshifts of cluster ($z_c=0.1, 0.2, 0.3, 0.8$), using the same color codes for the three clusters as in Fig. 6 (A1689: green dotted line, A1835: blue dot-dashed line and AC114: red solid line)

again, improperly called "cosmic variance") as :

$$v_r = \frac{\sqrt{\langle N^2 \rangle - \langle N \rangle^2}}{\langle N \rangle} \quad (11)$$

Results are presented in the Table 5 for the three LF considered, and for the three typical clusters used in the simulations.

We note an important field to field variance with such a limiting magnitude ($AB \sim 25.5$) either in blank or lensing fields due to the small number counts previously derived from calculations (see Table 3). Nevertheless, the variance is smaller behind gravitational telescopes with the same differential trends mentioned before between the three clusters, i.e. A1689 exhibits a

stronger magnification bias (see Sect. 3.4) than the other clusters which have a similar behavior. Besides, with increasing redshift of sources, the expected number counts decrease leading to a larger field to field variance.

The second estimate was based on the Millennium simulation, carried out by the Virgo Consortium and described in detail in ? and ?. The simulation follows $N = 2160^3$ particles of mass $8.6 \cdot 10^8 h^{-1} M_\odot$ within a co-moving box of size $500 h^{-1} Mpc$ on a side. The cosmological model is a Λ CDM model with small differences in the cosmological parameters adopted in Sect. 1, but without impact on the final results. These cosmological parameters are consistent with recent determinations from the combined analysis of the 2dFGRS and 3rd year WMAP data (?). Given its high resolution and large volume, the Millennium simulation allows us to follow in enough details the formation history of a representative sample of high redshift galaxy environments. With these prescriptions and a realistic beam tracer we can study the field-to-field variations in the number counts of star forming galaxies at the epoch of interest.

Our pencil beam tracer is similar to the one developed by ?. We trace through the simulation box a parallelepiped where the base is a parallelogram, whose size is given by the reference field of view in comoving units, and the depth is the comoving depth arbitrarily taken to $\Delta z = 1$. The variation of angular distance versus redshift in the redshift interval of the selection window considered was properly taken into account. This $500 h^{-1} Mpc$ edge box is more than 2000 times larger than the effective volume probed by the $6' \times 6'$ FOV : $\sim 10.7 \times 10.7 \times 323.0 (Mpc/h)^3$ for instance at $z=6$. We carried out 10000 Monte Carlo realizations of the beam-tracing procedure by randomly varying the initial position of the beam in order to calculate the typical number counts of galaxies and the associated standard deviation in the field of view with the same hypothesis.

Although this procedure is well suited to determine the field to field variance, several studies on this topic suggest an over-prediction on the abundance of massive galaxies at high redshift (e.g. ?). For this reason, we consider this second approach as a cross check yielding a lower limit for the field to field variance. Results obtained from the Millennium simulation are displayed in Table 6. They are in fair agreement with those obtained with the first method.

Field to field variance on number counts obviously depends on the depth of the survey. In order to compare our results with existing photometric surveys, we calculated the number counts of sources in blank and lensing fields (here AC114) with the evolving LF(c) for different deeper magnitude limits ($m_{lim} = 27.0, 28.0$ and 29.0), in our reference field of view using the same parameters as in Sect. 3.2 (see Table 7). The correlation function was used to derive the cosmic variance. The total fractional error (v_r) strongly decreases with increasing photometric depth, as expected given the increasing number of sources detected in such a large FOV (e.g. at $m_{lim} = 29.0$, the total number of sources is 1000 times larger than in the ‘‘shallow’’ survey), both in blank and lensing fields. The fractional error appears slightly larger in lensing than in blank fields at $z=6$, but this effect reverses with increasing source redshift. These estimates for the blank field can be compared to present-day surveys. For instance, the field to field variations obtained by ? for a single ACS pointing at $z \sim 6$ for a limiting magnitude $z_{850} \sim 29$ is 35%. Using the same observational constraints (FOV, depth, ...), our simulations yield a $v_r \sim 30\%$, a value which is smaller but fairly compatible with the results quoted by ?.

Table 6. Number counts for $m_{AB} \leq 25.5$ and field to field uncertainties (v_r) calculated from the Millenium simulation in a $6' \times 6'$ blank field, for different source redshifts

	$z_s = 6$	$z_s = 7$	$z_s = 8$
$\langle N \rangle$	2.74	1.10	0.39
v_r	68%	100%	168%

4. Discussion

4.1. Survey parameters and efficiency

As discussed in Sect. 2.1.3, the FOV and the limiting magnitude are two important survey parameters used in these simulations. The influence of the FOV for a fixed limiting magnitude strongly depends on the shape of the LF. The highest ratio in number counts between lensing and blank fields can be achieved with the smallest FOV due to simple geometrical considerations. This section specifically addresses the evolution on the survey efficiency in lensing and blank fields as a function of the limiting magnitude.

For these purposes, we use the same approach as in Sect. 3.2 to derive number counts within a $6' \times 6'$ FOV in blank fields and behind lensing clusters. AC114 is used here as a representative lensing cluster. Fig. 9 displays the expected number counts as a function of the redshift of sources, for different depths ($AB \leq 26.0, 27.0, 28.0$ and 29.0). An opposite trend between blank and lensing fields appears, depending once again on the LF and on the redshift of sources. With increasing limiting magnitude, the efficiency of the survey towards a foreground cluster diminishes and becomes less effective than in blank fields leading to a negative magnification bias for the faintest limiting magnitudes (e.g. for LF(a) between $AB \sim 27.0 - 28.0$, for LF(b) between $AB \sim 28.0 - 29.0$ and for LF(c) beyond $AB \sim 29.0$). This trend, however, is highly sensitive to the FOV. In particular, the negative magnification bias appears towards the typical magnitudes achieved by space facilities (JWST). Fig. 10 displays the same results as in Fig. 9 but for a $2.2' \times 2.2'$ FOV (JWST-like). The main characteristics remain broadly unchanged, the general trends are just exacerbated, the inversion happening to lesser depth.

Lensing and blank field surveys do not explore the same intrinsic luminosities, as shown in Fig. 11 and 12. These figures compare the expected number density of sources as a function of their intrinsic UV luminosity (or equivalent SFR) for different limiting magnitudes ranging from $AB \leq 25.5$ to 29.0 . In the case of lensing fields, two different results are given, depending on the FOV around the cluster center. In this particular case, the source redshift is arbitrarily fixed to $z_s = 8$, assuming a strongly evolving LF(c), and the lensing cluster is AC114.

In summary, the number of $z > 8$ sources expected at the typical depth of JWST ($AB \sim 28 - 29$) is much higher in lensing than in blank fields if the UV LF is rapidly evolving with redshift (LF(c)), as suggested by ?. The trend should be the opposite if the LF remains unchanged between $z \sim 6$ and 8 . Lensing clusters are the only way to study the faintest building blocks of galaxies, with typical $SFR \leq 0.1$ to $1 M_\odot/yr$. On the contrary, wide field surveys covering 10^3 to $10^4 arcmin^{-2}$ are needed to set reliable constraints on the brightest part of the LF at $z \geq 6$, i.e. for galaxies with $SFR \geq 10 M_\odot/yr$.

Table 5. Number counts, field to field variance calculated with the correlation function both in blank and lensing fields, for $z = 6, 7$ and 8 within a $6' \times 6'$ FOV, for a shallow survey with $AB \leq 25.5$. **Field to field variance in lensing fields includes $1 - \sigma$ magnification errors.**

	Blank field			Lensed field								
	6	7	8	A1689			A1835			AC114		
z_s	6	7	8	6	7	8	6	7	8	6	7	8
LF (a)	4.61	2.43	1.31	$8.63^{+0.86}_{-0.76}$	$5.66^{+0.62}_{-0.59}$	$3.83^{+0.47}_{-0.44}$	$6.69^{+0.61}_{-0.58}$	$4.00^{+0.42}_{-0.39}$	$2.48^{+0.29}_{-0.27}$	$7.07^{+0.65}_{-0.61}$	$4.27^{+0.44}_{-0.41}$	$2.66^{+0.31}_{-0.29}$
v_r	58%	75%	97%	$47^{+1}_{-1}\%$	$56^{+2}_{-2}\%$	$66^{+3}_{-3}\%$	$51^{+1}_{-1}\%$	$63^{+2}_{-2}\%$	$77^{+3}_{-3}\%$	$50^{+1}_{-1}\%$	$62^{+2}_{-2}\%$	$75^{+3}_{-3}\%$
LF (b)	1.30	0.39	0.13	$10.07^{+1.808}_{-1.608}$	$5.66^{+1.24}_{-1.08}$	$3.53^{+0.89}_{-0.75}$	$4.69^{+0.78}_{-0.69}$	$2.21^{+0.47}_{-0.41}$	$1.23^{+0.30}_{-0.25}$	$4.96^{+0.80}_{-0.71}$	$2.35^{+0.47}_{-0.41}$	$1.28^{+0.30}_{-0.25}$
v_r	96%	165%	283%	$45^{+2}_{-2}\%$	$56^{+4}_{-4}\%$	$68^{+5}_{-6}\%$	$60^{+3}_{-3}\%$	$79^{+6}_{-7}\%$	$101^{+9}_{-10}\%$	$57^{+4}_{-4}\%$	$77^{+6}_{-6}\%$	$100^{+8}_{-9}\%$
LF (c)	1.30	0.07	< 0.01	$10.07^{+1.808}_{-1.608}$	$3.08^{+0.84}_{-0.71}$	$0.96^{+0.38}_{-0.29}$	$4.69^{+0.78}_{-0.69}$	$1.04^{+0.27}_{-0.23}$	$0.28^{+0.10}_{-0.08}$	$4.96^{+0.80}_{-0.71}$	$1.03^{+0.26}_{-0.22}$	$0.24^{+0.09}_{-0.07}$
v_r	96%	383%	-	$45^{+2}_{-2}\%$	$70^{+6}_{-7}\%$	$113^{+17}_{-16}\%$	$60^{+3}_{-3}\%$	$108^{+12}_{-10}\%$	$197^{+39}_{-25}\%$	$57^{+4}_{-4}\%$	$108^{+12}_{-10}\%$	$211^{+38}_{-29}\%$

Table 7. Field to field variance for 3 different magnitude limits : $m_{lim} = 27.0, 28.0$ and 29.0 , in a $6' \times 6'$ blank field and lensing field (behind AC114) for the LF(c). **Field to field variance in lensing fields includes $1 - \sigma$ magnification errors.**

	$m_{lim} = 27.0$		$m_{lim} = 28.0$		$m_{lim} = 29.0$	
	$\langle N \rangle$	v_r	$\langle N \rangle$	v_r	$\langle N \rangle$	v_r
Blank field						
$z = 6$	65.58	27%	256.71	21%	681.92	18%
$z = 7$	19.01	38%	107.27	26%	352.52	21%
$z = 8$	4.17	62%	39.78	34%	170.04	26%
$z = 10$	0.05	471%	2.92	72%	29.73	39%
$z = 12$	< 0.00	-	0.04	494%	2.56	77%
Lensing field						
$z = 6$	$83.88^{+6.60}_{-6.28}$	$26^{+0}_{-0}\%$	$253.92^{+13.20}_{-12.86}$	$23^{+0}_{-0}\%$	$537.27^{+17.23}_{-17.22}$	$22^{+0}_{-0}\%$
$z = 7$	$31.05^{+3.21}_{-3.00}$	$33^{+1}_{-1}\%$	$122.49^{+8.16}_{-7.85}$	$26^{+1}_{-1}\%$	$318.64^{+13.88}_{-13.66}$	$24^{+0}_{-0}\%$
$z = 8$	$10.03^{+1.39}_{-1.27}$	$45^{+1}_{-2}\%$	$54.01^{+4.57}_{-4.33}$	$31^{+1}_{-1}\%$	$174.64^{+9.75}_{-9.46}$	$26^{+0}_{-0}\%$
$z = 10$	$0.72^{+0.20}_{-0.16}$	$129^{+14}_{-14}\%$	$7.44^{+1.06}_{-0.96}$	$55^{+2}_{-2}\%$	$41.28^{+3.58}_{-3.39}$	$37^{+1}_{-2}\%$
$z = 12$	$0.06^{+0.03}_{-0.02}$	$411^{+107}_{-78}\%$	$0.64^{+0.17}_{-0.14}$	$137^{+15}_{-14}\%$	$6.46^{+0.92}_{-0.83}$	$59^{+2}_{-2}\%$

4.2. Influence of galaxy morphology and image sampling

Gravitational magnification (e.g. in the tangential direction) induces an elongation of images along the shear direction while preserving the resolution in the perpendicular direction and the surface brightness of high redshift galaxies. All the comparisons between lensing and blank fields in our simulations assumed that observations were conducted with the same instrument setup in terms of FOV and spatial sampling, and with the same observational conditions, in particular the same limiting surface brightness and PSF. However, when comparing magnitude-limited samples in lensing and blank fields, it is worth discussing the influence of galaxy morphology and image sampling on the present results. In particular, the evolution in the surface brightness of high redshift sources is susceptible to hinder the search efficiency in clusters if, for instance, number counts in clusters were dominated by sources below the limiting surface brightness.

As explained in Sect. 2.1.1, all the previous results have been obtained assuming that galaxies at $z > 7$ are compact as compared to spatial sampling. Indeed, high redshift sources are expected to be very small, typically $\lesssim 0.1''$ on the sky, based on cosmological simulations (e.g. ?), in such a way that the high resolution capability of JWST is needed for resolving such faint galaxies. Recent observations of LBGs candidates in the HUDF fully support this idea (???). In a recent paper, ? measured the average intrinsic size of $z \sim 7-8$ LBGs to be 0.7 ± 0.3 kpc. These galaxies are found to be extremely compact, with very little evolution in their half-light radii between $z \sim 6$ and 7 , roughly consistent with galaxies having constant comoving sizes, at least within the observed luminosity domain $\sim 0.1 - 1L^*(z = 3)$. Smaller physical sizes are expected for higher redshift and/or intrinsically fainter galaxies, based on the scaling of the dark matter halo mass or the disk circular velocity (?). This differential trend is actually observed between the bright ($\sim 0.3 - 1L^*$) and the faint ($\sim 0.12 - 0.3L^*$) samples of ?.

If all high- z galaxies exhibit the same compact and uniform morphology, the effective mean surface brightness of a lensed galaxy will be brighter or fainter with respect to a blank field galaxy with the same apparent magnitude depending on the spatial resolution (in practice, the instrumental PSF). The majority of lensed sources should remain spatially unresolved on their width on seeing-limited ground-based surveys, and even on their tangential direction up to a gravitational magnification $\mu \sim 5 - 10$. Hence, the apparent surface brightness of a lensed source is actually brighter than that of a blank field galaxy of similar apparent magnitude (by roughly $-2.5 \log(\mu)$ mags for a spatially unresolved galaxy). This situation is typically found in the “shallow and wide” near-IR surveys discussed above (e.g. for the $6' \times 6'$ FOV), where lensing clusters are particularly efficient.

On the contrary, for a fixed apparent magnitude, the effective mean surface brightness of a lensed galaxy is expected to become fainter with respect to a blank field galaxy when the image resolution is similar or better than its (lensed maximum) half-light radius, reaching $\sim 2.5 \log(\mu)$ mags in the worst case. This situation is typically expected in the “deep and narrow” near-IR surveys with space facilities. In practice, the best spatial resolution presently achieved with HST/WFC3 in the near-IR is $\sim 0.''10$, reaching $0.''065$ with JWST/NIRCam, i.e. the typical size of the brightest $z \sim 7 - 8$ LBGs candidates presently identified. Therefore, the majority of lensed sources should remain spatially unresolved on their width. A lensed source entering the apparent-magnitude limited sample because of its magnification μ has also a smaller physical size, by a factor of μ (assuming a constant M/L scaling with the halo mass) or $\mu^{1/2}$ (assuming a constant M/L scaling with the halo circular velocity), leading to an apparent increase on its surface brightness with respect to blank-field observations of the same galaxy. Given the spatial resolution achieved with HST and JWST, this intrinsic-size effect tends to compensate the image dilution described above, in such a way that the actual surface brightness of the lensed galaxy should get close to the surface brightness of a blank field galaxy of similar apparent magnitude.

For the reasons explained above, and to the best of present knowledge, we do not expect the apparent-magnitude limited number counts derived in clusters to be strongly biased by sources below the limiting surface brightness, provided that the usual scalings apply to the size of high- z sources.

4.3. Comparison with current survey results

We have compared our simulation results to recent observations looking for high- z LBGs. For instance, the discovery of a bright $z = 7.6 \pm 0.4$ lensed galaxy by ?, with $AB=24.7$ (intrinsic $AB \sim -22.6$), in a $2.5' \times 2.5'$ FOV survey around A1689 is in fair agreement with our expectations. Indeed, given the survey characteristics and including $\sim 100\%$ variance for $z_s = 7.6 \pm 0.4$, we expect between 0.2 and 0.8 such bright objects in this lensing field, if the LF remains constant between $z \sim 4$ and 8 (LF(a)). In case of a strongly evolving LF(c), the expected number of sources in this survey is 0.12 (i.e. ranging between 0 and 0.5 with $\sim 200\%$ variance) making the discovery of this bright source particularly fortunate. Our results for lensing fields are also consistent with the number of $z \sim 7.5$ LBGs found by ?, to the depth of their survey, using LF(b) or (c). Quantitatively, ? detected 5 sources with 12 pointings over 6 clusters. With our simulations, $2.6^{+0.7}_{-0.6}$ objects with a variance of $\sim 75\%$ are expected with the

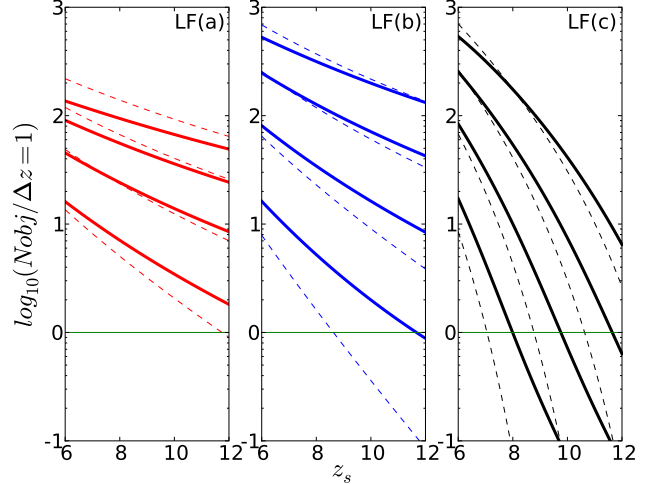


Fig. 9. Expected number counts of objects as a function of the redshift of sources in a $6' \times 6'$ FOV, for different limiting magnitudes 26.0, 27.0, 28.0 and 29.0 from bottom to top respectively. This calculation is provided both in blank (dotted line) and lensing fields (solid line) (here AC114) and for the three LFs (from right to left, (a) in red, (b) in blue and (c) in black)

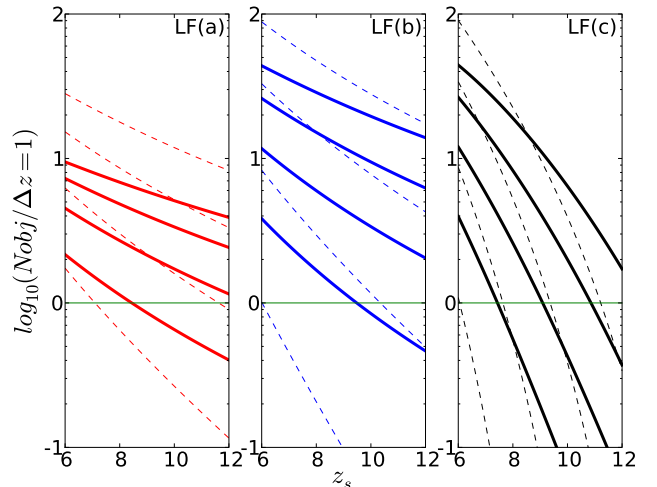


Fig. 10. The same as Fig. 9 but for a $2.2' \times 2.2'$ FOV. Some differences appear in comparison with the Fig. 9. For example, the total numbers of high- z galaxies expected behind lensing clusters (solid lines) and the field (dashed lines) are much larger at low limiting magnitude ($m_{AB} = 26.0$) but this phenomenon is reversed for deeper surveys ($m_{AB} = 28.0 - 29.0$) (see text for details).

LF(c) model. We also compared with the surface density of $z \sim 7$ candidates in the deep near-IR data behind clusters obtained by ?. ? found a surface density of $0.05^{+0.11}_{-0.04} \text{ arcmin}^{-2}$ with $AB \leq 25.5$ with a typical NICMOS3 FOV. With the strongly evolving LF(c) and the same survey characteristics used in our simulations, we expect a surface density of 0.01 arcmin^{-2} behind a typical cluster such as AC114, with a variance of $\sim 110\%$. This result shows a relatively good agreement by taking into account field to field variance.

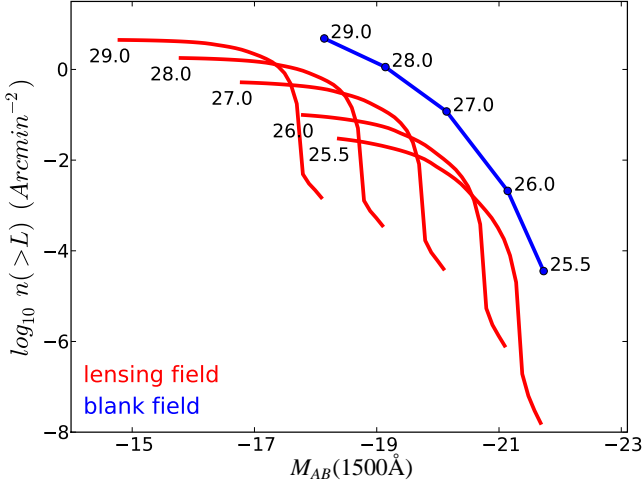


Fig. 11. Cumulative surface density of sources as a function of their intrinsic UV luminosity, in blank fields (blue solid line) and in the lensing fields with FOV ~ 5 arcmin² (JWST-like, red solid line), for different photometric depths ranging from shallow ($AB \sim 25.5$) to deep ($AB \sim 29.0$) surveys and a strongly evolving LF(c). The source redshift is arbitrarily fixed at $z=8$, with $\Delta z = 1$

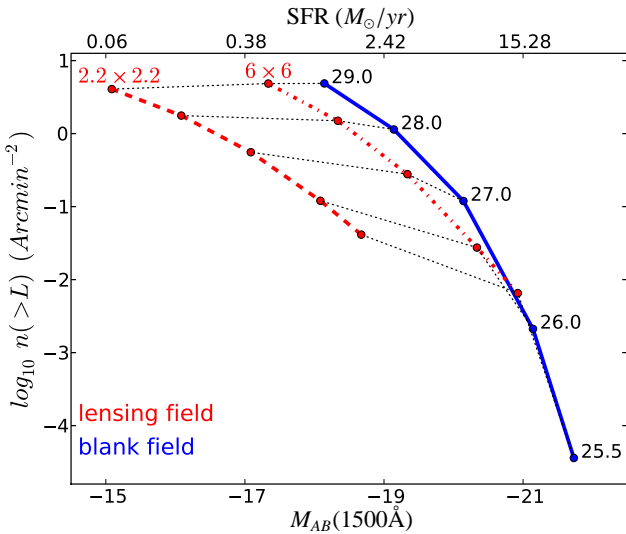


Fig. 12. Cumulative surface density of sources as a function of their intrinsic UV luminosity and SFR, in blank fields (blue solid line) and in the lensing fields with FOV $6' \times 6'$ (red dotted line) and $2.2' \times 2.2'$ (JWST-like, red dashed line), for different photometric depths ranging from shallow ($AB \sim 25.5$) to deep ($AB \sim 29.0$) surveys and a strongly evolving LF(c). The mean magnification over the whole the field is used to derive the lensing points, the true distribution is displayed in Fig. 11. The source redshift is arbitrarily fixed at $z=8$, with $\Delta z = 1$. The conversion from absolute magnitude to SFR is provided in Sect. 2.1.3 using the calibrations from ?.

4.4. Lyman Break versus NB searches

In this section, we discuss on the relative efficiency of blank and lensing fields on the detection of LAEs based on either NB surveys or the spectroscopic follow up of LBGs at $z > 6$. Although

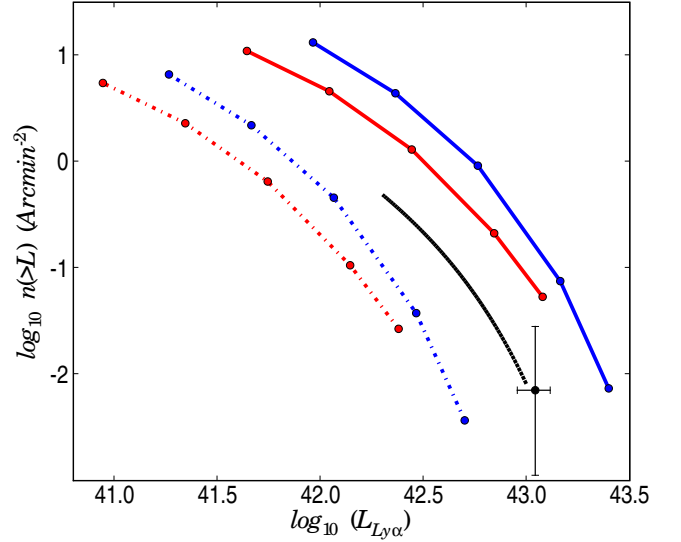


Fig. 13. Cumulative surface density of observed sources as a function of their Lyman alpha luminosity ($6' \times 6'$ FOV, $\Delta z = 1$, redshift of sources fixed at 6.6 for the LF(c)). The density is calculated in blank (blue solid line) and in lensing fields (red solid line) for different limiting magnitudes (from right to left: 25.5, 26.0, 27.0, 28.0 and 29.0). Dashed lines display number counts corrected by transmission value $\epsilon \sim 10\%$ (dashed red line in lensing fields and dashed blue line in blank field). For comparison, raw number counts extracted from the spectroscopic sample of LAEs by ? are also given (black solid line). The number density derived from ? at $z = 6.96$ is also indicated, together with corresponding error bars (see text for details). As in Fig. 12, the magnification used to derive the lensing points is averaged over the entire field.

the observational effort required to select $z \geq 7$ candidates using the dropout technique seems relatively cheap as compared to the NB approach, the two approaches are complementary, as emphasized by the fact that many objects found by Lyman α emission remain weak or undetected in the continuum (e.g. ?, ?, ?, ?). A quantitative comparison between the properties of LAEs and LBGs at $z \geq 7$ within the same volume should provide important information on the Lyman α transmission, SFR and other properties of these high- z galaxies.

Since the pioneering Large Area Lyman Alpha Survey (LALA, ?, ?), different NB surveys in blank fields have provided interesting galaxy samples in the $z \sim 5 - 7$ interval, e.g. the large sample of Ly α emitters at $z \sim 5.7$ by ?, the $z=6.17$ and 6.53 galaxies found respectively by ? and ?, the two $z \sim 6.6$ galaxies detected by ?, and the galaxy at a redshift $z=6.96$ found by ?. In the latter case, which should be representative of $z \sim 7$ samples, the authors used a combination of NB imaging at 8150\AA (SuprimeCam) and broad-band photometry in the optical bands to select candidates for a subsequent spectroscopic follow up with DEIMOS/Keck. Their confirmation rate is relatively high (18 sources out of 26 candidates), leading to 0.03 sources/arcmin² and redshift bin $\delta z = 0.1$. Similar results are reported by ?. All these sources have important Lyman α fluxes (a few $\times 10^{-17}$ erg cm⁻² s⁻¹), and display broad Lyman α lines ($\sigma_v \sim 200$ km/s). A strong evolution is found in the number density of LAEs at $z \geq 7$ with respect to the $z \sim 5 - 7$ interval (?, ?, ?).

The number of LAEs expected within a sample of LBGs at $z \geq 6$ can be estimated using the distribution of Lyman- α equivalent widths derived for the spectroscopic sample of LBGs at $z \sim 3$ by ?, assuming no evolution in the population of LAEs with respect to LBGs. This simplistic scaling should be enough for the simulation needs. We introduce a factor ϵ , defined below, which can be linked to the Lyman α transmission as follows:

$$\epsilon = \frac{L_{1500}}{L_{Ly\alpha}(1+z)} = \frac{1}{W_{Ly\alpha}} \quad (12)$$

where L_{1500} is the UV monochromatic luminosity at 1500 Å, $L_{Ly\alpha}$ is the Lyman- α luminosity and $W_{Ly\alpha}$ is the Lyman- α equivalent width. With this simple assumption, the average value for the Lyman- α equivalent width is ~ 10 Å, corresponding to $\epsilon \sim 10\%$. This value can be used to derive a rough estimate of expected number density of LAEs, from a population of LBGs. In addition, the number density is also corrected to take into account of the fraction of the LBGs sample displaying Ly α in emission.

Fig. 13 displays the cumulative number counts of sources at $z \sim 6.6$ integrated from the LF(c) as a function of the Lyman- α luminosity, scaled according to the UV luminosities (cf Sect. 2.1.1) in the typical $6' \times 6'$ FOV, together with a comparison of observations in a similar redshift domain ($z_s \sim 6.6$ for Kashikawa spectroscopic sample of LAEs and ? at $z=6.96$).

The number density of LBGs at $z=7$ (with $\delta z = 0.1$, close to the band-width of NB surveys) ranges between 0.001 (LF(c)) and 0.02 (LF(a)) sources/ $arcmin^2$ for a survey limited to $H(AB) \leq 25.5$, depending on the LF. Lensing clusters improve these numbers by a factor ranging between 6 (for LF(c)) and 2 (for LF(a)). In case of a deep survey limited to $H(AB) \leq 29.0$, the number densities reach 1 (LF(c)) to 2 (LF(a)) sources/ $arcmin^2$. In this case, there is a negative magnification bias of the order of 20%. These numbers, obtained with a simplistic model, are between a factor of ~ 10 (for bright sources) and a few (for faint sources) smaller than the number densities obtained by ? for their spectroscopic sample. With increasing z_s (see Fig. 9) for instance at $z=9$ with the strongly evolving LF(c), no sources can be detected for a shallow survey limited to $H(AB) \leq 25.5$ and for a deeper limited survey ($H(AB) \leq 29.0$), a minimum of 3 $arcmin^2$ surveyed area is needed to obtain 1 source in a blank field. In a lensing field with the (LF(c)), these number densities reach 0.002 for $H(AB) \leq 25.5$ and 0.32 sources/ $arcmin^2$ for $H(AB) \leq 29.0$. The relatively low-efficiency of lensing clusters with NB techniques in the $z \geq 9$ domain has been recently confirmed by the results of ?.

The preselection of $z \geq 6-7$ candidates in lensing fields has two main advantages with respect to blank fields. In the shallow ($AB \leq 25.5$) regime, there is an increase by a factor $\sim 8-10$ on the number of sources detected and a moderate gain in depth for a given exposure time (i.e. ~ 0.5 magnitudes at $AB \sim 25.5$). In the deep-survey regime ($AB \leq 28-29$), there is a gain in intrinsic depth, for a number of candidates which remains essentially constant (i.e. ~ 0.8 mags gain at $AB \leq 28$). The relative efficiency of lensing with respect to blank field counts in Fig. 12 depends on the FOV. The two predictions get close to each other with increasing values of the FOV in lensing surveys, and the trend goes in the opposite direction for smaller FOV. This trend is the same for both LBGs and LAEs. To explore the bright end of the LF, blank field surveys are needed with a large FOV, whereas lensing clusters are particularly useful to explore the faint end of the LF. This trend is further discussed in the next Section.

4.5. Towards the ideal survey: constraining the Luminosity Function of high- z sources

All present photometric surveys aimed at constraining the UV LF at $z > 7$, either space or ground-based, are still dramatically small in terms of effective surface. Wide and deep optical+near-IR surveys in lensing and blank fields are needed to set strong constraints on the LF and on the star-formation density at $z > 7$. An important issue is the combination between photometric depth and surveyed area which is needed to identify a representative number of photometric candidates, or to reach a significant non-detection limit in order to constrain the LF of $z > 7$ sources.

There are three different aspects to consider when designing an “ideal” survey aiming at constraining the LF: the depth and the area of the survey, and the corresponding field to field variance. In order to address these issues, we have computed the expected field to field variance corresponding to lensing and blank field surveys, for different survey configurations (area and depth). A summary of these results is given in Table 8 for different number of lensing clusters, and for two representative depths in the H-band (i.e. a “shallow” survey with $AB \leq 25.5$, and a “deep” survey with $AB \leq 28.0$) assuming a strongly evolving LF(c) in all cases. This table complements the results given in Tables 5 and 7 for blank and lensing fields as a function of depth. In all cases, we use AC114 as a reference for lensing clusters.

Regarding field-to-field variance in number counts, results are expected to be similar in blank and lensing fields for a relatively wide FOV ($\sim 40-50 arcmin^2$; see Sect. 3.5 and Table 7). As shown in Table 8, a deep lensing survey using ~ 10 clusters should be able to reach a variance $\leq 20\%$ on sources at $6 \leq z \leq 8$, irrespective of the actual LF. This value is better than present-day photometric surveys in blank fields, typically reaching 30-35% for $AB \leq 29.0$ (e.g. ?), which in turn is rather close to what could be achieved in a single lensing cluster for $AB \leq 28.0$.

A different survey strategy consists of increasing the number of lensing clusters with a shallow limiting magnitude. In this case, a few tens of lensing clusters (typically between 10 and 50, depending on the LF) are needed to reach a variance of $\sim 30\%$ at $z \leq 8$. Note that the difference in exposure time between the shallow and deep surveys reported in Table 8 is a factor ~ 100 , and that ~ 10 pointings are needed on blank fields in order to reach the same number of $z \sim 6-8$ sources as in a single “shallow” lensing field.

In the case of a strongly evolving LF(c), photometric surveys should reach a minimum depth of $AB \sim 28$ to achieve fair statistics on $z \sim 9-10$ sources using a lensing cluster (Table 7). In this case we expect between 20 ($z=9$, $\sim 40\%$ variance) and 8 ($z=10$, $\sim 40\%$ variance) sources per lensing cluster in a $\sim 40 arcmin^2$ FOV. The efficiency is a factor of 10 smaller at $z \sim 10$ in blank fields. Fair statistics at $z \sim 12$ should require a minimum depth close to $AB \sim 29$ both in lensing and blank fields.

Constraining the LF of star forming galaxies at $z \geq 7$ should require the combination of blank and lensing field observations. This is illustrated for instance in Fig. 11 and 12 for an example at $z_s = 8$. A survey towards a lensing cluster has several advantages. It increases the total number of sources available for spectroscopic follow up, and it helps extending the sample towards the faint edge of the LF and towards the highest possible limits in redshift. On the other hand, blank fields are needed to achieve fair statistics on the bright edge of the LF. Thus an “ideal” survey should combine both blank and lensing fields. Given the numbers presented in previous sections, a blank field used for these purposes should be a factor ranging between ~ 10 and 100 times

larger than a lensing field (depending on the redshift domain, photometric depth, and actual LF) in order to efficiently complete the survey towards $L > L^*$. This should be possible with the new upcoming surveys, such as the WIRCAM ultra deep survey (WUDS) at CFHT ($\sim 400 \text{ arcmin}^2$, with $YJHK \lesssim 25.5$), UKIDSS-UDS ($\sim 2700 \text{ arcmin}^2$, with $YJHK \lesssim 25$) or Ultra-Vista ($\sim 2600 \text{ arcmin}^2$, with $YJH \lesssim 26$, $K \lesssim 25.6$). The optimum number of lensing fields ranges between $\sim 10 - 20$ (for $z \sim 6 - 8$ studies with “shallow” photometry) to a few (for “deep” surveys targeting $z \sim 8 - 12$ sources).

5. Summary and conclusions

We have evaluated the relative efficiency of lensing clusters with respect to blank fields in the identification and study of $z \geq 6$ galaxies. The main conclusions of this study are given below.

For magnitude-limited samples of LBGs at $z \geq 6$, the magnification bias increases with the redshift of sources and decreases with both the depth of the survey and the size of the surveyed area. Given **the typical near-IR FOV** in lensing fields, the maximum efficiency is reached for clusters at $z \sim 0.1 - 0.3$, with maximum cluster-to-cluster differences ranging between 30 and 50% in number counts, depending on the redshift of sources and the LF.

The relative efficiency of lensing with respect to blank fields strongly depends on the shape of the LF, for a given photometric depth and FOV. The comparison between lensing and blank field number counts is likely to yield strong constraints on the LF.

The presence of a strong-lensing cluster along the line of sight has a dramatic effect on the observed number of sources, with a positive magnification effect in typical ground-based “shallow” surveys ($AB \leq 25.5$). The positive magnification bias increases with the redshift of sources, and also from optimistic to pessimistic values of the LF. In case of a strongly evolving LF at $z \geq 7$, as proposed by ?, blank fields are particularly inefficient as compared to lensing fields. For instance, the size of the surveyed area in ground-based observations would need to increase by a factor of ~ 10 in blank fields with respect to a typical $\sim 30 - 40 \text{ arcmin}^2$ survey in a lensing field, in order to reach the same number of detections at $z \sim 6 - 8$, and this merit factor increases with redshift. **All these results have been obtained assuming that number counts derived in clusters are not dominated by sources below the limiting surface brightness of observations, which in turn depends on the reliability of the usual scalings applied to the size of high- z sources.**

Ground-based “shallow” surveys are dominated by field-to-field variance reaching ~ 30 to 50% in number counts between $z \sim 6$ and 8 in a unique $\sim 30 - 40 \text{ arcmin}^2$ lensing field survey (or in a 400 arcmin^2 blank field), assuming a strongly evolving LF.

The number of $z > 8$ sources expected at the typical depth of JWST ($AB \sim 28 - 29$) is much higher in lensing than in blank fields if the UV LF is rapidly evolving with redshift (i.e. a factor of ~ 10 at $z \sim 10$ with $AB \lesssim 28$).

Blank field surveys with a large FOV are needed to probe the bright edge of the LF at $z \geq 6 - 7$, whereas lensing clusters are particularly useful to explore the mid to faint end of the LF.

Acknowledgements. We are grateful to D. Schaerer, A. Hempel, J.F. Le Borgne and E. Egami for useful comments. We acknowledge financial support from the European Commissions ALFA-II programme through its funding of the Latin-America European Network for Astrophysics and Cosmology (LENAC). This work was also supported by the French *Centre National de la Recherche Scientifique*, the French *Programme National de Cosmologie* (PNC) and *Programme National de Galaxies* (PNG). JR acknowledges support from a EU Marie-Curie fellowship.

Table 8. Field to field variance, including $1 - \sigma$ errors on the magnification factor, expected in a lensing survey, as a function of the number of clusters, for the three LFs (a), (b) and (c) (from top to bottom respectively). Simulations were performed using the same approaches in Sect. 3.5 (i.e. $6' \times 6'$ FOV, ...) for two different depths: $AB \leq 25.5$ (shallow survey) and $AB \leq 28.0$ (deep survey)

v_r LF(a)/ $N_{clusters}$	1	6	10	20	50	100
$z = 6$						
Shallow	50 ⁺³ ₋₃ %	28 ⁺¹ ₋₁ %	24 ⁺¹ ₋₁ %	19 ⁺⁰ ₋₀ %	14 ⁺⁰ ₋₀ %	10 ⁺⁰ ₋₀ %
Deep	25 ⁺¹ ₋₁ %	17 ⁺⁰ ₋₀ %	15 ⁺⁰ ₋₀ %	12 ⁺⁰ ₋₀ %	9 ⁺⁰ ₋₀ %	7 ⁺⁰ ₋₀ %
$z = 7$						
Shallow	62 ⁺² ₋₂ %	33 ⁺¹ ₋₁ %	28 ⁺¹ ₋₁ %	22 ⁺⁰ ₋₀ %	16 ⁺⁰ ₋₀ %	12 ⁺⁰ ₋₀ %
Deep	29 ⁺¹ ₋₁ %	19 ⁺⁰ ₋₀ %	17 ⁺⁰ ₋₀ %	13 ⁺⁰ ₋₀ %	10 ⁺⁰ ₋₀ %	7 ⁺⁰ ₋₀ %
$z = 8$						
Shallow	75 ⁺³ ₋₃ %	39 ⁺¹ ₋₂ %	32 ⁺¹ ₋₁ %	25 ⁺⁰ ₋₁ %	18 ⁺⁰ ₋₀ %	13 ⁺⁰ ₋₀ %
Deep	32 ⁺¹ ₋₁ %	21 ⁺⁰ ₋₀ %	18 ⁺⁰ ₋₀ %	15 ⁺⁰ ₋₀ %	11 ⁺⁰ ₋₀ %	8 ⁺⁰ ₋₀ %
v_r LF(b)/ $N_{clusters}$	1	6	10	20	50	100
$z = 6$						
Shallow	57 ⁺⁴ ₋₄ %	40 ⁺² ₋₂ %	33 ⁺² ₋₂ %	26 ⁺¹ ₋₁ %	18 ⁺⁰ ₋₀ %	14 ⁺⁰ ₋₀ %
Deep	23 ⁺¹ ₋₁ %	14 ⁺⁰ ₋₀ %	13 ⁺⁰ ₋₀ %	10 ⁺⁰ ₋₀ %	8 ⁺⁰ ₋₀ %	6 ⁺⁰ ₋₀ %
$z = 7$						
Shallow	77 ⁺⁶ ₋₆ %	40 ⁺² ₋₂ %	33 ⁺¹ ₋₁ %	25 ⁺⁰ ₋₁ %	18 ⁺⁰ ₋₀ %	13 ⁺⁰ ₋₀ %
Deep	24 ⁺¹ ₋₁ %	17 ⁺⁰ ₋₀ %	15 ⁺⁰ ₋₀ %	12 ⁺⁰ ₋₀ %	9 ⁺⁰ ₋₀ %	7 ⁺⁰ ₋₀ %
$z = 8$						
Shallow	100 ⁺⁸ ₋₉ %	48 ⁺² ₋₃ %	40 ⁺² ₋₂ %	30 ⁺¹ ₋₁ %	21 ⁺⁰ ₋₀ %	15 ⁺⁰ ₋₀ %
Deep	28 ⁺¹ ₋₁ %	19 ⁺⁰ ₋₀ %	16 ⁺⁰ ₋₀ %	13 ⁺⁰ ₋₀ %	10 ⁺⁰ ₋₀ %	7 ⁺⁰ ₋₀ %
v_r LF(c)/ $N_{clusters}$	1	6	10	20	50	100
$z = 6$						
Shallow	57 ⁺⁴ ₋₄ %	40 ⁺² ₋₂ %	33 ⁺¹ ₋₁ %	26 ⁺¹ ₋₁ %	18 ⁺⁰ ₋₀ %	14 ⁺⁰ ₋₀ %
Deep	23 ⁺⁰ ₋₀ %	14 ⁺⁰ ₋₀ %	13 ⁺⁰ ₋₀ %	10 ⁺⁰ ₋₀ %	8 ⁺⁰ ₋₀ %	6 ⁺⁰ ₋₀ %
$z = 7$						
Shallow	108 ⁺¹² ₋₁₀ %	51 ⁺³ ₋₄ %	42 ⁺² ₋₂ %	32 ⁺¹ ₋₁ %	22 ⁺¹ ₋₁ %	16 ⁺⁰ ₋₀ %
Deep	26 ⁺¹ ₋₁ %	18 ⁺⁰ ₋₀ %	15 ⁺⁰ ₋₀ %	12 ⁺⁰ ₋₀ %	9 ⁺⁰ ₋₀ %	7 ⁺⁰ ₋₀ %
$z = 8$						
Shallow	211 ⁺³⁸ ₋₂₉ %	92 ⁺⁸ ₋₈ %	73 ⁺⁶ ₋₆ %	53 ⁺⁴ ₋₄ %	35 ⁺¹ ₋₁ %	25 ⁺¹ ₋₁ %
Deep	31 ⁺¹ ₋₁ %	21 ⁺⁰ ₋₀ %	18 ⁺⁰ ₋₀ %	15 ⁺⁰ ₋₀ %	11 ⁺⁰ ₋₀ %	8 ⁺⁰ ₋₀ %